AD-774 525

PHOTOCHEMICAL ENHANCEMENT OF COMBUSTION AND MIXING ITS SUPERSONIC FLOWS

A. E. Cerkanowicz

Photochem Industries, Incorporated

Prepared for:

Air Force Office of Scientific Research

November 1973

UNCLASSIFIED
Security Classification

i. AD774 525

DOCUMENT CONTROL DATA - R & D

(Security classification of title, body of abstract and indexing annotation must be entered when the overall report is classified)

1. ORIGINATING ACTIVITY (Corporate author) Photochem Industries, Inc. 123 Clinton Road Fairfield, New Jersey 07006	2a. REPORT SECURITY CLASSIFICATION UNCLASSIFIED 2b. GROUP n/a

3. REPORT TITLE

PHOTOCHEMICAL ENHANCEMENT OF COMBUSTION AND MIXING IN SUPERSONIC FLOWS

4. DESCRIPTIVE NOTES (Type of report and inclusive dates)

- Final

5. AUTHOR(S) (First name, middle initial, last name)

Anthony E. Cerkanowicz

6. REPORT DATE November 1972	7a. TOTAL NO. OF PAGES 136	7b. NO. OF REFS 53
8a. CONTRACT OR GRANT NO. F44620-70-C-0051 b. PROJECT NO. 9711-02 c. 61102F d. 681308	9a. ORIGINATOR'S REPORT NUMBER(S) PII-3036-2 9b. OTHER REPORT NO(S) (Any other numbers that may be assigned this report) AFOSR - TR - 74 - 0158	

10. DISTRIBUTION STATEMENT

Approved for public release; distribution unlimited

11. SUPPLEMENTARY NOTES	12. SPONSORING MILITARY ACTIVITY AF Office of Scientific Research 1400 Wilson Boulevard Arlington, Virginia 22209

13. ABSTRACT

Initiation and combustion enhancement of gaseous (vaporized or atomized) fuel-air mixtures can be produced photochemically by ultraviolet irradiation in both stationary and flowing mixtures. Induced combustion characteristics are different from normal thermal ignition (e.g., spark plug), and could provide for ignition and enhanced combustion at conditions where thermal ignition is unreliable or impossible. The potential for practical application of photochemically induced effects in chemical energy conversion devices (e.g., aircraft gas turbines, ramjets) is further facilitated by the recent availability of higher efficiency ultraviolet light sources. The designer is thus provided with a novel and practical method of combustion initiation and enhancement which departs from the usual thermal method,

This report presents a summary of the observed combustion effects and the intrinsic wavelength effects related to the photochemical combustion initiation and enhancement principle. Specific in-depth attention is given to radiant penetration into the reactant mixture, the possible use of laser sources and the role of the electronically excited oxygen atom in the photochemical processes.

Analytical description of the phenomena provides correlation of the experimental results and extension of the findings to other conditions not directly observed by experiment.

136

DD FORM 1 NOV 65 1473

UNCLASSIFIED
Security Classification

14 KEY WORDS	LINK A		LINK B		LINK C	
	ROLE	WT	ROLE	WT	ROLE	WT
Photochemical Ignition						
Enhanced Combustion						
Supersonic Combustion						
Unsensitized Ignition						
Ultraviolet Radiation						
Oxygen Photodissociation						
Spark Ignition						
Fuel Lean Mixtures						
Atomized Liquid Fuels						
Phase Plane Analysis						
Laser Ignition						
Excited State Kinetics						
Combustion Instability						

AFOSR Scientific Report
AFOSR-TR-73-

FINAL REPORT

PHOTOCHEMICAL ENHANCEMENT OF COMBUSTION AND MIXING IN SUPERSONIC FLOWS

By: A. E. Cerkanowicz

Photochem Industries, Inc., Fairfield, N. J.

November 1973

Research Partially Sponsored by
Air Force Office of Scientific Research

under

Contract No. F44620-70-C-0051

FOREWORD

This is a report on research studies conducted with the partial support of the Air Force Office of Scientific Research under Contract F44620-70-C-0051 with Dr. B. T. Wolfson as the AFOSR project monitor. As such, Photochem furnished scientific effort together with all the necessary related services, facilities, supplies and materials to conduct theoretical and experimental studies to better understand, demonstrate and measure the enhancement effect due to photochemically induced reactions on the combustion and mixing of two high-speed, fuel and air streams. Portions of this work, particularly the UV radiant source development and the non-aerospace applications, have been supported by Photochem Industries, Inc. internal funds (primarily under Photochem project numbers 1017 and 2060).

This is a final report on the progress of research through August 31, 1973 - at Photochem Industries, Inc., Fairfield, New Jersey (under Photochem project number 3036), with Dr. A. E. Cerkanowicz as principal investigator.

TABLE OF CONTENTS

	Page
FOREWORD	ii
ABSTRACT	iii
OBJECTIVE	1
PHOTOCHEMICAL IGNITION PRINCIPLE	1
SUMMARY OF PHOTOCHEMICAL COMBUSTION EFFECTS	3
INTRINSIC WAVELENGTH EFFECTS	6
EXTENSION AND APPLICATION OF PRINCIPLE	8
SUMMARY/CRITIQUE	9
REFERENCES	10
APPENDIX I - COMPUTER PROGRAM - ATOMIC OXYGEN CONCENTRATION	11
A. Introduction	11
B. Computer Program	11
C. Results	17
D. References	17
APPENDIX II - FLOWING REACTANT MIXTURES	19
A. Introduction	19
B. Exposure Time	19
C. Photochemical Ignition Energy	22
D. Comparison with Experiment	25
E. Discussion	26
F. Summary	28
G. References	28
APPENDIX III - REPETITIVE PULSE IGNITION	30
A. Introduction	30

Page

B. Pulsed Power Supply 30

C. Experimental Results 35

D. References 35

APPENDIX IV - PHOTOCHEMICAL VS SPARK IGNITION 36

A. Introduction 36

B. Experimental Results 36

C. Fuel Lean Mixtures 38

D. Low Pressure Mixtures 39

E. Summary 43

F. References 43

APPENDIX V - PENETRATION OF PHOTODISSOCIATIVE EFFECT . . 44

A. Introduction 44

B. Window Transmission 45

C. Molecular Oxygen Absorption 52

D. Radiant Energy Flux 55

E. Correction of Previous Analysis 55

F. Discussion 58

G. Summary 59

H. References 62

APPENDIX VI - PHOTOCHEMICAL COMBUSTION ENHANCEMENT . . . 63

A. Introduction 63

B. Phase Plane Considerations 63

C. Penetration of Combustion Enhancement 66

D. Summary 72

E. References 72

Page

APPENDIX VII - LASER CALCULATIONS 73

A. Fundamental Absorption Considerations 73

B. Atomic Oxygen Production 74

C. Solution of Differential Equation 75

D. Evaluation of Series Coefficients 77

E. Laser Photochemical Ignition Energy 79

F. Comments on Laser Ignition Techniques. 80

i. Direct Laser Action 80

ii. Frequency Multiplication 82

iii. Two Photon Absorption 83

G. Laser Radiant Penetration 85

H. Dissociation Wave Velocity 85

I. Summary 87

J. References 88

APPENDIX VIII - EXCITED STATE KINETICS 90

A. Introduction 90

B. General Comments on Excited State Chemistry. . 91

C. Analysis of $O(^1D)$ Reaction Kinetics 93

D. Analysis of Electronically Excited O_2 Kinetics 102

E. Photochemistry of H_2-N_2-O_2 System 105

F. Discussion 112

G. Summary 117

H. References 119

APPENDIX IX - COMBUSTION INSTABILITY PEHNOMENA 122

A. Discussion 122

B. References 124

Page

APPENDIX X - COMPENDIUM: DISSEMINATION OF PHOTOCHEMICAL COMBUSTION KNOWLEDGE. 125

A. Reports and Papers 125

B. Presentations 126

DD Form 1473

OBJECTIVE

The major objective of the subject research program is to elucidate the mechanism by which exposure to ultraviolet irradiation initiates and augments combustion of fuel-air mixtures under conditions encountered in air breathing aircraft engines and other chemical energy conversion devices. Practical photochemical devices are being developed in a parallel effort to this fundamental work to provide for rapid initiation and combustion enhancement where normal (i.e., spark) initiation and combustion are impossible. Operation of engines in regimes beyond their normal flight corridors would then be possible.

PHOTOCHEMICAL IGNITION PRINCIPLE

Based on qualitative and quantitative analysis of, and subsequent agreement with, the experimental results, a mechanism for the photochemical initiation and enhancement of sustained combustion in unsensitized fuel-air systems has been developed.

The initiation and enhancement mechanism is considered to follow a photochemical path wherein the critical intermediary species are oxygen atoms. The atoms are generated by photodissociation of oxygen molecules via radiant energy absorption below 2450 Å

$$O_2 + \text{radiant energy} \rightarrow O + O \qquad (1)$$

However, the most efficient photodissociative production of atoms occurs primarily at wavelengths below 1800 Å where one of the atoms produced is in an excited electronic state.

When a critical concentration of oxygen atoms, on the order of 10^{14} atoms/cm^3, is achieved or exceeded at any point in the reactant mixture, combustion initiation (not ignition) occurs. Subsequent reaction of the atomic oxygen with fuel molecules (as well as other combustion species) leads to ignition and sustained combustion via chain reactions. For example,

$$O + RH \rightarrow OH + R \qquad (2)$$

These reactions are different from the usual high temperature oxygen atom reactions since the process starts at a low temperature and not (as is usually the case) at the thermal ignition temperature. Additionally, since radiant absorption below 1800 Å is primarily responsible for initiation, the presence of electronically excited oxygen atoms further alters and enhances the kinetics. Combustion enhancement (lowering of the ignition temperature) is effectively produced by radiant absorption of all wavelengths below 2450 Å and typically involves oxygen atom concentrations of 10^6 atoms/cm^3, or greater. The experimental results indicate that the radiant energy consumed for photochemical ignition by the photochemical technique is only on the order of μJ/100 Å at 1500 Å.

Absorption of radiant energy by the fuel is postulated to be unnecessary. Qualitative verification of this is found in the fact that the hydrogen-oxygen-nitrogen mixtures and the methane-oxygen-nitrogen mixtures can be ignited photochemically using sapphire as the window material for radiant transmission. In these cases, the only radiative process which can occur involves oxygen photodissociation.

For a radiant pulse at the threshold energy initiation level, the initiation time (not ignition time) will be equal to the radiant pulse time. This is a consequence of the fact that the radiant energy input is essentially integrated over the time of the pulse by the reactant mixture. During this period, the absorbed radiant input is insufficient to cause any excessive heating effects and thus the initiation will occur under isothermal conditions. Additionally, only a small percentage of molecules are dissociated during the initiation period and thus the initial species concentrations are constant. Combining this information with the ideal gas equation of state shows that the pressure within the chamber is also constant during the initiation phase. Consequently, the photochemical combustion initiation and enhancement mechanism occurs at constant pressure, temperature and initial specis concentration.

The underlying physical phenomena involved in modeling the initiation process are photo-absorption--followed by photo-dissociation, gas phase reactions, diffusion and wall recombination. It is through the gas phase reactions that the process passes from the initiation phase to the ignition or self-sustaining phase. For flowing reactant mixtures, the added effect of "smearing" the oxygen atom density distribution due to mixture velocity past the radiant source window must be considered.

SUMMARY OF PHOTOCHEMICAL COMBUSTION EFFECTS

o Experiment[+]

Since photochemical ignition relies on dissociation of oxygen, the principle is applicable to a wide variety of fuels. This is supported by the achievement of successful photochemical ignition at room temperature of hydrogen, carbon monoxide, methane, acetylene, commercial gasoline and varsol (kerosene) fueled mixtures. Threshold energy requirements of these fuels (liquids in the atomized state) vary depending on the fuel-oxidant combination tested. Higher hydrocarbon fuels or the use of air instead of oxygen results in higher energy requirements. However, for all possible fuel-oxidant variations, the photochemical ignition threshold energy requirements are of the same order of magnitude.

Changing the mixture stoichiometry from stoichiometric to fuel-lean results first in a threshold energy decrease, then an increase. Again, however, the variation in threshold energy requirement is well within an order of magnitude, even beyond the stoichiometry range considered. For example, the energy typically required for photochemical ignition is increased by a factor of only 2 for a 16-fold decrease in fuel concentration[1]. A comparison of photochemical ignition with thermal (spark) ignition for fuel-lean mixtures (see Appendix IV) illustrates the vastly different characteristics that can be obtained by using the photochemical technique.

The required threshold energy level for photochemical ignition as a function of pressure has a relatively flat minimum between approximately 5 and 15 psia, but increases sharply at pressures below 2 psia. An increase of pressure to above 80 psia is necessary before a two-fold increase in energy above the minimum value occurs. The majority of the photochemical ignition experiments have been performed at initial temperatures of about 80°F. However, on the basis of some limited experiments at slightly elevated temperatures, and analytical considerations of kinetic requirements at increased temperatures, it is expected that photochemical ignition energy requirements decrease rapidly with increasing temperature.

[+]The majority of photochemical combustion effects reported in this section are detailed in references 1 thru 3.

A reactant mixture which is flowing past the optical window through which the radiant energy is transmitted will not require an increase in photochemical ignition energy above that required for ignition of stationary mixtures until a critical velocity is exceeded. A linear increase of photochemical ignition energy requirements with increasing mixture velocity is experienced for flows above the critical value (see Appendix II).

Photochemical ignition time delays of 0.1 to 1.0 msec have been measured for hydrogen and methane fueled mixtures at an initial temperature of about 80°F. Variation of the delay time with stoichiometry, pressure, or temperature is similar to that observed for the threshold ignition energies. Decreasing the radiant pulse time or increasing the input radiant energy (for a fixed pulse time) results in a reduction of the time delay. The "true" photochemical ignition delay would be defined by the delay time for instantaneous energy input (zero radiant pulse time).

Measured velocities of photochemically initiated flame fronts are about an order of magnitude greater than corresponding thermally (spark) initiated fronts[4]. However, the reported photochemical data was measured in laboratory coordinates and has not been corrected relative to the unreacted gas coordinates which differs due to the fact that the experiment involved ignition at one end of a closed horizontal reactant chamber. This correction is expected to be minor.

- Analysis

Since oxygen atoms are the key species in the photochemical combustion initiation and enhancement mechanism, a description of the variation of oxygen atom concentration (generated as a result of photodissociation) as a function of various applicable parameters is considered to be essential. Such an analysis was developed previously and provided satisfactory correlation of the experimentally observed photochemical combustion effects. The effect on photochemical ignition energy requirements of mixture type, stoichiometry, pressure, and temperature, as well as the influence of various light source parameters (window material, pulse time, etc.) have been analytically defined. However, although a closed form expression for oxygen atom concentration and thus photochemical ignition energy requirements was obtained, it proved to be very lengthy and arduous to use for numerical calculation. For this reason, a Fortran computer program has been compiled for

calculation of atom concentrations. Appendix I reviews the parameters involved in computing the oxygen atom concentration and the related computer program.

Extension of the analysis to flowing reactant mixtures is covered in detail in Appendix II. Computation of the time (exposure time) over which an element of gas is exposed to the ultraviolet radiant flux as it passes in front of the source window, provides for determination of the effect of reactant mixture velocity on the distribution of oxygen atom concentration. As the flow rate is increased, the distribution becomes "smeared," and eventually results in a decrease in peak oxygen atom concentration once a critical velocity is exceeded. A general expression for the dependence of ignition energy on mixture velocity (or Mach number) which applies for either laminar, turbulent or slug flow is obtained (Equations 12, 13 and 14). The analysis of the energy required to ignite, photochemically, flowing mixtures as a function of velocity results in predictions which adequately fit the data points and demonstrates the occurrence of a critical flow velocity (Figure 3), thus providing a basis for reliable extrapolation of the photochemical ignition characteristics to regions where data are presently lacking.

Additional reactant flow experiments were initiated using a repetitively pulsed radiant source system in place of the single pulse system. As discussed in Appendix III, an approximate 10 joule discharge energy level was provided at selectable rates from 10 to 100 pulses per second to a type PC-4 ultraviolet source. Feasibility of photochemical ignition under repetitive pulsed conditions was successfully demonstrated. However, limitations on repetitive pulse operation of the source precluded completion of the contemplated test program. Based on state-of-the-art technology and operating experience of commercially available pulsed radiant sources for application in the visible region of the spectrum, it is expected that suitable ultraviolet source life can eventually be achieved to allow for continuation of this aspect of the photochemical ignition study.

- Review

A review of the observed photochemical combustion effects indicate that a new class of igrition and combustion characteristics is provided by the photochemical technique. An appraisal of the unique combustion aspects involved can best be obtained by comparison with other ignition techniques. A limited comparison of this nature with regard to spark ignition is provided in Appendix IV. The comparison indicates that a stronger ignition kernel and propagating reaction front as well as a completely different ignition mechanism is involved in the

photochemical ignition technique. Coupled with the availability of practical ultraviolet radiant sources, these findings provide a new degree of freedom in optimizing the design of chemical energy conversion devices.

INTRINSIC WAVELENGTH EFFECTS

As delineated above, photochemical ignition involves the photodissociative creation of oxygen atoms by ultraviolet radiant absorption below 2450 Å. This has been verified by the use of ultraviolet window materials which cut off at various wavelengths within the 1000 Å to 2000 Å region. And by the analysis of required photochemical ignition energy (or peak oxygen atom concentration generated), as described in the previous section. Since photo-absorption by molecular oxygen followed by photodissociation to atomic oxygen is the vital process of the photochemical combustion technique, a more detailed and extensive study of this process is warranted.

Re-examination of the assumptions on which the previous analysis is based leads to a more rigorous consideration of the wavelength dependence of parameters such as window transmission, species absorption coefficient and radiant intensity. Appendix V follows this direction and the end result is substantial correction, which indicates that a considerably more gradual decrease in oxygen atom concentration with distance from the radiant source window occurs than previously calculated (Figure 5). This increased radiant penetration results from detailed consideration of radiant absorption at higher wavelengths (above 1800 Å) which were essentially neglected in the past analysis. As a result, it is possible to identify various wavelength absorption regions of importance at different distances into the mixture.

For reactant mixture regions near or at the window, where the photochemical ignition kernel is created, the previous analysis (and thus the previously calculated photochemical ignition energy requirements) can be used with negligible error. However, consideration of in-depth photochemical effects necessitates using the more detailed analysis presented in Appendix V. The design of an ultraviolet radiant system that could effect photochemical ignition after penetration of a fuel-free boundary air layer between the radiant source window and the reactant mixture, would be an example where such considerations are necessary (see Appendix V for details).

Appendix VI couples the radiant penetration analysis with complementary phase plane data. The result indicates that the photochemical combustion technique creates sufficient oxygen atom concentrations at in-depth regions of a reactant mixture to result in a combustion enhancement effect which reduces the temperature increase required for ignition below that normally required. As illustrated in the appendix, the temperature reduction can be considerable and is brought about by the creation of oxygen atom concentrations in excess of about 10^3 to 10^6atoms/cm^3. As before, different wavelength regions are identified as being effective in combustion enhancement at various distances into the mixture. Consequently, an ultraviolet ignition system design could be optimized to the achievement of a specific goal.

Since the enhancement mechanism is inherent in the photochemical ignition technique when a broad-band radiant source is employed, it probably represents the mechanism whereby stronger ignition kernels and propagating reaction fronts are created in comparison with the usual ignition techniques.

The feasibility of using laser radiant sources in photochemical ignition systems is an aspect of intrinsic wavelength effects which is considered in Appendix VII. Following development of a general laser photochemical ignition equation, which accounts for bleaching of the absorbing species, the optimum laser wavelengths for photochemical ignition are established (Figure 1). However, outside of a few fundamental laboratories, laser sources are not available in this region of the spectrum (vacuum ultraviolet). If such lasers did exist, it is doubtful if they could compete with plasma arc sources for practical application on the basis of complexity, reliability, size, weight and cost considerations. Further, in comparison with plasma arc sources, laser sources would be inappropriate in practical systems since they cannot produce in-depth enhancement of combustion, as well as ignition. This is a consequence of the inherent monochromatic nature of the laser which precludes its simultaneous use in both the ignition and enhancement wavelength regions.

Finally, an intrinsic factor in the photochemical ignition process, which has not been previously assessed, is the presence of electronically excited oxygen atoms. These atoms are a direct result of ultraviolet radiant absorption below 1760 Å and pre-empt the use of normal ground state chemical kinetics. Appendix VIII provides a detailed consideration of excited state kinetics and the effect of excited species on the photochemical ignition process.

Although the reported literature regarding excited state species kinetics is limited and often conflicting, the results indicate that the presence of electronically excited state species cannot be neglected in photochemical kinetic calculation. The two species which have been identified as being important [excited atomic oxygen $O(^1D)$ and excited molecular oxygen $O_2(^1\Sigma_g^+)$] are metastable since radiative decay to the ground state is spin forbidden. Consequently, the excitation energy can only be lost via collisional transfer with another species in the reactant system. For this reason, a comprehensive review of this type of interaction is provided in Appendix VIII for species of interest in combustion systems.

Detailed calculations of the chemical kinetics for hydrogen-oxygen-nitrogen mixtures, including excited state kinetics, are also illustrated in Appendix VIII. The results demonstrate that species excitation cannot be neglected without appreciably affecting the calculation of intermediary species concentration and therefore required photochemical ignition energy. Further, inclusion of excited state kinetics results in alteration of the ignition kernel characteristics due to the formation of greater concentrations of OH and H species than possible when only ground state kinetics are assumed. The results also indicate that the use of leaner fuel-air mixtures does not deplete the concentration of intermediary species in the ignition kernel. Thus the ignition energy required by the photochemical technique will not be affected by the use of fuel lean mixtures.

EXTENSION AND APPLICATION OF PRINCIPLE

The results presented on photochemical combustion initiation and enhancement indicate that a new departure from the usual combustion schemes is provided by the photochemical technique. Combustion characteristics and energy transfer mechanisms (ultraviolet light beam) which are unique to the photochemical technique are realized. Application to fundamental combustion research as well as practical energy conversion devices should be extensively pursued. For example, in addition to combustion initiation and enhancement, the photochemical technique may find application in combustion instability investigation or control as suggested by the discussion in Appendix IX.

The cornerstone of application of the photochemical combustion principle is the availability of practical vacuum ultraviolet radiant sources. Various types of singly pulsed

ultraviolet sources have already been developed by Photochem Industries, Inc. for application in photochemical combustion research (see Appendix I, Ref. 3). Recent advances have resulted in the development of a singly pulsed ultraviolet source suitable for application to practical devices, due mainly to a reduction of the stored energy requirement to only about 150 millijoules (the first ultraviolet sources used required stored energies on the order of 7 kilojoules). Size, weight and cost of this source is competitive with typical aircraft spark igniters. As a consequence of the reduced size and energy requirement of the ultraviolet source, the established photochemical ignition and combustion enhancement principles can now be applied to some practical hardware needs.

Two programs which are related to eventual practical application of the photochemical ignition technique are currently in progress. The first involves an exploratory investigation of photochemical ignition for turbine engine combustors and is monitored by the Air Force Aero Propulsion Laboratory. Testing has commenced using a General Electric F101 sector test rig assembly. The second program involves high speed combustion studies to be carried out at the Johns Hopkins University supersonic combustion facilities under Navy sponsorship.

Further improvement in ultraviolet radiant source design is expected to result in additional reductions in required stored energy per pulse for photochemical ignition. Advances in source pulse life to 10^8 pulses are also expected. This would effectively widen the range of application of the photochemical combustion technique. For example, photochemical flame holding could eventually be achieved. Thus instead of requiring a physical protrusion into the reactant flow stream to hold the flame, a simple beam of light could be used. The eventual development of a steady state light source would further widen the areas for practical application.

SUMMARY/CRITIQUE

Combustion initiation and enhancement of practical, unsensitized fuel-air mixtures by irradiation with a beam of light in the vacuum ultraviolet has been demonstrated. The photochemical combustion initiation mechanism involves photodissociation of oxygen molecules via absorption of about 10 μJ of radiant energy below 1800 Å, which results in the creation of a peak oxygen atom concentration on the order of

10^{14} atoms/cm^3. Subsequent interaction of the highly reactive oxygen atoms with fuel species results in ignition and sustained combustion. Photochemical combustion enhancement involves a reduction of ignition temperature via radiant absorption below 2450 Å and requires oxygen atom concentrations on the order of 10^3 to 10^6 atoms/cm^3. The photochemical technique results in combustion characteristics which are completely different than those normally encountered.

Exploration of the photochemical combustion principle unveils new and unique considerations in combustion applications. The advanced concepts developed have a potentially wide application in practical propulsion and energy conversion devices and provide a new departure from the usual combustion schemes in the design of such devices.

A compendium of all photochemical combustion reports, papers and presentations is given in Appendix X.

REFERENCES

1. Cerkanowicz, A. E., Levy, M. E., and McAlevy III, R. F., "Photochemical Ignition of Gaseous Fuel-Oxidizer Mixtures at Subatmospheric Pressures," Final AFOSR Scientific Report No. 70-1664, April 1970.

2. Cerkanowicz, A. E., "Photochemical Initiation of Sustained Combustion in Unsensitized Gaseous Fuel-Oxygen Mixtures," Ph.D. Dissertation, Stevens Institute of Technology, June 1970.

3. Cerkanowicz, A. E., "Photochemical Enhancement of Combustion and Mixing in Supersonic Flows," Interim Scientific Report No. AFOSR-TR-73-0563.

4. Lewis, B., and von Elbe, G., Combustion Flames and Explosions of Gases, Academic Press, Inc., 1961.

APPENDIX I

COMPUTER PROGRAM - ATOMIC OXYGEN CONCENTRATION

A. INTRODUCTION

Prior analysis of photochemical ignition provided a general expression, in closed form, for the oxygen atom concentration as a function of the following explicit variables[1,2]: (1) time - measured from the onset of the radiant pulse, (2) distance - measured from the window, (3) initial reactant pressure, (4) initial reactant temperature, (5) initial species type, (6) initial species composition or mole fraction, (7) window transmission, (8) radiant pulse length and (9) radiant intensity. The following implicit parameters are included as well: (1) reaction rate constant for three body ozone formation, (2) reaction rate constant for two body reactions between fuel and atomic oxygen species, (3) absorption cross section of molecular oxygen, (4) diffusion coefficient of atomic oxygen and (5) surface recombination effectiveness of atomic oxygen.

The general expression relating the atomic oxygen concentration to the factors listed above, is very lengthy and arduous to use for numerical calculation. Consequently, a simple Fortran computer program using the results of the cited analysis has been written to facilitate its use.

B. COMPUTER PROGRAM

The resulting computer program is given in Table 1. Lines 112 thru 118 represent data within the program on the following factors (the numerical value used in the illustrated program is given by the number in parenthesis):

- XØ2, mole fraction molecular oxygen (0.3333)
- XH2, mole fraction hydrogen (0.6667)
- XCH4, mole fraction methane (0.0)
- K1, reaction rate constant for $O+O_2+M \rightarrow O_3+M$ (1.61 x 10^{-34} cm^6/particle^{2}sec)
- K2, reaction rate constant for $O+H_2 \rightarrow OH+H$ (6.40 x 10^{-17} cm^3/particle sec)
- K3, reaction rate constant for $O+CH_4 \rightarrow CH_3+OH$ (1.69 x 10^{-17} cm^3/particle sec)

Table 1

Fortran Computer Program for Photochemical Ignition Computations--Calculation of Atomic Oxygen Concentrations Generated

```
100 REAL K0,K1,K2,K3,K4,N0I,N0F,N02,NM,N02,NH2,NCH4
110 DIMENSION X(100),N0I(100),N0F(100),N02(100)
112 DATA X02,XH2,XCH4/0.3333,0.6667,0.0/
114 DATA K1,K2,K3/1.61E-34,6.40E-17,1.69E-17/
116 DATA GAMA,D0,TAU/0.0,0.28,0.0001/
118 DATA SIGMA,S11/9.3E-18,187.0/
120 1 CONTINUE
130 PRINT,"P,T,T0,XMIN,XINC,N"
140 PRINT 876
150 876 FORMAT(//)
160 INPUT,P,T,T0,XMIN,XINC,N
165 PRINT,P,T,T0,TAU,X02,XH2,XCH4,D0,K1,K2,K3,GAMA
170 10 CONTINUE
180 IF(N.LE.100)GO TO 11
190 PRINT,"N TOO LARGE"
200 STOP
205 11 P0=P/(X02+XH2+XCH4)
210 D0M=D0*(760./P0)*((1/293.)**1.8)
211
220 NM=2.686E+19*(P0/760.)*(293./T)
230 N02=NM*X02
240 NH2=NM*XH2
250 NCH4=NM*XCH4
```

Table 1 (Continued)

```
260 A=0.5/SQRT(D0M*TAU)
270C  SET THE VALUE OF X
280 XSUM=XMIN
290 DO 111 IX=1,N
300 X(IX)=XSUM
310 X0=A*X(IX)
320 K0=TAU*((K1*N02)*NM+K2*NH2+K3*NCH4)
330 S0=(SIGMA*N02)/(2.0*A)
332 IF(K0.NE.S0**2) GO TO 22
334 PRINT,"K0 EQUAL TO S0 SQUARED"
336 STOP
338 22 CONTINUE
340 K4=GAMA*SQRT(1.2966E+07*TAU*T/D0M)
350 C0=K0-S0*S0
360 C1=X0/SQRT(T0)
370 C2=S0*SQRT(T0)
380 C3=SQRT(K0*T0)
390 C4=0.5*K4*SQRT(T0)
400 B=K4+2.0*S0
410 C5=B/(K4-2.0*S0)
420 C6=B/(K4-2.0*SQRT(K0))
430 C7=B/(K4+2.0*SQRT(K0))
440 C8=(4.0*K4)/((K4-2.0*S0)*(K4*K4-4.0*K0))
450 H0=0.5*S11*TAU*N02/C0
```

Table 1 (Continued)

```
460 H1=EXP((-C0)*T0)
470 H2=EXP((0.25*K4*K4-K0)*T0)
480 F1=EXP((-2.0)*S0*X0)
490 F2=F1*H1*ERFC(C2-C1)
500 F3=H1*EXP(2.0*S0*X0)*ERFC(C1+C2)
510 F4=EXP(2.0*SQRT(K0)*X0)*ERFC(C1+C3)
520 F5=EXP((-2.0)*SQRT(K0)*X0)*ERFC(C1-C3)
530 F6=H2*EXP(K4*X0)*ERFC(C1+C4)
540 F7=0.5*(2.0*F1-F2+C5*F3-C6*F4-C7*F5+2.0*(C8*C0*F6)
550 N0I(IX)=H0*(2.0*F1-F2+F3-F4-F5)
560 N0F(IX)=2.0*H0*F7
570 N0Z(IX)=H0*(2.0*F1-F2-F3-(S0/SQRT(K0))*(F5-F4))
580 XSUM=XSUM+XINC
590 111 CONTINUE
640 PRINT 908
650 DO 6 IX=1,N
660 PRINT 900,X(IX),N0I(IX),N0F(IX),N0Z(IX)
670 6 CONTINUE
680 PRINT 876
690 PRINT 876
700 900 FORMAT(F8.4,3E16.8)
710 908 FORMAT(5X,1HX,10X,3HN0I,12X,3HN0F,13X,3HN0Z)
750 PRINT,"TO CONTINUE TYPE 1, OTHERWISE 0."
760 INPUT,I02
```

Table 1 (Continued)

```
770 IF(IQ2.EQ.0)GO TO 999
780 PRINT,"IF YOU WISH TO CHANGE ONLY XMIN,XINC AND N TYPE 1;OTHERWISE 0
790 INPUT,IQ2
800 IF(IQ2.EQ.0)GO TO 1
810 PRINT,"SPECIFY XMIN,XINC AND N"
820 INPUT,XMIN,XINC,N
830 GO TO 10
840 999 STOP
850 END
860 FUNCTION ERFC(XXX)
870 Q=SIGN(1.,XXX)
880 XXX=ABS(XXX)
890 A1=0.0705230784
900 A2=0.0422820123
910 A3=0.0092705272
920 A4=0.0001520143
930 A5=0.0002765672
940 A6=0.0000430638
950 ERF=1.0-(1.0/(1.0+A1*XXX+A2*XXX**2+A3*XXX**3+A4*XXX**4+A5
960 &  *XXX**5+A6*XXX**6)**16)
970 ERF=Q*ERF
980 ERFC=1-ERF
990 RETURN
1000 END
```

- GAMMA, surface recombination effectiveness for $2O \rightarrow O_2$ (10^{-3})
- DØ, atomic oxygen diffusion coefficient (0.28 cm^2/sec)
- TAU, radiant pulse width (10^{-4}sec)
- SIGMA, average molecular oxygen absorption cross-section in the wavelength region of interest ($9.3 \times 10^{-18} cm^2$/molecule)
- S11, variable given by $2\overline{T\sigma_{O_2}} I_O^*/D'$ ($187\ sec^{-1}$)

  where $\overline{T\sigma_{O_2}}$ is the integral over the wavelength region of interest of the product of window transmission and molecular oxygen absorption cross section ($24.22 \times 10^{-14} cm^2 Å$/molecule - this corresponds to the use of a lithium fluoride window, see p. 107 ref. 2)

  I_O^* is the ultraviolet radiant flux incident on the window in the wavelength region of interest (3.16×10^{-4} joules/cm^2 sec Å - this corresponds to an averaged energy discharge of 1 micro-joule per 100 Å thru a 1/4 inch diameter opening in 10^{-4}sec)

  D' is the representative dissociation energy for molecular oxygen (5.11 ev)

Line 160 represents input data selected in operating the program and is defined as follows:

- P, initial pressure of reactant mixture
- T, initial temperature of reactant mixture
- TØ, nondimensional time - real time/radiant pulse time
- XMIN, distance from window at which calculation will start
- XINC, increment in distance at which successive calculations will be performed
- N, total number of distances for which calculations will be performed

Line 660 represents the output information which consists of atomic oxygen concentrations (NØ) as a function of distance from the window (x) for surface (window) recombination rates which are infinite (NØI), finite (NØF) and zero (NØZ).

C. RESULTS

A typical set of results is given in Figure 1, where the oxygen atom density for infinite surface recombination rates (NØI) is plotted as a function of distance from the window (x) for a stoichiometric hydrogen-oxygen mixture at various initial reactant mixture pressures. The effect of reactant mixture pressure on the location and magnitude of the maximum oxygen atom concentration and on the oxygen atom density profiles is clearly apparent. At low pressure, weak absorption occurs while diffusion is fast; therefore, the density profile is relatively flat and the recombination effect at the window is sensed by the mixture relatively far from the window (greater than 0.07 cm). As the pressure is increased the effect of diffusion and hence window recombination decreases, while radiation absorption increases. This results in the production of higher oxygen atom concentrations at some point in the mixture. Finally, as the pressure is increased further, gas-phase reactions begin to dominate resulting in decreased oxygen atom densities. As a consequence, there exists an optimum pressure for which the atomic oxygen concentration reaches a maximum value.

Since photochemical ignition is related to the oxygen atom concentration[1,2], the results of the computer program can be utilized to characterize the effect of the photochemical ignition technique at various conditions of interest.

D. REFERENCES

1. Cerkanowicz, A. E., Levy, M. E., and McAlevy III, R. F., "Photochemical Ignition of Gaseous Fuel-Oxidizer Mixtures at Subatmospheric Pressures," Final AFOSR Scientific Report No. 70-1664, April 1970.

2. Cerkanowicz, A. E., "Photochemical Initiation of Sustained Combustion in Unsensitized Gaseous Fuel-Oxygen Mixtures," Ph.D. Dissertation, Stevens Institute of Technology, June 1970.

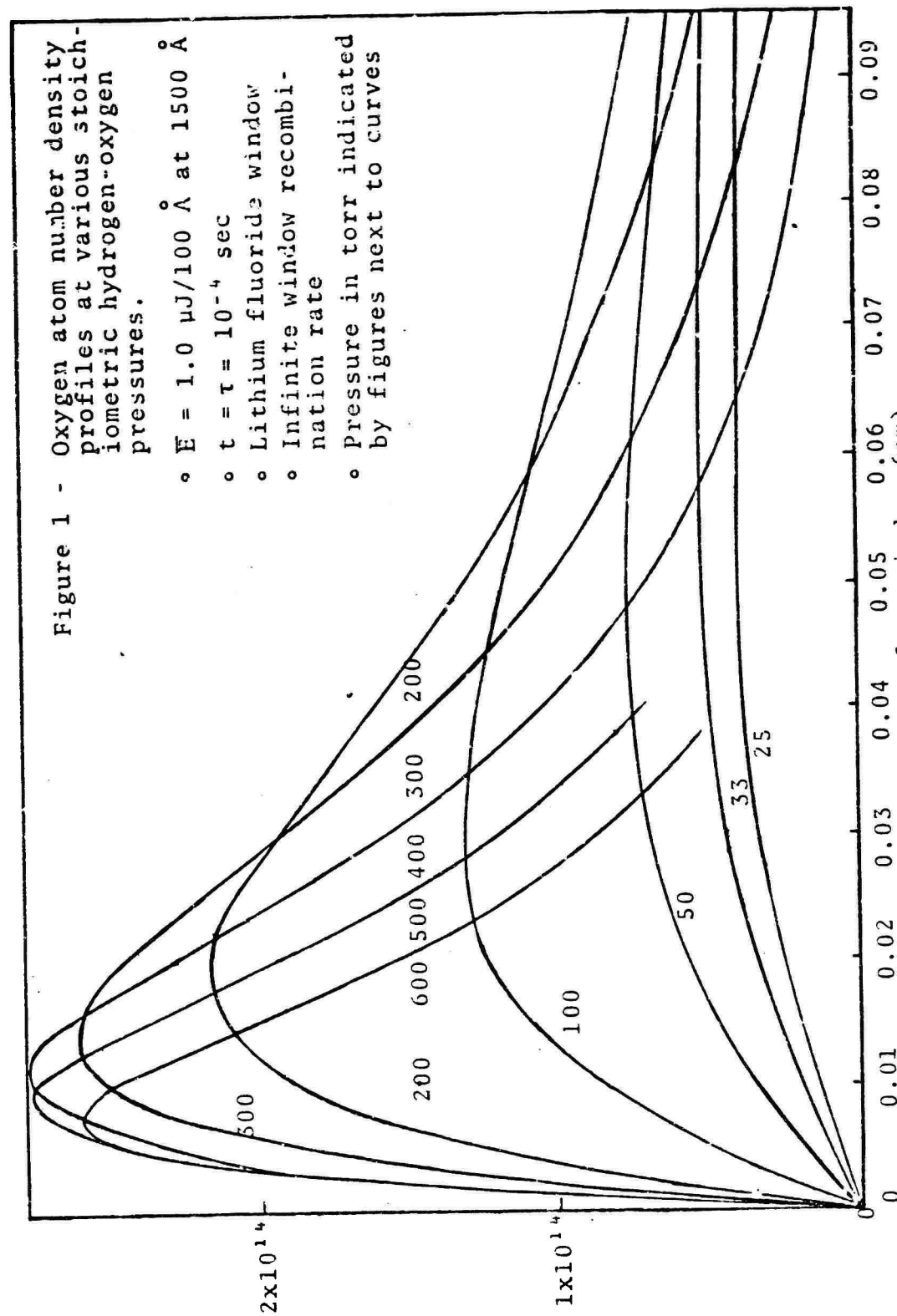

Figure 1 - Oxygen atom number density profiles at various stoichiometric hydrogen-oxygen pressures.

- E = 1.0 μJ/100 Å at 1500 Å
- t = τ = 10^{-4} sec
- Lithium fluoride window
- Infinite window recombination rate
- Pressure in torr indicated by figures next to curves

APPENDIX II

FLOWING REACTANT MIXTURES

A. INTRODUCTION

Analysis of the requirements for photochemical ignition of flowing combustible mixtures will require coupling boundary layer theory with the established criterion for photochemical ignition. Detailed description of the mixture velocity in the boundary layer is necessary since the radiant absorption responsible for ignition occurs very close to the window for the mixtures of interest[1,2], presumably within the boundary layer. Figure 1 presents the situation being considered, along with a definition of some of the appropriate parameters.

Coupling between the reactant mixture velocity and the photochemical ignition mechanism is provided by determining the period of time over which an element of gas is exposed to the radiant flux (exposure time). Some elements of the reactant mixture will be able to integrate the radiant input (via absorption) for this time period which effectively becomes a pseudo pulse time.

B. EXPOSURE TIME

A radiant absorbing gas flowing past a window of characteristic dimension (d^*) at a velocity (U^*) when subjected to a radiant pulse of duration (τ) will absorb energy over a distance ($d^* + \tau U^*$). The exposure time (t_e) to the radiant flux of a given element of gas in front of the window varies with the position (x) of that element within the total length irradiated. The dependence of exposure time with position is given by the following set of equations, the results of which are depicted in Figure 2.

For pulse time $\tau < d^*/U^*$ or equivalently for velocities $U^* < d^*/\tau$ the following equations apply:

$$t_e = x/U^* \qquad 0 < x < \tau U^* \qquad (1\text{-a})$$

$$t_e = \tau \qquad \tau U^* < x < d^* \qquad (1\text{-b})$$

$$t_e = \tau - (x-d^*)/U^* \qquad d^* < x < d^* + \tau U^* \qquad (1\text{-c})$$

For pulse time $\tau < d^*/U^*$ or equivalently for velocities $U^* > d^*/\tau$ the following equations apply:

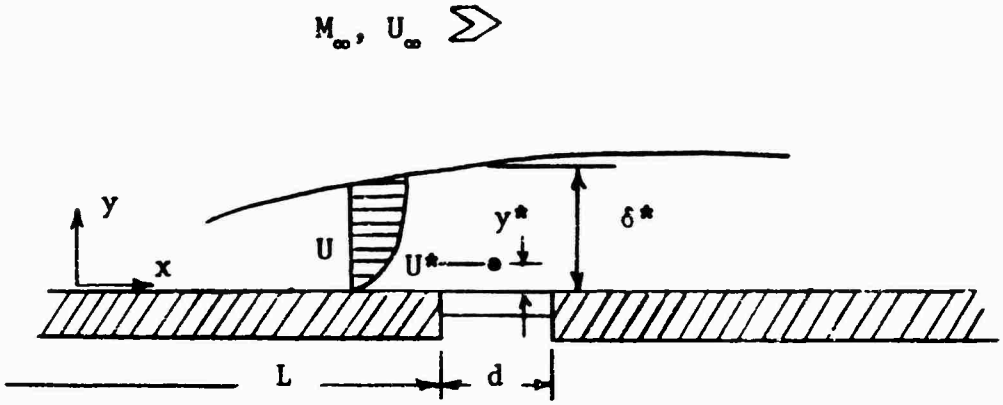

x distance measured along wall

y distance measured normal to wall

L distance from window to leading edge of boundary layer

d window diameter

δ^* boundary layer thickness at window

y^* characteristic radiant absorption depth for ignition, not a function of flow velocity[1,2]

U^* boundary layer velocity at y^*

U boundary layer velocity

U_∞ free stream velocity

M_∞ free stream Mach Number

Figure 1 - Schematic of the Reactant Mixture Boundary Layer Flow Near the Radiant Source Window

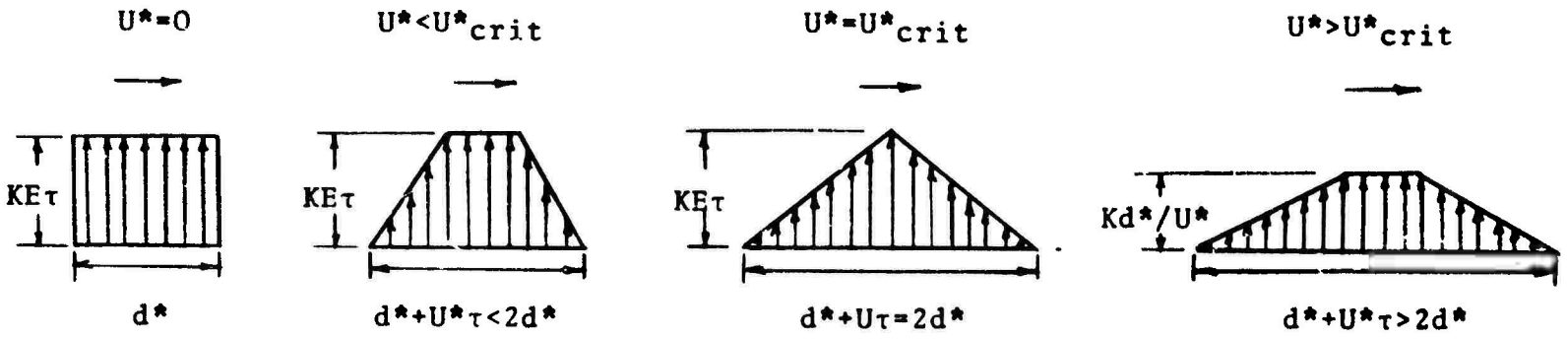

Figure 2 - Effect of Mixture Flow Past the Radiant Source Window on Oxygen Atom Distribution for Pulsed Irradiation

$$t_e = x/U^* \qquad 0 < x < d^* \qquad (2\text{-a})$$

$$t_e = d^*/U^* \qquad d^* < x < \tau U^* \qquad (2\text{-b})$$

$$t_e = \tau - (x-d^*)/U^* \qquad \tau U^* < x < d^* + \tau U^* \qquad (2\text{-c})$$

Where the juncture between the two sets of equations is given by

$$\tau = d^*/U^*_{crit} \text{ or } U^*_{crit} = d^*/\tau \qquad (3)$$

For the photochemical ignition of flowing reactant mixture experiments, the window diameter used was 0.25 inch and the pulse time was 50×10^{-6} sec which implies (according to equation 3) a critical velocity of 417 ft/sec. For reactant mixture flow rates corresponding to conditions below the critical Mach number, the maximum exposure time of any element to the radiant flux is given by equation 1-b. For reactant mixture flow rates corresponding to conditions above the critical Mach number, the maximum exposure time of any element to the radiant flux is given by equation 2-b.

The effect of reactant mixture velocity on the distribution of oxygen atom concentration is illustrated in Figure 2. As the flow rate is increased, the distribution becomes "smeared," and the result is a decrease in peak oxygen atom concentration for flows above the critical velocity.

C. PHOTOCHEMICAL IGNITION ENERGY

As shown in the previous work on photochemical ignition of static mixtures[1,2] for a square wave radiant pulse, neglecting diffusion, kinetics and wall recombination, the maximum oxygen atom concentration is achieved at the end of the time available for absorption. This is also true with small error for the case where kinetics and diffusion are included. Thus, in a static system the time available for absorption is the pulse time. In a flow system, the time available for absorption is directly proportional to the exposure time, t_e. Consequently, the maximum oxygen atom concentration, $n_{O_{max}}$, for pulsed UV irradiation of flowing mixtures is given by the following equation

$$n_{O_{max}} = KEt_e \qquad (4)$$

where E is the stored pulse energy and K is the constant of proportionality for the rate of conversion of the stored energy into oxygen atoms via photodissociation by the

generated UV pulse. Assuming that ignition occurs when a critical concentration of oxygen atoms, $n_{O\text{-}crit}$, is achieved[1,2], the stored energy requirement according to equation 4 becomes

$$E = n_{O\text{-}crit}/Kt_e \tag{5}$$

(a) $M < M_{crit}$

In this region the maximum exposure time of any element of the mixture is given by equation 1-b which upon substitution into equation 5 gives

$$E = n_{O\text{-}crit}/K\tau = \text{constant} = E_O \tag{6}$$

where E_O is the required stored energy for photochemical ignition of a static mixture. Thus the required energy for ignition is independent of the free stream number and is equal to that required for ignition of a static system. The value of E_O was experimentally determined to be 340 joules for hydrogen-air and 180 joules for hydrogen-oxygen mixtures.

(b) $M > M_{crit}$

In this region the maximum exposure time of any element of the mixture is given by equation 2-b which upon substitution into equation 5 gives

$$E = n_{O\text{-}crit}\ U^*/Kd^* \tag{7}$$

Combining this with equation 6 then gives

$$E = E_O U^*\tau/d^* = E_O U^*/U^*_{crit} \tag{8}$$

Since U^*_{crit} is fixed by the characteristic window dimension and the radiant pulse duration, equation 3, this result indicates that the required energy for photochemical ignition varies linearly with the mixture boundary layer velocity at the ignition site.

The expression for the required photochemical ignition energy given by equation 8 is independent of the type of flow

(laminar, turbulent or slug), since it is given in terms of boundary layer velocities. In order to convert to free stream velocities or Mach numbers, the appropriate boundary layer equations must be used. For example, using the typical 1/7 power law[3], the turbulent boundary layer velocity at a distance y* above the window can be related to the free stream Mach number, M_∞, by the following set of equations,

$$M_\infty = U_\infty / C_o \tag{9}$$

$$\delta^* = 0.37\ L\ (U_\infty L/\nu)^{-1/5} \tag{10}$$

$$U^*/U_\infty = (y^*/\delta^*)^{1/7} \tag{11}$$

while similar expressions can be written for laminar and slug flows. It should also be noted that compressibility (Mach Number), Prandtl Number and pressure gradient effects contribute only minor corrections to the above equations for Mach numbers less than 1.5[3].

(c) General Expression

A general expression for the required stored energy for photochemical ignition of flowing reactant mixtures can be written based on the analysis presented in parts (a) and (b).

$$E = E_o [M_\infty / M_{\infty crit}]^N \tag{12}$$

where $$M_{\infty crit} = \alpha [U^*_{crit}/C] [U^*_{crit} L/\nu]^{-\beta} [y^*/L]^{-\delta} \tag{13}$$

and $$U^*_{crit} \equiv d/\tau \tag{14}$$

The constants in equations 12 and 13 depend on the type of flow and are given in Table 1, below.

Table 1

Flow	α	β	δ	N $M_\infty < M_{crit}$	N $M_\infty > M_{crit}$
laminar	2.14	1/3	2/3	0	3/2
turbulent	0.87	1/36	5/36	0	36/35
slug	1	0	0	0	1

The results indicate that, for reactant mixture flows above the critical Mach number, the required stored energy for photochemical ignition varies as the free stream Mach number is raised to tne power N. For slug flow and as a close approximation for turbulent flow, a value of 1 can be used for this exponent indicating a linear dependence of photochemical ignition energy on the free stream Mach number.

D. COMPARISON WITH EXPERIMENT

Experimental data has been obtained on the stored energy required for photochemical ignition of stoichiometric hydrogen-air and hydrogen-oxygen mixtures at various mixture velocities[5]. And the following parameters are typical for the experimental conditions of interest:

$d^* \sim d = 0.25$ inch

$y^* \sim 0.01$ cm $= 0.0039$ inch (see Ref. 1,2)

$L \sim 15.7$ inches

$P_{test} \sim 14.7$ psia

$T_{test} \sim 80°F$

For stoichiometric hydrogen-air flow

$\mu_1 \sim 0.0358$ lbm/hr ft (calculated according to Ref. 4)

$\rho_1 \sim 0.0532$ lbm/ft^3 (hence $\nu_1 = 0.675$ ft^2/hr)

$C_{o_1} \sim 1328$ ft/sec (sound speed)

For stoichiometric hydrogen-oxygen flow

$\mu_2 \sim 0.0372$ lbm/hr ft (calculated according to Ref. 4)

$\rho_2 \sim 0.03404$ lbm/ft^3 (hence $\nu_2 = 1.22$ ft^2/hr)

$C_{o_2} \sim 1755$ ft/sec (sound speed)

As mentioned before, the critical boundary layer velocity, U^*_{crit}, for the experimental conditions of interest is 417 ft/sec and consequently, ignition energy-mixture velocity dependency will occur for velocity regions above this value. Since the free stream velocity, U_∞ is always higher than the

boundary layer velocity, this region corresponds to Reynolds numbers (based on length L) greater than 10^6 for the mixtures of interest. According to Schlichting[3], this indicates that turbulent boundary layer theory should be used.

Using the appropriate forms of equations 12 to 14 for turbulent flow, the critical Mach number is calculated to be about 0.57 for hydrogen-air mixtures and about 0.44 for hydrogen-oxygen mixtures. The exponential dependency is nearly unity which indicates that the required energy for photochemical ignition is essentially linearly dependent on the free stream Mach number for Mach number values above the critical value. Substitution of the appropriate values for the required static ignition energy, E_o, allows evaluation of the slope of this dependence, which is calculated to be about 620 joules/Mach No. for hydrogen-air mixtures and 425 joules/Mach No. for hydrogen-oxygen mixtures.

A comparison between the above analytical results and experimental results on the stored photochemical ignition energy requirement as a function of free stream Mach number for hydrogen-air and hydrogen-oxygen mixtures is presented in Figure 3. Experimental results are indicated by data points while the solid lines drawn through the data points represent the requirements of the theory. As can be seen, good agreement between theory and experiment is obtained, especially considering the simplicity of the analysis.

E. DISCUSSION

The satisfactory agreement between experiment and theory indicates that coupling the previously reported analytical work on photochemical ignition of stationary reactant mixtures with the appropriate boundary layer equations provides a suitable approach to determining the photochemical ignition requirement of flowing reactant mixtures. Thus, results from the static experiments can be extended to a flow system when the appropriate corrections are applied to account for the "smearing out" of radiant absorption due to flow past the window.

Two important points are also obvious as a result of the analysis. First, the appropriate position (based on energy required) of a photochemical igniter within a combustion chamber is in a region where the mixture flow is still laminar. This results in lower boundary layer velocities than would occur in turbulent flows for the same free stream Mach number.

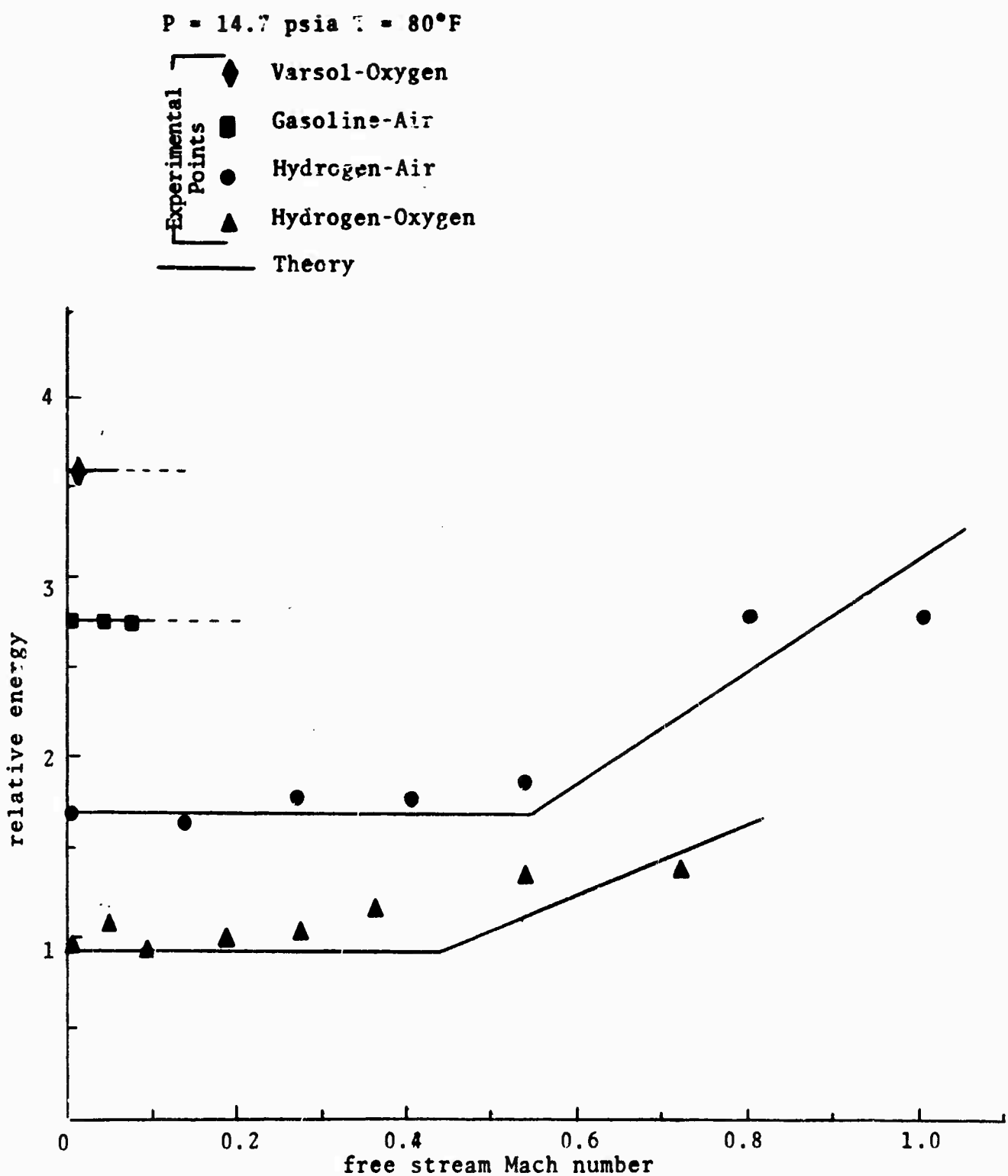

Figure 3 - Relative Photochemical Threshold Initiation Energy as a Function of Velocity for Various Mixtures

Consequently, the critical Mach number will increase and the increase in energy required can be delayed to higher flow rates. Second, a similar effect can be realized by either increasing the window diameter or by decreasing the pulse time of the radiant source.

It should be noted that the details of the analysis presented above are restricted to regions close to the window, within the boundary layer. A mechanism does exist, however, whereby the ignition site can be moved outside a fuel-free boundary layer, details of which are given in a separate appendix.

Finally, the experimental results (indicated in Figure 3) using liquid fuels were limited to low mixture flow rates and consequently never reached critical flow values. However, the results demonstrate the applicability of the photochemical ignition principle to a wide variety of fuels, including atomized liquid fuels typical of those used in practical engines.

F. SUMMARY

- An analysis is developed which successfully describes the required stored energy for photochemical ignition of flowing reactant mixtures.
- The analysis indicates the existence of a critical flow Mach number, below which the required energy is independent of mixture velocity and above which the required energy is dependent on mixture velocity.
- Extrapolation of existing photochemical ignition data for static mixtures to flow conditions is possible.
- Criteria for the design and location of a photochemical ignition source for flow systems are indicated by the results of the analysis.

G. REFERENCES

1. Cerkanowicz, A. E., Levy, M. E., and McAlevy III, R. F., "Photochemical Ignition of Gaseous Fuel-Oxidizer Mixtures at Subatmospheric Pressures," Final AFOSR Scientific Report No. 70-1664, April 1970.

2. Cerkanowicz, A. E., "Photochemical Initiation of Sustained Combustion in Unsensitized Gaseous Fuel-Oxygen Mixtures," Ph.D. Dissertation, Stevens Institute of Technology, June 1970.

3. Schlichting, H., Boundary Layer Theory, McGraw Hill, 1960.

4. Hirschfelder, J. O., Curtiss, C. F., and Bird, R. B., Molecular Theory of Gases and Liquids, John Wiley and Sons, 1954.

5. Cerkanowicz, A. E., "Photochemical Enhancement of Combustion and Mixing in Supersonic Flows," Interim Scientific Report, March 1972.

APPENDIX III

REPETITIVE PULSE IGNITION

A. INTRODUCTION

A series of experiments using a repetitively pulsed photochemical source in conjunction with the blow-down tunnel system were planned in order to provide a quasi-steady photochemical ignition capability (see illustration of Figure 1). The quasi-steady state condition established would then allow reasonable diagnostic measurements on the photochemical effects to be performed at the ignition site and downstream of the ignition site. An advanced ultraviolet source (type PC-4) was to be used in conjunction with a nominal 1 kw pulsed power supply which had an adjustable pulse rate between 10 and 100 pulses per second.

A description of the blow-down tunnel and ultraviolet radiation source was reported previously[1]. The power supply was fabricated since the last report and a description is provided below.

B. PULSED POWER SUPPLY

The power supply is a digital logic controlled, high frequency converter design which provides a pulsed output up to one kilowatt. It is designed to provide an approximate 10 joule discharge into an ionized gap at various repetition rates. The pulse rate is switch selectable from 10 to 100 discharges/second.

The power supply design consists of five major blocks and associated sub-blocks, as illustrated in Figure 2. These blocks are listed below and will be discussed in that order.

- AC to DC Power Converter
- Low Voltage Power Supply
- Control Logic Circuitry
  - Oscillator
  - Digital Counter
  - Control Logic
- DC to DC Power Converter
  - Driver
  - Power
- Discharge Circuit
  - Trigger Circuit
  - Power Discharge

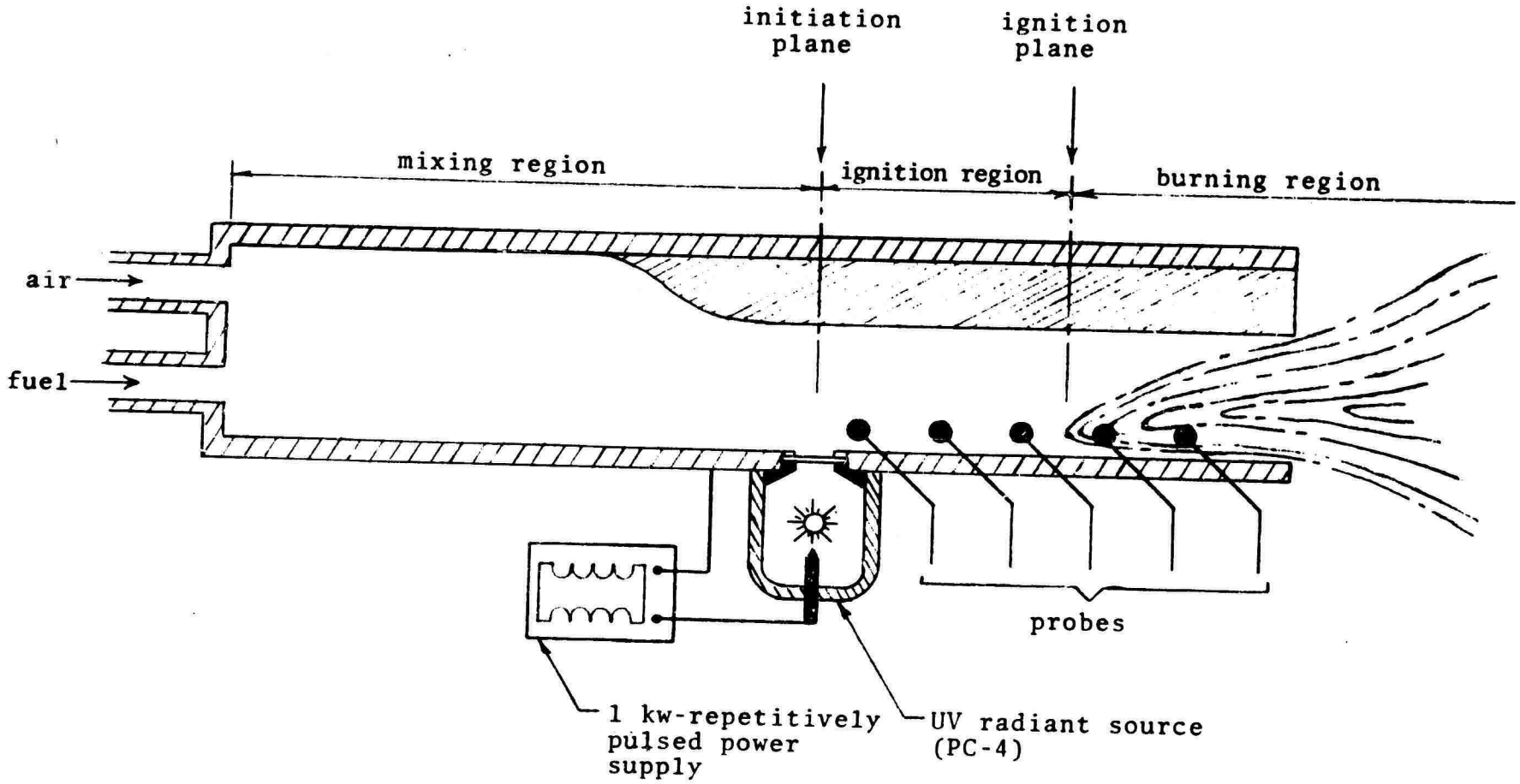

Figure 1 - Schematic of Blowdown Combustion Tunnel Showing the Formation of a Stationary Reaction Region

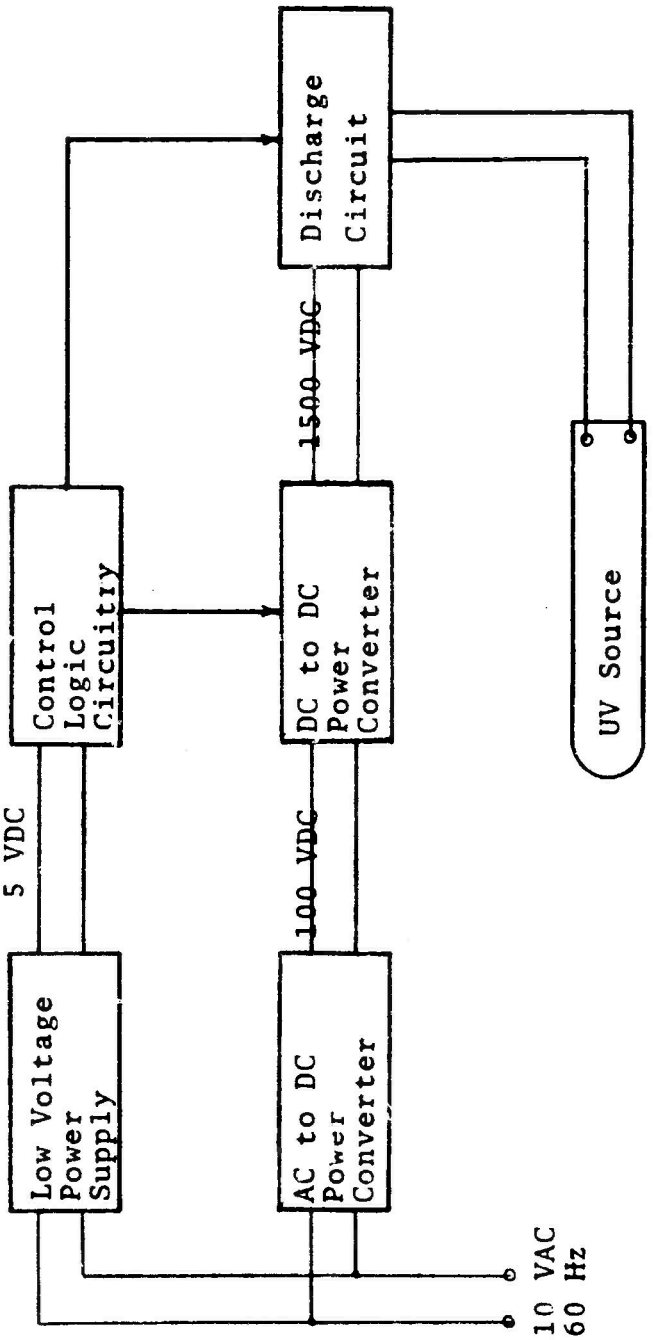

Figure 2 - Block Diagram of 1 kw Pulsed Power Supply

The AC to DC Power Converter accepts a standard 110 VAC 60 Hz line directly; there is no line isolation at this point. The 110 volt line is full-wave rectified and the output is passed through a single stage L-C filter which provides an output of approximately 100 VDC under full load conditions. It should be noted that under low repetition rates the DC output may rise to 140 volts as this is an unregulated supply.

The Low Voltage Supply provides the necessary DC voltage (5 volts) to operate the digital control circuitry and the DC to DC converter drivers. This supply design is a standard step-down transformer with center-tapped, full-wave rectification and an L-C filter network at the output of the rectifiers. There are, in effect, two outputs from this supply. The first is taken directly from the L-C filter and is used in the converter driver circuitry. No regulation is provided in this portion of the supply. A second output (5 VDC) is Zener diode regulated and is used to power the oscillator and digital logic circuitry.

A Control Logic Circuitry oversees the entire operation of the power supply. It provides the timed driving signals for the DC to DC converter, the disabling of the converter during discharge periods, the switch selected time between discharges, the discharge circuit control signals and an external sync output at time of discharge.

The control circuitry is initiated by an oscillator which is a standard two-transistor multivibrator operating at 2000 Hz. Provisions are made for an external clock if more precise timing is required or if a slight variation in operating frequency is desired. The 2 kHz signal is digitally divided, providing a 1 kHz signal which drives both a two-stage digital counter and the buffer drivers for the DC to DC converters.

The two-stage counter is used to fix the time between discharges. Content of the counter is fed to two switches located on the unit front panel which are set to the desired time between discharges. As the counter is accepting one pulse every millisecond, the exact time between discharges may be controlled with the unit firing when the selected count is reached. After firing the counter is reset to zero to start the next cycle.

The same 1 kHz signal used for the timing counter is used to drive the DC to DC converter. This digital logic signal is used to drive a pair of IC gate circuits which drive a transistorized transformer circuit which, in turn, drives the final power transistors of the converter thereby providing

the isolation of the logic and low voltage circuitry from the AC line. The entire converter drive circuitry is logically disabled during the discharge period. Disabling of the DC to DC converter during the discharge cycle is of importance as operation of the power converter during this time would introduce new and undetermined amounts of power into the arc discharge.

In addition, the Control Logic, through timed gating logic circuits, provides a properly timed fire command pulse to the Discharge Circuit. Fire command may be disarmed by the action of a front panel switch. When this switch is not in the "enable" position, the firing cycle is halted; however, the power converter continues to operate.

The DC to DC Converter is an externally driven type, operating at a frequency determined by the control circuitry, typically 1 kHz. As previously mentioned, the converter drive is obtained through an isolating driver transformer which is operated in the low voltage section of the circuitry providing only base drive to power converter transistors.

The power circuitry of the converter is a bridge inverter configuration with full-wave bridge rectifier output on the secondary winding of the converter transformer. It is this converter transformer that provides the isolation of the discharge circuitry from the AC power line. Selection of the bridge inverter design was based on its independence of operating frequency to load and decreased electrical stress on the power transistors used. The power converter provides a rectified 1500 volt square wave to the discharge circuit.

The Discharge Circuit accepts the 1500 VDC output of the power converter, energy being stored in a single 10 μfd capacitor. At the proper time, as determined by the control logic, a signal is sent to the trigger circuit which consists of a SCR firing circuit operating at 100 VDC in a capacitor discharge mode. It is used to generate the high voltage pulse (700 volts) needed to fire the Krytron in the power discharge circuit.

The power discharge circuit is also a capacitor discharge transformer circuit, operating at the full 1500 VDC of the supply. The 1500 VDC is stepped up to approximately 20,000 volts in the discharge transformer in order to provide for ionization of the arc gap. After ionization has occurred, the entire energy stored in the 10 μfd discharge capacitor dumps into the gap. It should be noted that all the current flowing during this discharge goes through the secondary of a specially wound discharge transformer.

C. EXPERIMENTAL RESULTS

The ultraviolet source-power supply system proved capable of initiating photochemical combustion when used in the flow system. Hydrogen-oxygen and hydrogen-air mixtures were used. However, operation of the system was severely limited due to unsatisfactory source pulse-lifetime. For the particular sources available, an inherent source lifetime only on the order of 50 to 100 pulses was obtained, due to internal fouling when operated in the pulsed mode. Consequently, detailed diagnostic tests could not be performed under the operating life constraint.

The experiments did indicate that ignition is possible when a pulse system is employed. But detailed measurements will have to be deferred until a suitable ultraviolet radiant source becomes available. It should be noted, that based on state-of-the-art technology and operating experience of commercially available radiant sources for application in the visible region of the spectrum, it is expected that a source life greater than 10^8 pulses can eventually be achieved.

D. REFERENCES

1. Cerkanowicz, A. E., "Photochemical Enhancement of Combustion and Mixing in Supersonic Flows," Interim AFOSR Scientific Report, March 1972.

APPENDIX IV

PHOTOCHEMICAL VS SPARK IGNITION

A. INTRODUCTION

An equitable comparison between spark ignition and photochemical ignition is difficult at best (even in an experimental system). The difficulty stems from the extremely complicated nature of the spark.

First, the spark is an in-situ form of ignition, presumably acting on the principle of large sensible heat generation due to ohmic heating. However, in addition to sensible heating, there must be some contribution from the radiant energy generated, the extent of which is not presently assessable. To this must also be added the unknown contribution of the high voltage potential impressed locally on some of the combustion species.

Second, direct control of the energy dump independently from the other discharge parameters (capacitance, breakdown voltage, impressed voltage, etc.) is not possible. Consequently, more energy is used than would be required for threshold ignition.

Finally, the discharge of an in-situ spark disturbs the fluid dynamics in the location of the source. This further alters the ignition and initial local propagation characteristics.

The net effect of the above factors is that a general comparison between spark and photo-ignition is not possible within the present scope of the subject program. And comparison must be restricted to the particular spark sources employed in the experiments described below or in the pertinent literature.

B. EXPERIMENTAL RESULTS

A direct experimental comparison of spark and photochemical ignition could be obtained by measurement of reaction propagation velocity and time delay for spark ignition in the same experimental apparatus used for photochemical ignition studies[1,2]. This system consists of a replaceable radiant source (including an ultraviolet transmitting window) mounted in the end wall of a cylindrical, quartz reactant chamber of variable length and approximately 25 mm diameter. The chamber axis is oriented in the horizontal direction. For the spark ignition experiments,

the radiant source was replaced with a spark source consisting of two tungsten wires, 1/4 inch apart, which barely protruded through an electrically nonconductive end wall. A variable, high voltage tester coil was used to establish a "continuous" 1/4 inch spark discharge between the wires, which discharge would subsequently ignite the mixture. Ignition delay and reaction front propagation velocity were measured by photocells stationed at distances of 1.35 cm, 6.35 cm and 11.35 cm away from the ignition source, along the length of the tube. Signal rise time for these devices is about 1.5 microseconds and sensitivity is in the wavelength range 4,000 to 11,000 Å.

In order to provide a rational comparison of the two forms of ignition, some basis for selection of the input energy must be formed. A requirement of equal energy deposition in the mixture by the ignition source would provide one basis for comparison. However, with the apparatus generally available, determination of the spark energy input was not possible. The only other acceptable basis for comparison would be for each method to provide just the amount of energy dictated by its threshold limit requirement. When this approach was attempted, the spark ignition results became very erratic and the ensuing propagation velocity was difficult to determine since the emission from the reaction front proved to be very weak. Further, the fact that the spark process provided more than one spark pulse makes it difficult to establish at what time (or spark pulse) sufficient conditions for ignition were established. Thus to provide for more consistent results, the spark system was run at maximum input even though data interpretation becomes difficult.

Typical results for stoichiometric mixtures of hydrogen-oxygen, methane-oxygen and methane-air are shown in Table 1.

TABLE 1

Stoichiometric Mixture (Pressure in Torr)	V_{12}(m/sec)		V_{23}(m/sec)		τ(msec)	
	spark	photo	spark	photo	spark	photo
Hydrogen-Oxygen (300)	298	245	172	227	0.26	0.24
Methane-Oxygen (300)	190	176	282	305	0.25	0.25
Methane-Air (600)	10	7.2	2.1	13.9	6.87	3.00

Note: V_{12} and V_{23} are the mean propagation velocities between photo-cell stations 1-2 and 2-3, respectively, while τ is the estimated time delay.

For methane-air mixtures, the results were erratic since the particular spark ignition method used appeared to be near the threshold spark ignition limit for these mixtures. For the particular experimental conditions explored (and only those conditions) the results indicate that the propagating wave for spark ignition decays faster than that for photochemical ignition. For hydrogen-oxygen mixtures, the velocity of the propagating front decreased in going from region 1-2 to region 2-3 by 42% for spark ignition, but only 7% for photochemical ignition. For methane-oxygen mixtures, the velocity of the front increased in this interval by 43% for spark ignition, as compared to 73% for photochemical ignition. A different effect was observed in methane-air mixtures. While the reaction front velocity decreased by 79% for spark ignition it increased by 93% for photochemical ignition! Thus, although the particular spark ignition method used tended to result in a somewhat higher initial propagation velocity compared with photochemical ignition, the propagation was stronger when photochemically initiated, especially for the methane-air mixtures.

When consistent spark ignitions were produced, as was the case for the hydrogen-oxygen and methane-oxygen mixtures, the ignition time delay was similar for both spark and photochemical ignitions. However, when the spark ignition was inconsistent and unreliable, as was the case for methane-air mixtures, the time delay for spark ignition was considerably greater (130%) than for photochemical ignition. It should be noted that a few of the hydrogen-oxygen data runs showed the same behavior. With regard to ignition delay, it must also be noted that the spark duration is many orders of magnitude less than the "photo-flash" duration. Reduction of the radiant pulse period would result in a significant reduction of the photo-ignition time delay as well.

The one general result which appears to be indicated in the above results is that the propagating front is affected by the photochemical ignition technique even at reasonable distances into the mixture as compared with a spark ignited front. Clearly, a detailed general comparison cannot be formulated by the above techniques. However, an indirect comparison is possible by comparing the characteristics of photochemical and spark ignition at various mixture stoichiometries and pressures. This approach is taken in the following sections.

C. FUEL LEAN MIXTURES

A series of photochemical ignition experiments were run (using a type PC-1 ultraviolet radiation source and a lithium

fluoride window) on off-stoichiometric mixtures of hydrogen-oxygen at room temperature and 600 torr pressure[3]. The primary measurement was the threshold energy level required for photochemical ignition, no photo-cell data was taken. The data covers oxidizer/fuel ratios of 1/6 to 15/1 (1/2 is stoichiometric) and the results indicate that, changing the mixture stoichiometry from stoichiometric to fuel lean results first in a threshold energy decrease, then an increase. However, the variation in threshold energy requirement is well within an order of magnitude, even beyond the stoichiometry range indicated. For example, the energy typically required for photochemical ignition is increased only by a factor of 2 for a 16-fold decrease in fuel concentration.

Using this data, a comparison can be made between the minimum ignition energy for spark and photochemical ignition as a function of air-fuel ratio. Figure 1 shows this comparison for hydrogen-air mixtures, the thermal or spark data being obtained from Lewis and von Elbe[4], while the photochemical data is obtained from the hydrogen-oxygen photochemical ignition experiments corrected to hydrogen-air requirements[3]. The results clearly show that two different mechanisms are at work, with the photochemical method being stronger as it is relatively unaffected by the fuel lean state of the mixture. For example, a 16-fold decrease in fuel concentrations requires that the ignition energy be increased by a factor of 70 for spark initiation as opposed to a factor of 2 for photochemical initiation.

D. LOW PRESSURE MIXTURES

A comparison between photochemical and spark ignition for various subatmospheric pressures of reactant mixtures can also be formulated. Typical threshold ignition energy data for photochemical ignition of subatmospheric methane-air and methane-oxygen mixtures is presented in the previous reports[1,2], while the corresponding data for spark ignition can be obtained from Lewis and von Elbe[4]. A comparison of these results is illustrated by the curves presented in Figures 2 and 3. As in the previous section, the results clearly show that two different mechanisms are involved, with the photochemical method being stronger as it is relatively unaffected by decreasing mixture pressure. For example, an order of magnitude decrease in mixture pressure below sea level conditions requires that the ignition energy be increased by well over one (methane-oxygen) or two (methane-air) orders of magnitude for spark ignition, while virtually no change is required for photochemical ignition. It should be noted that the spark data is given for a vertically oriented chamber which imposes less of a restriction than horizontally oriented chambers.

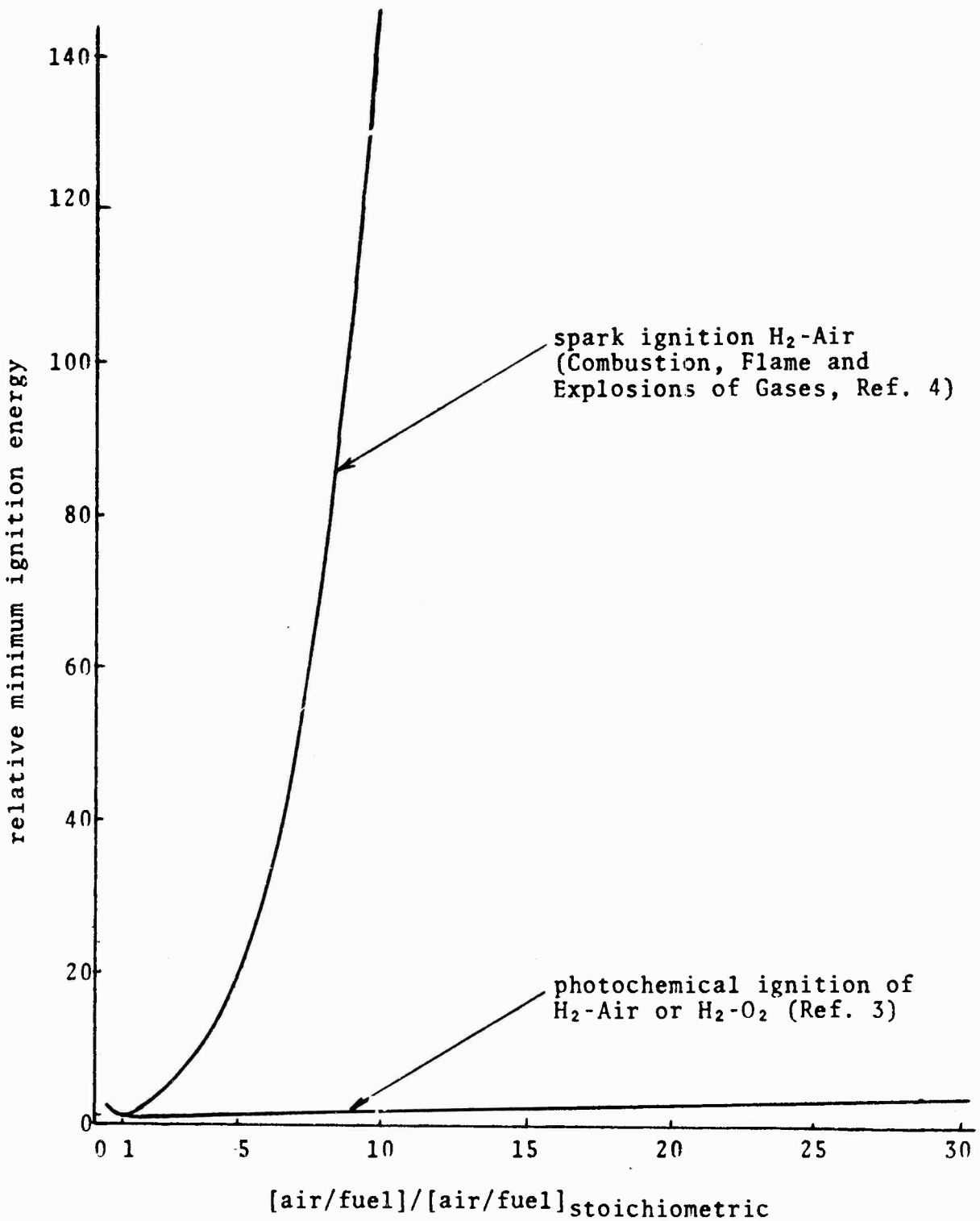

Figure 1 - Comparison of Minimum Ignition Energy vs Air-Fuel Ratio Curves for Thermal (Spark) and Photochemical Ignition

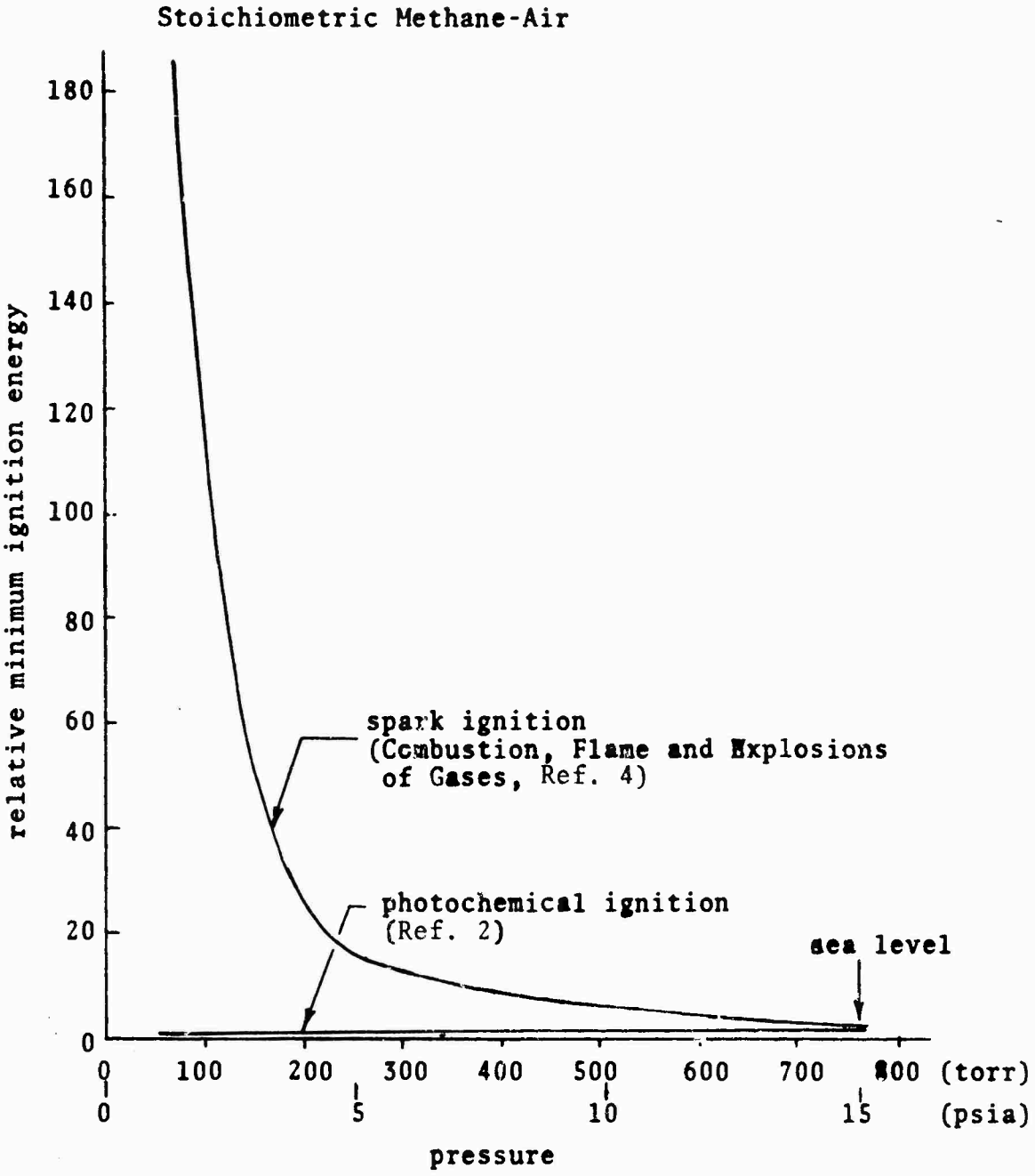

Figure 2 - Comparison of Minimum Ignition Energy vs Mixture Pressure for Spark and Photochemical Ignition

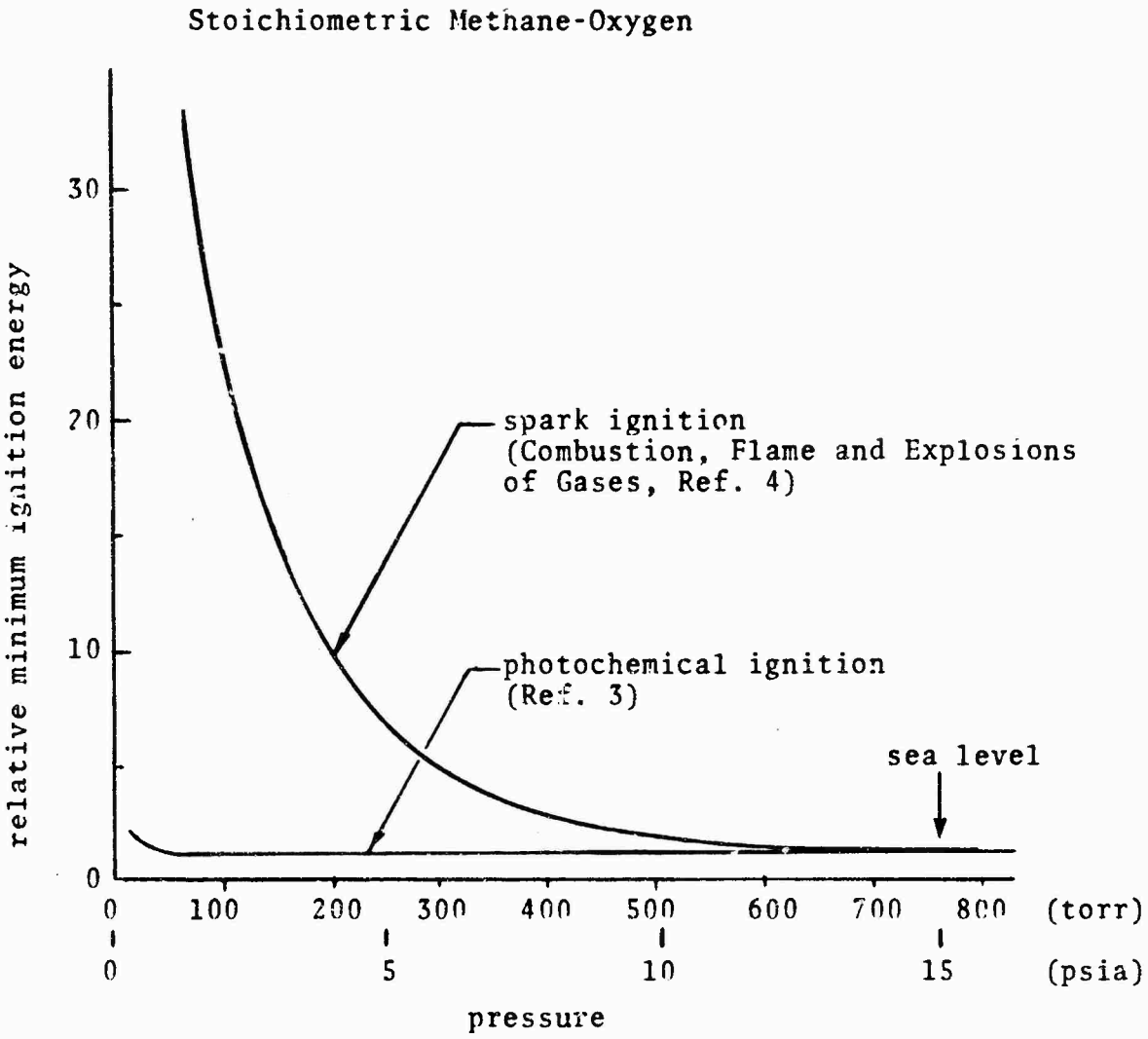

Figure 3 - Comparison of Minimum Ignition Energy vs Mixture Pressure for Spark and Photochemical Ignition

E. SUMMARY

A stronger ignition kernel and propagating reaction front as well as a completely different ignition mechanism is involved in the photochemical ignition technique in comparison with spark ignition techniques. This finding is supported by direct experimental comparison of reaction front velocities and ignition delay for both photochemical and spark ignition. And by indirect comparison of required ignition energy using spark sources (literature data), and photochemical source (experimental data) for fuel lean and for low pressure reactant mixtures.

F. REFERENCES

1. Cerkanowicz, A. E., Levy, M. E., and McAlevy III, R. F., "Photochemical Ignition of Gaseous Fuel-Oxidizer Mixtures at Subatmospheric Pressures," Final AFOSR Scientific Report No. 70-1664, April 1970.

2. Cerkanowicz, A. E., "Photochemical Initiation of Sustained Combustion in Unsensitized Gaseous Fuel-Oxygen Mixtures," Ph.D. Dissertation, Stevens Institute of Technology, June 1970.

3. Cerkanowicz, A. E., "Photochemical Enhancement of Combustion and Mixing in Supersonic Flows," Interim AFOSR Scientific Report, March 1972.

4. Lewis, B., and von Elbe, G., Combustion Flames and Explosions of Gases, Academic Press, Inc., 1961.

APPENDIX V

PENETRATION OF PHOTODISSOCIATIVE EFFECT

A. INTRODUCTION

Neglecting diffusion (and hence wall effects as well) the variation of oxygen atom density as a function of time, distance (from the UV transmitting window into the reactant mixture), thermodynamic and optical parameters was previously determined (for a square wave radiant pulse)[1,2] to be given by the following expression,

$$n_O = (2n_{O_2}/D')(t_p k_O)[1-\exp(-k_O t_O)]\int_0^\infty I_O T_\lambda \sigma_{O_2} \exp(-\sigma_{O_2} n_{O_2} x)d\lambda \quad (1)$$

where n_O = oxygen atom concentration

n_{O_2} = molecular oxygen concentration

D' = energy of dissociation of oxygen molecule

t_p = radiant pulse time

k_O = overall reaction rate constant (see ref. 1 & 2)

t_O = nondimensional time = t/t_p

I_O = radiant energy flux (wavelength dependent)

T_λ = window transmission (wavelength dependent)

σ_{O_2} = molecular oxygen absorption cross section (wavelength dependent)

x_2 = distance, measured from the window into the mixture

λ = wavelength

Prior work[1,2] made the approximation of replacing σ_{O_2} in the exponential with its average or mean value $\bar{\sigma}_{O_2}$ and assuming that I_O is constant over the wavelength region where σ_{O_2} is appreciably different from zero. These approximations reduced the integral of equation (6) to the simple form $\int_0^\infty T_\lambda \sigma_{O_2} d\lambda$ which could be graphically integrated to give a constant valued number (see pages 106-107, reference 2).

For reactant mixture regions near or at the window, where the photochemical ignition kernel is created, the above approximations can be used with minimal error. However, consideration of in depth photochemical effects, such as photodissociative penetration, necessitates abandoning these approximations and the detailed consideration of the wavelength dependent terms, as will be shown below. Three terms are involved; the window transmission (T_λ), the molecular oxygen absorption cross section (σ_{O_2}), and the radiant energy flux (I_O). In addition to exploring the details of wavelength dependency at these terms, the following sections also review their inherent characteristics which should be considered in application of the photochemical technique. Following these treatments, a graphical integration of equation 1 is performed and the results are reviewed.

B. WINDOW TRANSMISSION (T_λ)

Application of the photochemical combustion initiation technique requires the use of window material with good transmission characteristics in the vacuum ultraviolet region below 2000 Å (see ref. 1 and 2). Various candidate window materials in this region are presented in Table 1, while the relation of some of these window materials to the strong oxygen-photodissociation region is illustrated in Figure 1. As can be seen, the best UV transmitting materials are fluorides (lithium fluoride transmits as low as 1040 Å) which, unfortunately, are water soluble and hydroscopic with softening points between 400 and 600°C[3]. For practical applications, synthetic single crystal sapphire (UV or Czochralski grade) represents the best UV transmitting material (lower cut-off at 1400 Å)[4]. The next best window material would be synthetic single crystal quartz* (crystal designation X-246[5] or Cultured quartz[6]). Experiments have shown that about three times the energy is required for photochemical ignition of a standard reactant mixture when Cultured quartz is used in place of UV grade sapphire as the window material. Amorphous quartz (Supersil or type 151 fused silica) and polycrystalline alumina (Lucalux) also transmit in the UV region of interest, but only at a limited efficiency with regard to the photochemical ignition mechanism. Therefore, a considerably more powerful light source would be required than is the case when sapphire windows are used. This is substantiated by the inability to observe ignition using Supersil windows in the laboratory experiments.

*Insufficient information on this type of quartz exists regarding UV cut-off and temperature limitations to make a final appraisal at this time.

Table 1

Low Wavelength Cut-off of Various Far-UV Transmitting Materials

Material	Formula	Cut-off Å
Lithium Fluoride*	LiF	1040
Magnesium Fluoride*	MgF_2	1100
Calcium Fluoride*	CaF_2	1250
Strontium Fluoride*	SrF_2	1300
Sodium Fluoride*	NaF	1300
Barium Fluoride*	BaF_2	1345
Sapphire (UV Grade)(1)	Al_2O_3	1400
Cultured Quartz(2)	SiO_2	1450
Potassium Fluoride*	KF	1600
Suprasil(3)	SiO_2 (amorphous)	1600
Lucalux(4)	Al_2O_3 (polycrystalline)	1700

Notes:

* Softening points between 400 and 600°C - water soluble and hydroscopic.

(1) Melting point 2040°C, loses some inertness at about 1700°C.

(2) Melting point 1800°C, crystal change α to β at 550°C - transmission comparable with UV grade sapphire above about 1500 Å.

(3) Melting point 1800°C, devitrification starts 1000°C - transmission better than sapphire above 1680 Å.

(4) Melting point 2040°C - transmission less than 20% over entire region of interest.

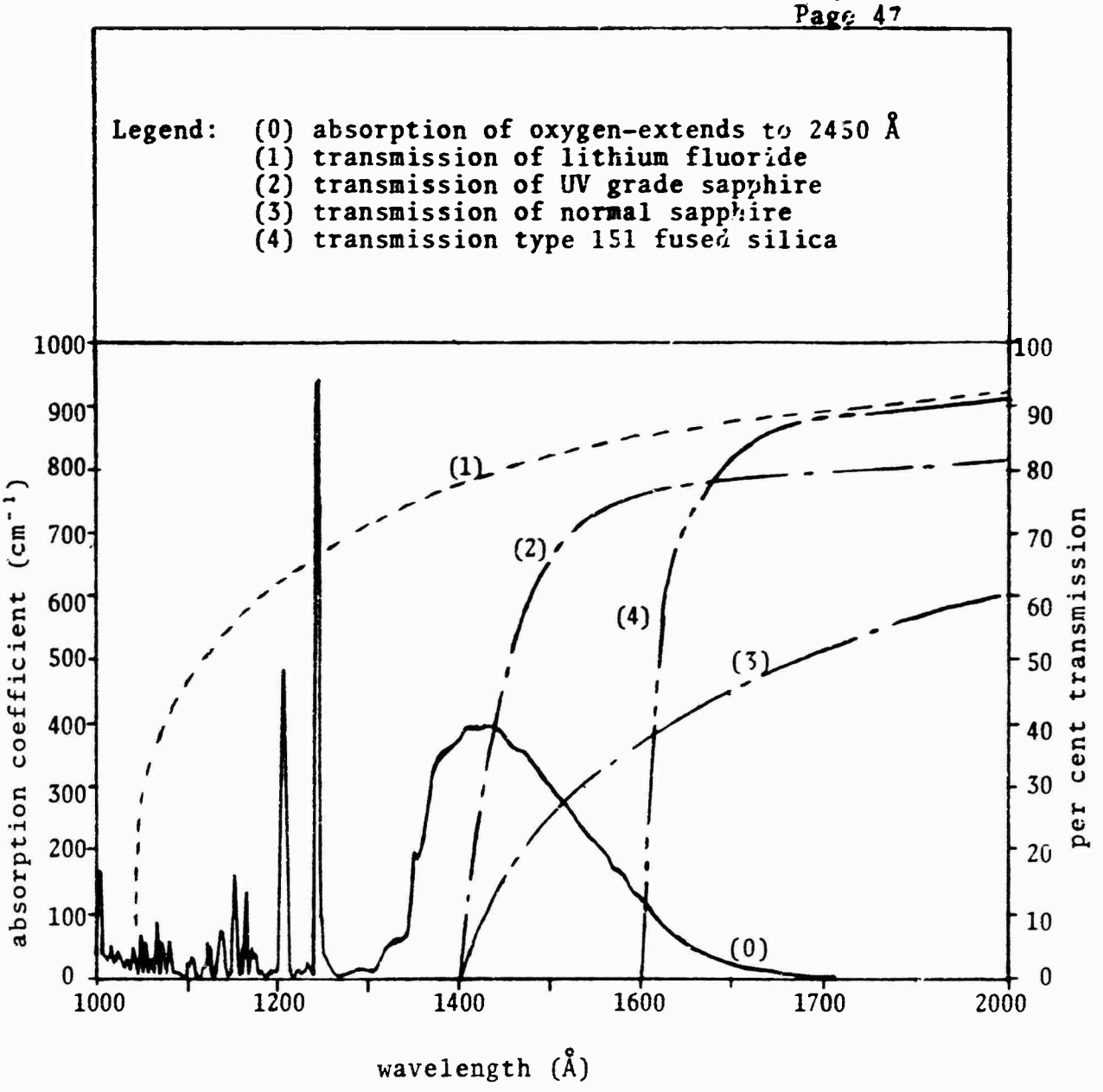

Figure 1 - Superposition of Window Transmission and Molecular Oxygen Absorption in the Wavelength Range 1000 Å to 2000 Å

In addition to the differences in UV transmission and cut-off, the following comparisons can be made regarding the characteristics of sapphire and quartz.

- Sapphire has a higher operating temperature limitation than quartz. The melting point of sapphire is about 2040°C but in some gas atmospheres the surface can be damaged via reactions at temperatures of about 1700°C. Cultured quartz, however, undergoes a crystal change at about 550°C (the effect of this change on transmission is not known but is most probably negative) while amorphous quartz starts to devitrify at about 1000°C.

- The ultraviolet cut-off for reasonable thickness sapphire windows is determined by surface reflection loss while for quartz windows it is determined primarily by the bulk material absorption. It is possible that a suitable anti-reflecting coating may be found for sapphire to increase its transmission.

- The thermal expansion coefficient of sapphire is approximately ten times that of quartz. High temperature "glass" to metal type seals are therefore possible with sapphire due to a better match to the expansion coefficient of some metals. This is also aided by the higher temperature capability of the sapphire.

- Sapphire is harder, more scratch resistant and inert to chemical attack than quartz. Quartz, however, is easier to machine and the amorphous variety can be flame worked.

- Quartz is less costly than sapphire, probably by a factor of 5 to 10. However, recent advances in the technique of sapphire growth does allow for sapphire to be economically used in commercial applications.

Based on superior ultraviolet transmission and physical characteristics important for practical application, UV grade sapphire is the prime candidate window material for use in application of the photochemical combustion technique. A detailed tabulation of sapphire transmission in the wavelength region of interest is given in Table 7, along with that possible when standard grade sapphire or non-cultured quartz windows are used. As can be seen, above 1680 Å, quartz transmission is about 10% greater than sapphire.

Table 2

Oxygen Absorption and Window Transmission for Wavelength Region 1400 Å to 2450 Å

(average values every 10 Å)

Wavelength Å	Oxygen Absorption (cm^{-1})	UV Grade Sapphire Transmission	Std. Grade Sapphire Transmission	UV Grade Quartz Transmission
1400-1410	380	0.065	0.015	--
1410-1420	396	0.200	0.048	--
1420-1430	397	0.300	0.080	--
1430-1440	395	0.365	0.110	--
1440-1450	390	0.427	0.134	--
1450-1460	375	0.480	0.160	--
1460-1470	355	0.529	0.185	--
1470-1480	344	0.570	0.205	--
1480-1490	330	0.606	0.224	--
1490-1500	308	0.635	0.240	--
1500-1510	290	0.659	0.251	--
1510-1520	277	0.678	0.267	--
1520-1530	260	0.692	0.279	--
1530-1540	240	0.703	0.290	--
1540-1550	218	0.712	0.302	--
1550-1560	200	0.722	0.315	--
1560-1570	182	0.731	0.327	--
1570-1580	167	0.739	0.339	--
1580-1590	151	0.747	0.350	--
1590-1600	135	0.751	0.361	--
1600-1610	122	0.757	0.370	0.170
1610-1620	107	0.760	0.380	0.414
1620-1630	93.0	0.761	0.390	0.535
1630-1640	79.0	0.763	0.399	0.620
1640-1650	65.0	0.768	0.408	0.679
1650-1660	55.0	0.769	0.417	0.728
1660-1670	45.0	0.770	0.423	0.745
1670-1680	36.0	0.770	0.430	0.768
1680-1690	30.0	0.772	0.438	0.788
1690-1700	25.0	0.774	0.446	0.802
1700-1710	20.4	0.778	0.454	0.820
1710-1720	17.2	0.779	0.461	0.830
1720-1730	14.1	0.780	0.468	0.840
1730-1740	11.1	0.781	0.473	0.845
1740-1750	8.50	0.782	0.478	0.850

Table 2 (Continued)

Wavelength Å	Oxygen Absorption (cm^{-1})	UV Grade Sapphire Transmission	Std. Grade Sapphire Transmission	UV Grade Quartz Transmission
1750-1760	3.00	0.783	0.483	0.853
1760-1770	1.00	0.785	0.489	0.857
1770-1780	0.520	0.788	0.497	0.860
1780-1790	0.350	0.789	0.504	0.862
1790-1800	0.182	0.790	0.511	0.864
1800-1810	0.113	0.790	0.519	0.866
1810-1820	0.0720	0.791	0.526	0.869
1820-1830	0.0480	0.792	0.531	0.871
1830-1840	0.0310	0.793	0.538	0.873
1840-1850	0.0202	0.795	0.544	0.876
1850-1860	0.0133	0.797	0.550	0.879
1860-1870	0.00920	0.799	0.556	0.881
1870-1880	0.00620	0.800	0.562	0.883
1880-1890	0.00430	0.800	0.568	0.886
1890-1900	0.00290	0.800	0.574	0.888
1900-1910	0.00202	0.801	0.582	0.890
1910-1920	0.00150	0.802	0.587	0.891
1920-1930	0.00110	0.804	0.592	0.891
1930-1940	0.000890	0.805	0.597	0.892
1940-1950	0.000700	0.807	0.602	0.892
1950-1960	0.000580	0.807	0.607	0.893
1960-1970	0.000510	0.807	0.612	0.893
1970-1980	0.000450	0.807	0.617	0.894
1980-1990	0.000400	0.808	0.622	0.894
1990-2000	0.000358	0.808	0.627	0.895
2000-2010	0.000349	0.808	0.632	0.895
2010-2020	0.000340	0.808	0.637	0.896
2020-2030	0.000330	0.808	0.642	0.897
2030-2040	0.000321	0.808	0.647	0.898
2040-2050	0.000312	0.808	0.652	0.899
2050-2060	0.000303	0.808	0.657	0.900
2060-2070	0.000293	0.809	0.662	0.901
2070-2080	0.000283	0.809	0.667	0.902
2080-2090	0.000274	0.809	0.672	0.903
2090-2100	0.000264	0.809	0.677	0.904
2100-2110	0.000254	0.809	0.682	0.904
2110-2120	0.000245	0.809	0.685	0.905
2120-2130	0.000235	0.809	0.687	0.906
2130-2140	0.000235	0.809	0.690	0.907
2140-2150	0.000216	0.809	0.692	0.907

Table 2 (Continued)

Wavelength Å	Oxygen Absorption (cm^{-1})	UV Grade Sapphire Transmission	Std. Grade Sapphire Transmission	UV Grade Quartz Transmission
2150-2160	0.000206	0.810	0.695	0.908
2160-2170	0.000197	0.810	0.697	0.909
2170-2180	0.000188	0.810	0.700	0.909
2180-2190	0.000179	0.810	0.702	0.910
2190-2200	0.000170	0.810	0.705	0.911
2200-2210	0.000161	0.810	0.707	0.912
2210-2220	0.000153	0.810	0.710	0.912
2220-2230	0.000144	0.811	0.712	0.913
2230-2240	0.000135	0.811	0.715	0.914
2240-2250	0.000126	0.811	0.717	0.915
2250-2260	0.000119	0.811	0.720	0.915
2260-2270	0.000111	0.811	0.722	0.915
2270-2280	0.000104	0.811	0.725	0.916
2280-2290	0.0000964	0.811	0.727	0.916
2290-2300	0.0000886	0.811	0.729	0.916
2300-2310	0.0000841	0.811	0.731	0.916
2310-2320	0.0000752	0.812	0.733	0.916
2320-2330	0.0000663	0.812	0.735	0.916
2330-2340	0.0000604	0.812	0.737	0.917
2340-2350	0.0000546	0.812	0.739	0.917
2350-2360	0.0000495	0.812	0.741	0.917
2360-2370	0.0000452	0.812	0.743	0.917
2370-2380	0.0000410	0.812	0.745	0.917
2380-2390	0.0000368	0.812	0.747	0.918
2390-2400	0.0000327	0.813	0.749	0.918
2400-2410	0.0000287	0.813	0.751	0.918
2410-2420	0.0000249	0.813	0.752	0.918
2420-2430	0.0000210	0.813	0.754	0.918
2430-2440	0.0000185	0.813	0.755	0.919
2440-2450	0.0000160	0.813	0.757	0.919

Since the photochemical combustion application depends on good transmission near the ultraviolet cut-off, it is important to know how this region is affected by operating parameters. It has been found that the transmittance of all these windows is temperature dependent[7,8]. Typical transmission wavelength-temperature curves for sapphire[8], given in Figure 2, indicate a shift of the transmission curves toward higher wavelengths with increasing temperature of about 0.3 Å/°C

C. MOLECULAR OXYGEN ABSORPTION (σ_{O_2})

The results of this work have indicated that the primary mechanism of photochemical combustion initiation and enhancement is the photodissociation of molecular oxygen[1,2]. This is energetically possible only when photons in the wavelength region below 2450 Å are provided. (It should be noted that when radiant energy below 1760 Å is used, at least one of the two resulting oxygen atoms will be in an excited electronic state[9].) Coupled with the wavelength limitations of the window (previous section) this defines the wavelength region of interest.

Since sapphire is the most practical window material, the wavelength region of interest for molecular oxygen absorption is 1400 Å to 2450 Å. Table 2 provides a listing of the molecular oxygen absorption coefficient for every 10 Å interval within this region, taken from the excellent review paper of Sullivan and Holland[10]. As is evident from this table and the curves of Figure 1, the most intense absorption occurs in the wavelength region below about 1760 Å and, consequently, this region is of prime importance in the photochemical ignition mechanism. Over the entire wavelength region from 1400 Å to 2450 Å, the absorption coefficient decreases in an exponential manner by seven orders of magnitude. However, even though the higher wavelength absorption is weak, it represents a major factor in the creation of a photochemical combustion enhancement effect, as will be demonstrated later. The exponential type decrease in the absorption coefficient is smooth except for the region near 1760 Å where an order of magnitude change is experienced over only about a 25 Å interval.

A strong temperature dependence as well as wavelength dependence exists for the molecular oxygen absorption coefficient[11]. This is illustrated by the results presented in Figure 3 which indicate an increase in absorption coefficient of two to three orders of magnitude for a 600°C temperature rise above room temperature! This will have a considerable

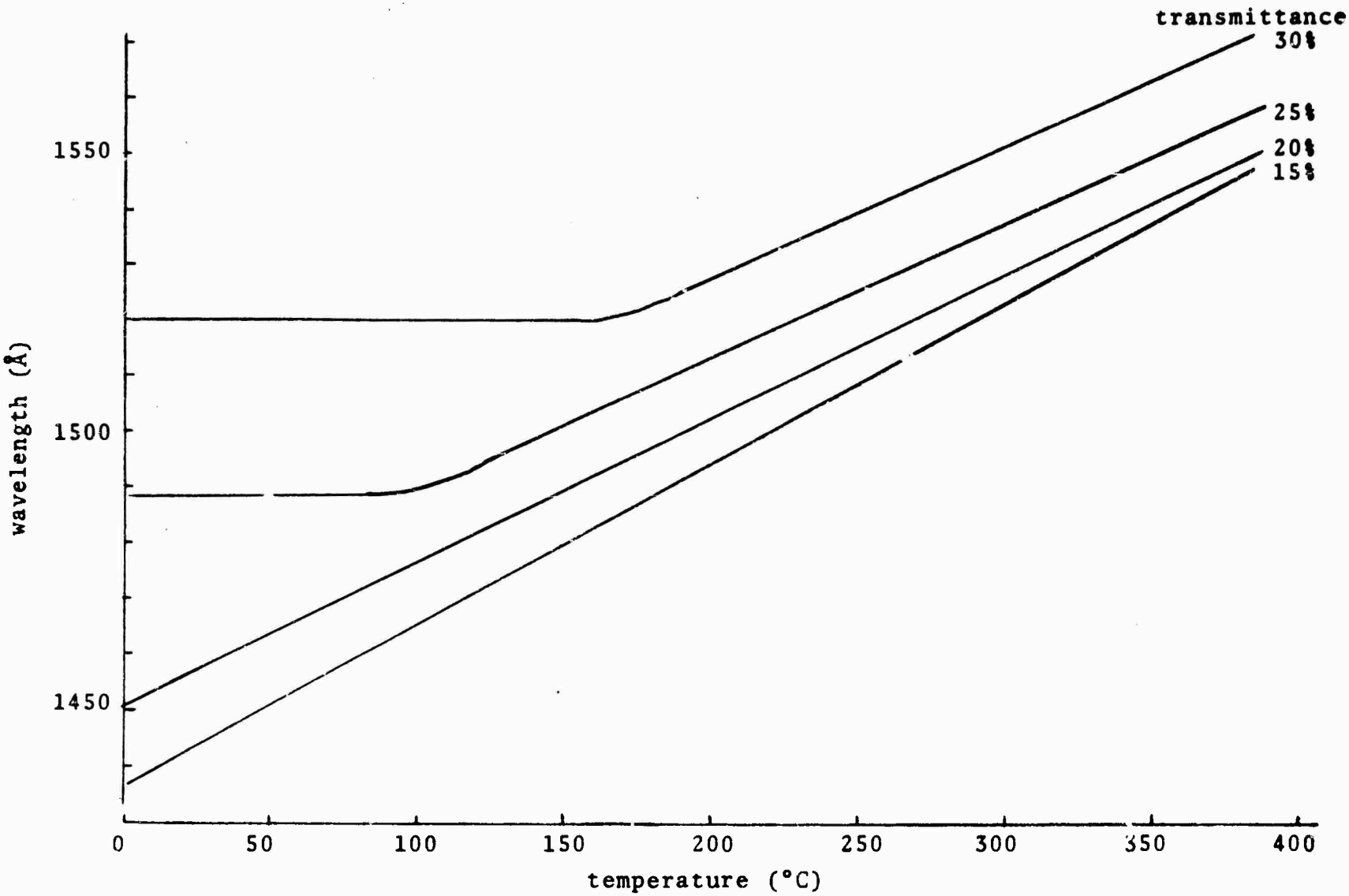

Figure 2 - Variation of Transmittance Wavelength vs. Temperature for Standard Grade Sapphire

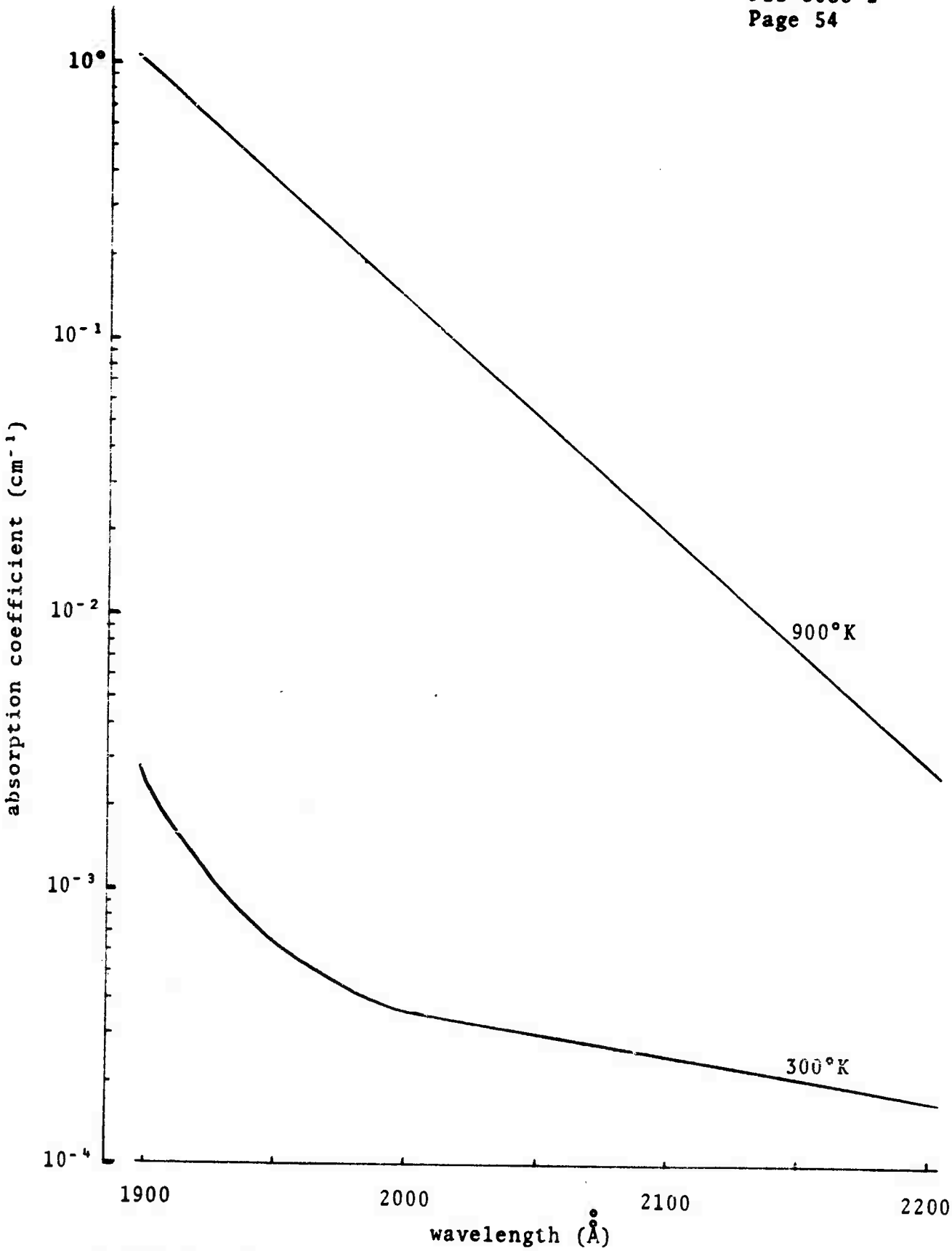

Figure 3 - Absorption Coefficient of Molecular Oxygen vs. Wavelength for Temperatures of 300°K and 900°K

effect on the solution of equation 1, resulting in a proportionally stronger photochemical effect than calculated for room temperature conditions. This caution should be remembered when reviewing the results which follow as they are based on room temperature conditions.

D. RADIANT ENERGY FLUX (I_o)

Earlier analysis of photochemical ignition assumed that the radiant intensity was constant in the wavelength region of interest, based on limited experimental measurements at three wavelengths (1300 A, 1500 A and 1700 A). While this representation may be valid for some sources in a limited wavelength region (say the ignition region), it will not necessarily be valid for all sources or over the extended wavelength region of 1400 A to 2450 A (which includes both the ignition and enhancement regions).

In the ultraviolet regions of the spectrum, the intensity of the radiant flux from a light source typically increases in an exponential manner with increasing wavelength and, consequently, will compensate, to some extent, for the decrease in absorption coefficient. A typical curve for a xenon plasma arc source intensity as a function of wavelength in the region of interest is illustrated in Figure 4[12]. For most plasma arc sources the intensity-wavelength variation will not be a smooth, continuous curve, but will be featured by intensity peaks due to line radiation. The magnitude and width of the peaks will be controlled by various source parameters such as, electrode gap, type of fill gas, fill pressure, etc. For the present purpose, however, the variation given in Figure 4 will be used to model the general trend expected and thereby represent a slightly better approach to reality than the assumption of constant intensity.

E. CORRECTION OF PREVIOUS ANALYSIS

The information presented in the three previous sections can be used to graphically integrate equation 1, section A, thereby avoiding the necessity of having to resort to the approximations made in the previous analysis[1,2]. In general, the results of following this procedure indicate that the previous analysis is sufficiently correct for regions near the window where ignition occurs, but is grossly in error when applied to regions away from the window.

Typical results of the corrected analysis are shown in Figure 5, which presents curves of the log of oxygen atom density divided by oxygen atom density at the window (i.e.,

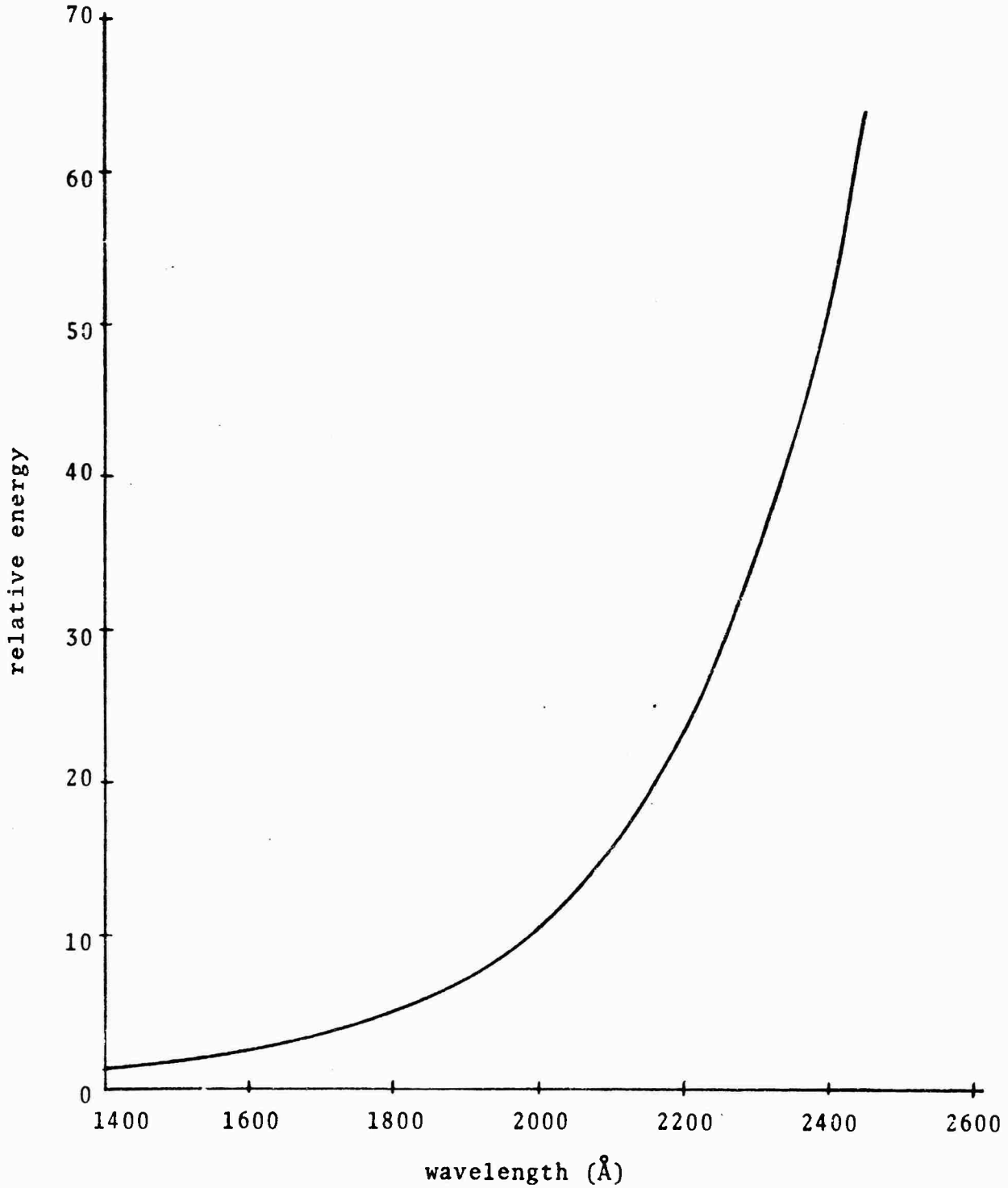

Figure 4 - Typical Continuum Intensity Variation of Low Pressure Vacuum UV Sources in the Wavelength Range 1400 Å to 2500 Å

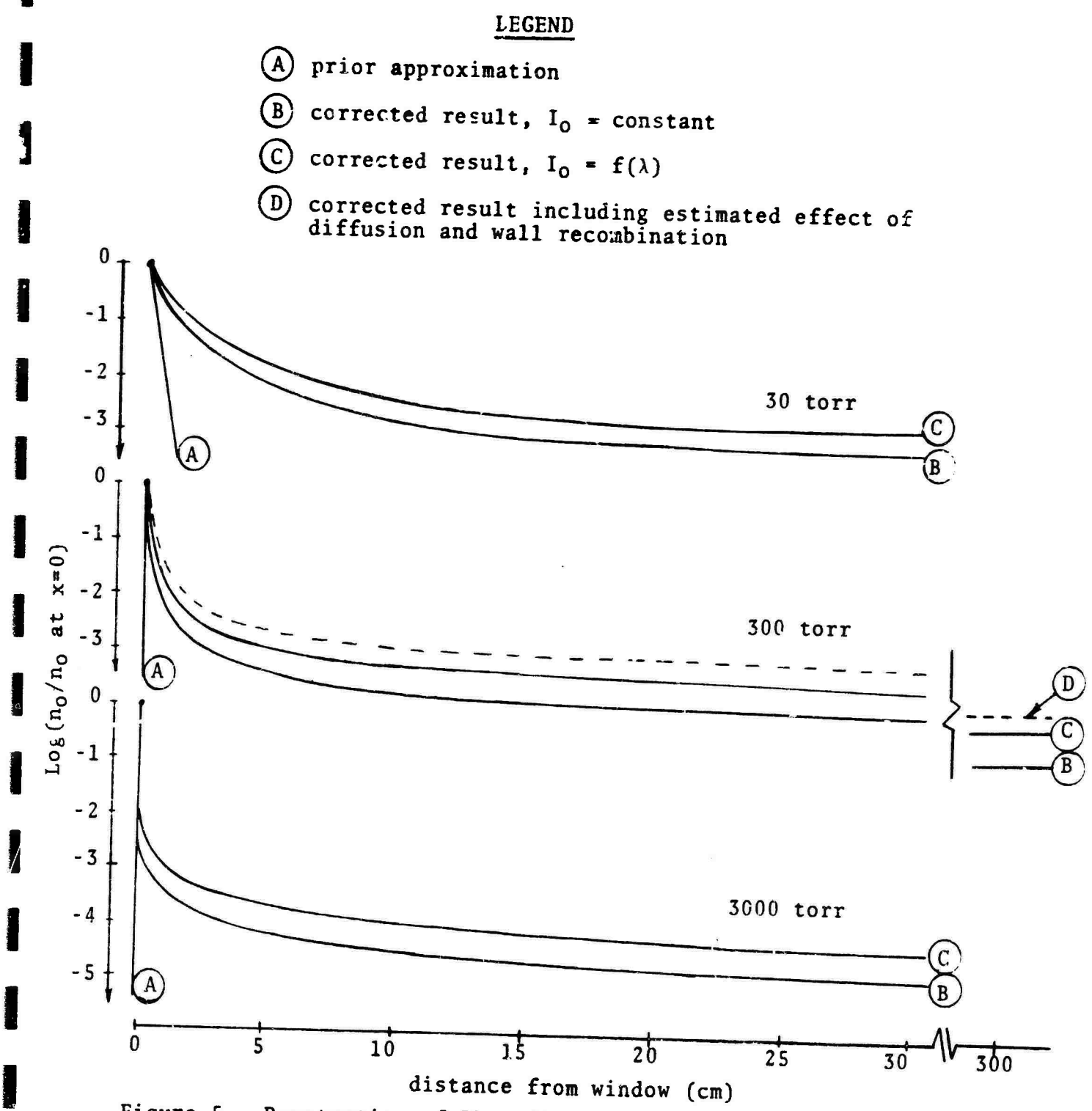

Figure 5 - Penetration of Photodissociative Effect into a Stoichiometric Hydrogen-Oxygen Mixture at Various Pressures (UV grade sapphire window, 300°K temperature)

Following the same reasoning, if the gas near the window was a fuel-free layer of air, a photochemical ignition site could still be created in the in-depth region by an increase in radiant energy input. Such a situation will exist if a photochemical igniter is positioned in the side wall of a combustor which is cooled by the presence of a fuel-free boundary layer of air. Figure 6 shows a typical curve for radiant energy increase required to penetrate various air layers and still create the critical oxygen atom concentration needed for ignition. For boundary layers of about 1/8 inch, less than an order of magnitude increase in the radiant energy would be required. Such increases are entirely within the realm of practical light source design.

Finally, it is possible to identify that different wavelength regions are instrumental in creating atomic oxygen species at various distances from the window. A typical detailed breakdown for a 300 torr, stoichiometric hydrogen-oxygen mixture is given in Table 3. As can be seen, for regions close to the window, lower wavelength absorption (1450-1650 Å) is of primary importance. As distance from the window increases, the higher wavelength absorption (1750-1900 Å) becomes more important until even absorption above 2000 Å contributes. Consequently, appropriate tailoring of the radiant source output could allow for either ignition, enhancement or both ignition and enhancement. It is also apparent that quartz optics is more than satisfactory if only enhancement effects are of interest.

G. SUMMARY

- A correction of the previous analysis on radiant flux penetration indicates that a considerably more gradual decrease in oxygen atom concentration with distance from the window occurs than previously calculated, with a leveling off after about 2 to 3 orders of magnitude decrease.
- This difference indicates that wavelength dependent terms should not be averaged.
- Sufficient oxygen atom concentrations are created in-depth to provide for a combustion enhancement effect.
- Penetration of a fuel-free boundary air layer between the radiant source window and reactant mixture is possible with a reasonable increase in energy expenditure.
- Different wavelength absorption regions of importance at various distances into the mixture have been identified.

order of magnitude changes in oxygen atom density) as a function of distance into the mixture measured from the source window for a stoichiometric hydrogen-oxygen mixture at pressures of 30, 300 and 3000 torr. Mixture temperature is 300°K and the window material selected is UV grade sapphire. Curve A indicates the linear curve which results from the previous analysis, while curves B, C and D indicate the corrected results at various degrees of scrutiny. As can be seen, the oxygen atom concentration produced is maximum near the window, where both analyses agree, and decreases with distance from the window into the mixture. Thus at threshold photochemical ignition energies, the critical oxygen atom concentration for ignition (10^{14} atoms/cm^3)[1,2] is produced near the window. At reasonable distances into the mixture, however, a substantial difference exists between the new results and those obtained using the prior approximations. A considerably higher degree of radiant flux penetration (or photodissociative effect) is indicated than previously thought possible. In fact, in the example cited (Figure 5), the logarithmic decrease in oxygen atom concentration levels off after only two to four orders of magnitude decrease (even at distances of 300 cm from the window) instead of decreasing continuously (over a hundred orders of magnitude at comparable distances). The indicated penetration is increased even further when the wavelength dependency of the radiant flux (I_0) is included in the analysis, in addition to molecular oxygen absorption (σ_{O_2}) and window transmission (T_λ) dependency, and when the effects of diffusion and wall recombination are also included.

F. DISCUSSION

Although the in-depth decrease in oxygen atom concentration is a few orders of magnitude, the concentrations generated are still sufficient to result in enhancement of the combustion processes. Details regarding this enhancement will be given in the following appendix.

Further, it should be noted that increasing the radiant energy input above the threshold ignition level raises the penetration curve proportionately, thus increasing the ignition and combustion enhancement effect at any given distance into the mixture. This could result in broadening the ignition kernel from a small volume near the window to a larger volume extending from the window to the point in the mixture where the oxygen atom concentration has decreased to the threshold ignition level. Additionally, the enhancement effect at greater distances into the mixture would also be increased. Ultimately, with a sufficiently powerful radiant source, ignition sites could be created throughout the entire mixture within the optical path of the radiant source.

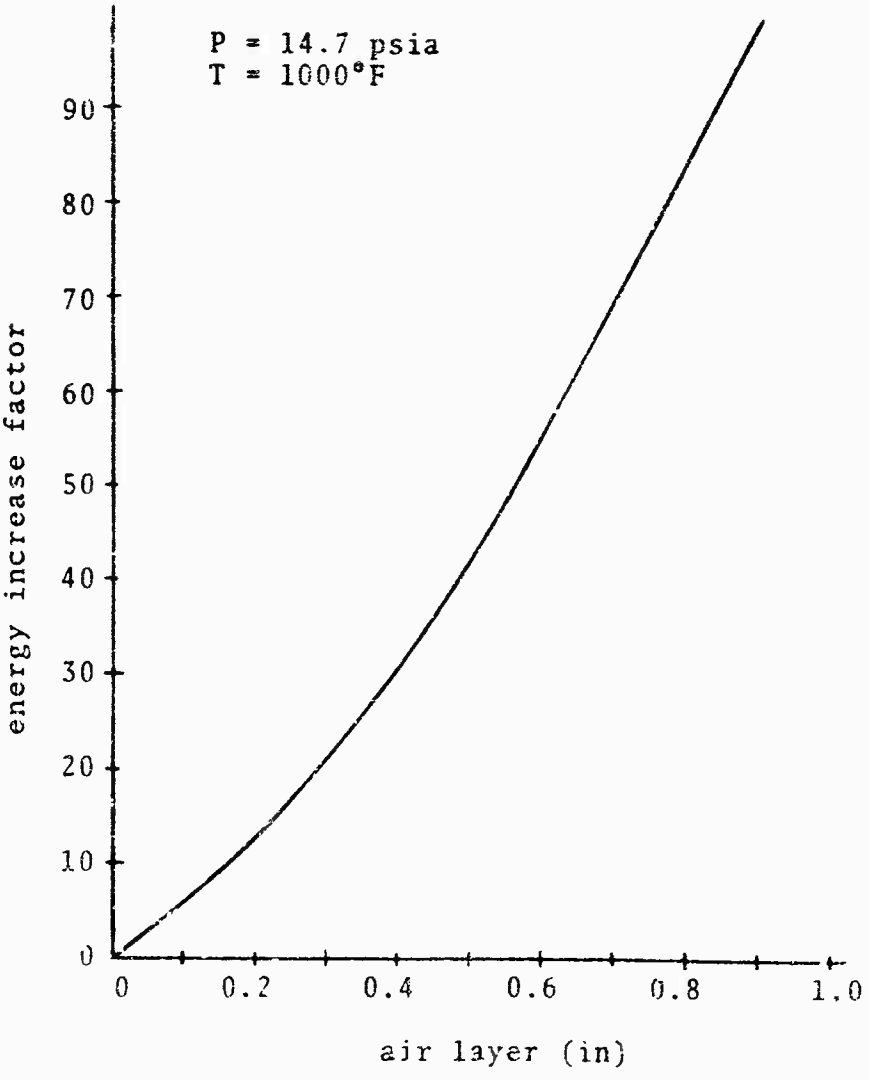

Figure 6 - Energy Increase Required to Achieve Photochemical Ignition after Penetration of an Air Layer at 1000°F and 1 Atmosphere

Table 3

Fractional Contribution of Indicated Wavelength Region in Oxygen Formation for Various Distances from a UV Grade Sapphire Window and a 300 Torr Stoichiometric Hydrogen-Oxygen Mixture

wavelength region (Å)	distance from window (cm)					
	x=0	x=0.01	x=0.30	x=3.0	x=30.0	x=300.0
1400-1450	0.099	0.0788	--	--	--	--
1450-1500	0.214	0.181	--	--	--	--
1500-1550	0.241*	0.228*	--	--	--	--
1550-1600	0.202	0.216	0.0097	--	--	--
1600-1650	0.140	0.163	0.104	--	--	--
1650-1700	0.0698	0.0878	0.382	--	--	--
1700-1750	0.0316	0.0413	0.436*	0.136	--	--
1750-1800	0.0026	0.0035	0.0610	0.734*	0.437*	--
1800-1850	--	--	0.0046	0.099	0.403	0.315*
1850-1900	--	--	--	0.0157	0.0804	0.296
1900-1950	--	--	--	0.0034	0.0177	0.0842
1950-2000	--	--	--	--	0.0082	0.0403
2000-2050	--	--	--	--	0.00720	0.0355
2050-2100	--	--	--	--	0.00738	0.0364
2100-2150	--	--	--	--	0.00755	0.0373
2150-2200	--	--	--	--	0.00737	0.0366
2200-2250	--	--	--	--	0.00705	0.0350
2250-2300	--	--	--	--	0.00613	0.0306
2300-2350	--	--	--	--	0.00485	0.0242
2350-2400	--	--	--	--	0.00352	0.0176
2400-2450	--	--	--	--	0.00228	0.0114

- Creation of a homogeneous ignition zone throughout the mixture or at least at reasonable distances into the mixture may eventually be possible.

H. REFERENCES

1. Cerkanowicz, A. E., Levy, M. E., and McAlevy III, R. F., "Photochemical Ignition of Caseous Fuel-Oxidizer Mixtures at Subatmospheric Pressures," Final AFOSR Scientific Report No. 70-1664, April 1970.

2. Cerkanowicz, A. E., "Photochemical Initiation of Sustained Combustion in Unsensitized Gaseous Fuel-Oxygen Mixtures," Ph.D. Dissertation, Stevens Institute of Technology, June 1970.

3. Harshaw Optical Crystals Catalogue, The Harshaw Chemical Company, 1967.

4. Optical Properties and Applications of Linde C_Z Sapphire, Technical Bulletin, Union Carbide, 1972.

5. Ballman, A. A., Dodd, D. M., Kuebler, N. A., Landisc, R. A., Wood, D. L., and Rudd, D. W., "Synthetic Quartz with High Ultraviolet Transmission," App. Optics, Vol. 7, pp. 1387-1390, July 1968.

6. Optical Cultured Quartz, Technical Bulletin, Sawyer Research Products, 1961.

7. Hunter, W. R., and Malo, S. A., J. Phys. Chem. Solids, Vol. 30, p. 2739, 1969.

8. Samson, J. A., Techniques of Vacuum Ultraviolet Spectroscopy, John Wiley and Sons, pp. 180-184, 1967.

9. Calvert, J. G., and Pitts, J. N., Photochemistry, John Wiley and Sons, pp. 205-207, 1967.

10. Sullivan, J. U., and Holland, A. C., "A Congeries of Absorption Cross Sections for Wavelengths Less Than 3000 Å," NASA-CR-371, 1966.

11. Ben-Aryeh, Y., "Spectral Emissivity of the Schumann-Runge Bands of Oxygen," J. Optical Soc., Vol. 58, No. 5, pp. 679-684, 1968.

12. Cerkanowicz, A. E., Levy, M. E., Simon, D. R., and Strowe, R. J., "Atomic Oxygen Absorption Cell System," Final Report, AFCRL-72-0249, 1972.

APPENDIX VI

PHOTOCHEMICAL COMBUSTION ENHANCEMENT

A. INTRODUCTION

Description of photochemical combustion enhancement is facilitated by the use of an appropriate phase plane diagram, as indicated by the previous work on photochemical ignition[1,2]. Detailed construction of a phase plane diagram, however, requires the solution of coupled energy and species conservation equations for the mixture of interest, along with the inclusion of a suitable kinetic scheme[3,4]. For the purpose of illustration, the work presented below will avoid these complications by using a simplified, approximate technique for specific reactant conditions. The results will then be combined with those related to penetration of the photochemical effect to indicate the mechanism of photochemical combustion enhancement. And although the calculations presented will be for specific reactant conditions, the results can be assumed to portray the general behavior to be expected.

B. PHASE PLANE CONSIDERATIONS

For a given reactant mixture and stoichiometry (in the present case, $2H_2 + O_2$), the oxygen atom concentration at room temperature and the pressure of interest is calculated (point S - stable point) via the equilibrium requirements of the oxygen atom formation reaction

$$O_2 \rightleftarrows O + O \qquad (1)$$

Using information on the equilibrium constant of equation 1 as a function of temperature[5], and the thermal ignition temperature-pressure requirements of the reactant mixture[6], the oxygen atom concentration at the thermal ignition (point T) for slow heating of the mixture (path S-T) is calculated. Based on previous photochemical ignition tests[1,2], the threshold photochemical ignition requirement (point P) and the isothermal route by which it is achieved (path S-T) can easily be calculated for the various pressures of interest. The phase plane separatrix is then approximated by a straight line between the thermal (T) and photochemical (P) ignition points.

Results of this calculation procedure for stoichiometric hydrogen-oxygen mixtures at pressures of 30, 300 and 3000 torr are listed in Table 1 and the corresponding phase plane diagrams are illustrated in Figure 1. Details of the appropriate kinetic scheme are inherently considered in the construction procedure since it utilizes experimental results. Interpretation of Figure 1 follows below.

Table 1

Phase Plane Points for
Stoichiometric Hydrogen-Oxygen Mixture

Point	Pressure (torr)	Temperature (°K)	Oxygen Atoms (atoms/cm^3)
S	30	300	1.55×10^{-22}
S	300	300	4.91×10^{-22}
S	3000	300	1.55×10^{-21}
T	30	747	$5.55 \times 10^{+3}$
T	300	853	$2.18 \times 10^{+6}$
T	3000	773	$2.40 \times 10^{+5}$
P	30	300	$3.94 \times 10^{+14}$
P	300	300	$8.29 \times 10^{+14}$
P	3000	300	$4.15 \times 10^{+14}$

Thermal ignition of a combustible mixture by slow heating follows the path S→T while photochemical ignition follows the path S→P. In the photochemical case, ignition is achieved, without the need of any temperature increase, by the photodissociative production of oxygen atom concentrations equal to or greater than that indicated by the photochemical ignition point (P). If, however, the radiant flux is only sufficient to produce an oxygen atom concentration less than or equivalent to that which would exist at the thermal ignition point (T), then a temperature increase to the thermal ignition temperature will still be required before ignition can occur. Thus, no obvious gain is incurred by irradiating the mixture. The situation is different when the radiant flux results in the creation of oxygen atom concentrations which are higher than the concentration at the thermal ignition point (T) but lower than the concentration at the photochemical ignition point (P). In this case, although a temperature rise is necessary for ignition, the required increase is less than that normally needed for pure thermal ignition and thus the mixture ignition and combustion properties are enhanced due to the ultraviolet irradiation.

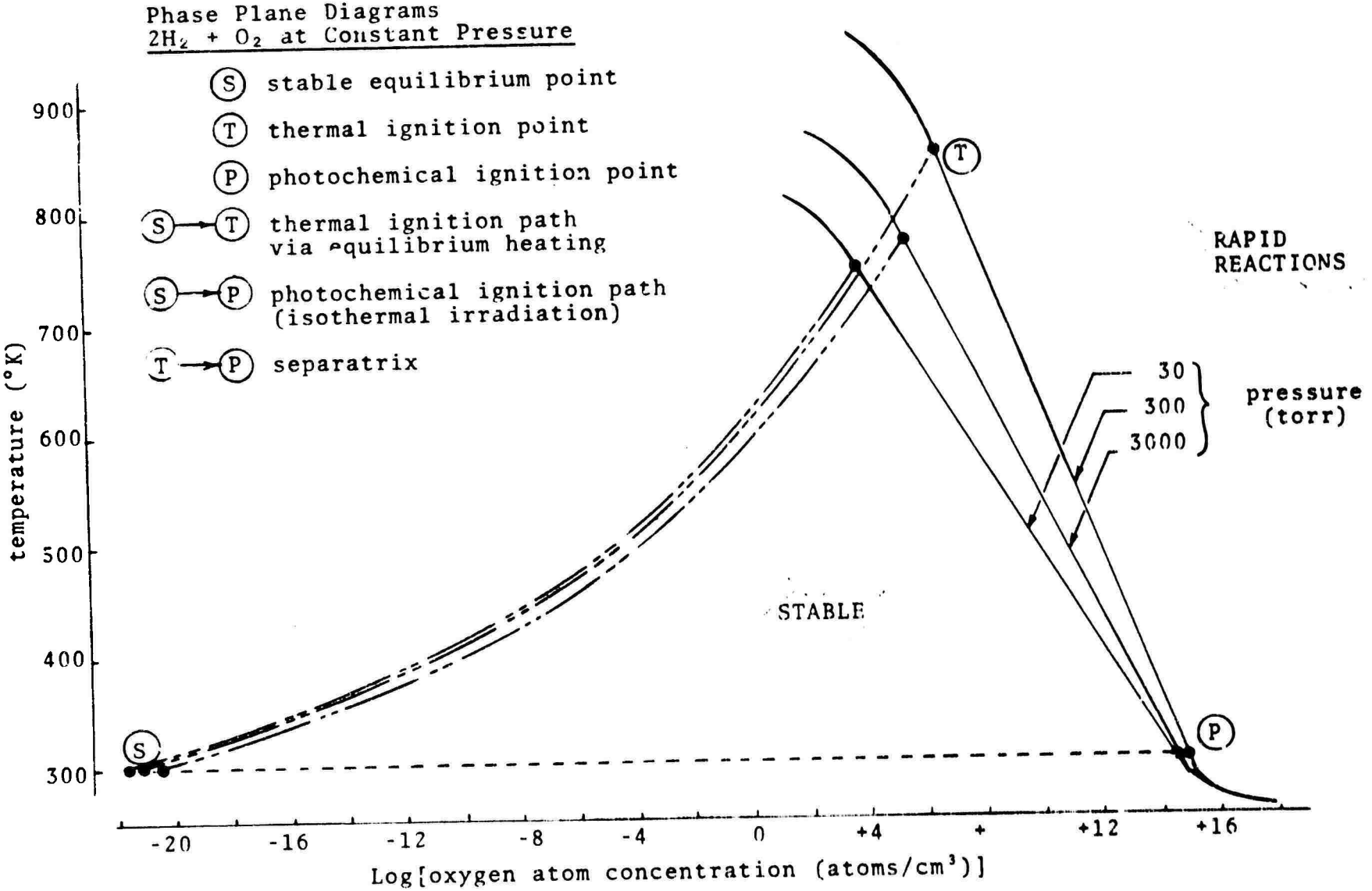

Figure 1 - Phase Plane Diagrams for Stoichiometric Hydrogen-Oxygen Mixtures

As an example of the above analysis, consider the phase plane characteristics (see Table 1 and Figure 1) of a 300 torr stoichiometric hydrogen-oxygen mixture. Thermal ignition is achieved by heating the mixture to 853°K at which condition the oxygen atom concentration has also increased from its room temperature value of 4.91×10^{-2} atoms/cm^3 to $2.18 \times 10^{+6}$ atoms/cm^3. In comparison, photochemical ignition is achieved at constant temperature by the photodissociative creation of oxygen atom concentrations of at least 8.29×10^{14} atoms/cm^3. Now, if the critical radiant flux for threshold photo-ignition is reduced by two orders of magnitude, only about 8.29×10^{12} atoms/cm^3 will be generated. Consequently, the mixture will not ignite unless a temperature increase is imposed on the mixture as well as the atomic oxygen species. However, since the oxygen atom concentration is higher than the concentration normally achieved in thermal ignition ($2.18 \times 10^{+6}$ atoms/cm^3), the required temperature increase is only 130°C as compared with the 553°C normally needed for thermal ignition. Thus the mixture combustion characteristics are enhanced by exposure to the ultraviolet flux. This enhancement effect can penetrate considerable distances from the window and therefore affect the mixture combustion in depth, as will be shown in the section.

C. PENETRATION OF COMBUSTION ENHANCEMENT

A wide range of oxygen atom concentration exists below the threshold photochemical ignition concentration for which combustion enhancement occurs (9 to 11 orders of magnitude indicated in Table 1). Further, the corrected analysis of radiant penetration indicates that contrary to a prior analysis, only a relatively modest decrease in generated oxygen atom concentration (2 to 4 orders of magnitude) occurs for reasonably in-depth volumes of the reactant mixture. As a result, use of the photochemical ignition technique will result in the creation of considerable, in-depth combustion enhancement within the reactant mixture.

Coupling of phase plane information and radiant penetration provides a description of the penetration of radiative combustion enhancement. The results for a stoichiometric hydrogen-oxygen mixture are given in Figures 2A, 2B and 2C for mixture pressures of 30, 300 and 3000 torr, respectively. The basic curves for the relative oxygen atom concentration variation with distance from the source window are taken from the work on radiative penetration. A second ordinate scale indicates the temperature rise required for ignition, which is derived from phase plane data on the location of the separatrix above the oxygen atom concentration of interest. The third ordinate scale indicates the temperature that would be required to produce comparable oxygen atom concentrations under equilibrium conditions. In all three figures, the intercept of the

ordinate scales with the abscissa designates the temperature-concentration conditions at the equilibrium thermal ignition point.

The oxygen atom concentration, and hence the enhancement effect as well, is a maximum at the window and decreases with distance from the window into the mixture. At threshold photochemical ignition energies, the critical oxygen atom concentration (approximately 10^{14} atoms/cm^3) is produced at the window and, thus, ignition with zero temperature increase required will originate in this region. Using Figure 2B as an example, the use of threshold ignition energy levels, will result in a reduction of the oxygen atom concentration by three orders of magnitude (approximately 10^{11} atoms/cm^3) at a penetration distance of about 30 cm into the mixture. Although this concentration is insufficient for direct ignition, it does result in a combustion enhancement effect since the additional temperature increase required for ignition is lowered to only 180°C (as opposed to the 553°C normally needed for thermal ignition). Under equilibrium conditions, a temperature of over 1000°C would be required to obtain the corresponding oxygen atom concentration! Even at a distance of 300 cm into the mixture, sufficient oxygen atoms (greater than 10^{10} atoms/cm^3) are present to result in lowering the additional temperature rise required for ignition to only 240°C.

These results clearly suggest the mechanism (in-depth preconditioning or enhancement of the mixture) whereby increased flame propagation velocities are observed in photochemical ignition of combustion. Coupled with the information on the effect of various wavelength regions on radiant penetration, the results provide for the identification of which wavelength regions are instrumental in the creation of combustion enhancement. Table 2 illustrates the relations in question, indicating that the higher wavelength regions, including wavelengths above 2000 Å, are important when in-depth enhancement is desired. This information can be used to attempt to optimize ultraviolet source design where specific photochemical effects are required.

Finally, it should be noted that increasing the radiant energy input above the threshold ignition level will result in proportionately increasing the penetration of radiative combustion enhancement at any given distance into the mixture. This provides another degree of freedom available in the design of photochemical combustion devices.

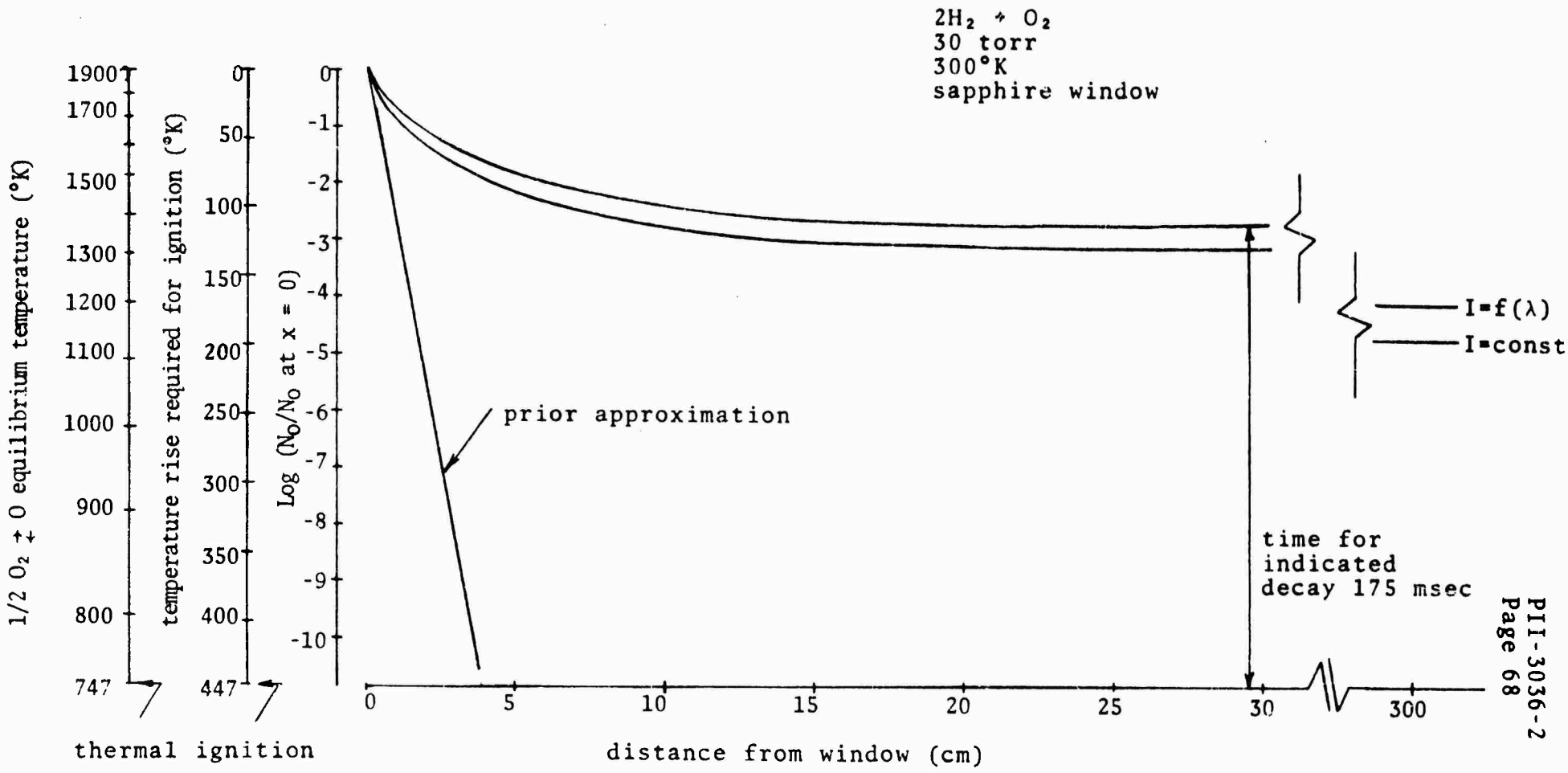

Figure 2A - Penetration of Radiative Combustion Enhancement for a Stoichiometric Hydrogen-Oxygen Mixture at a Pressure of 30 torr

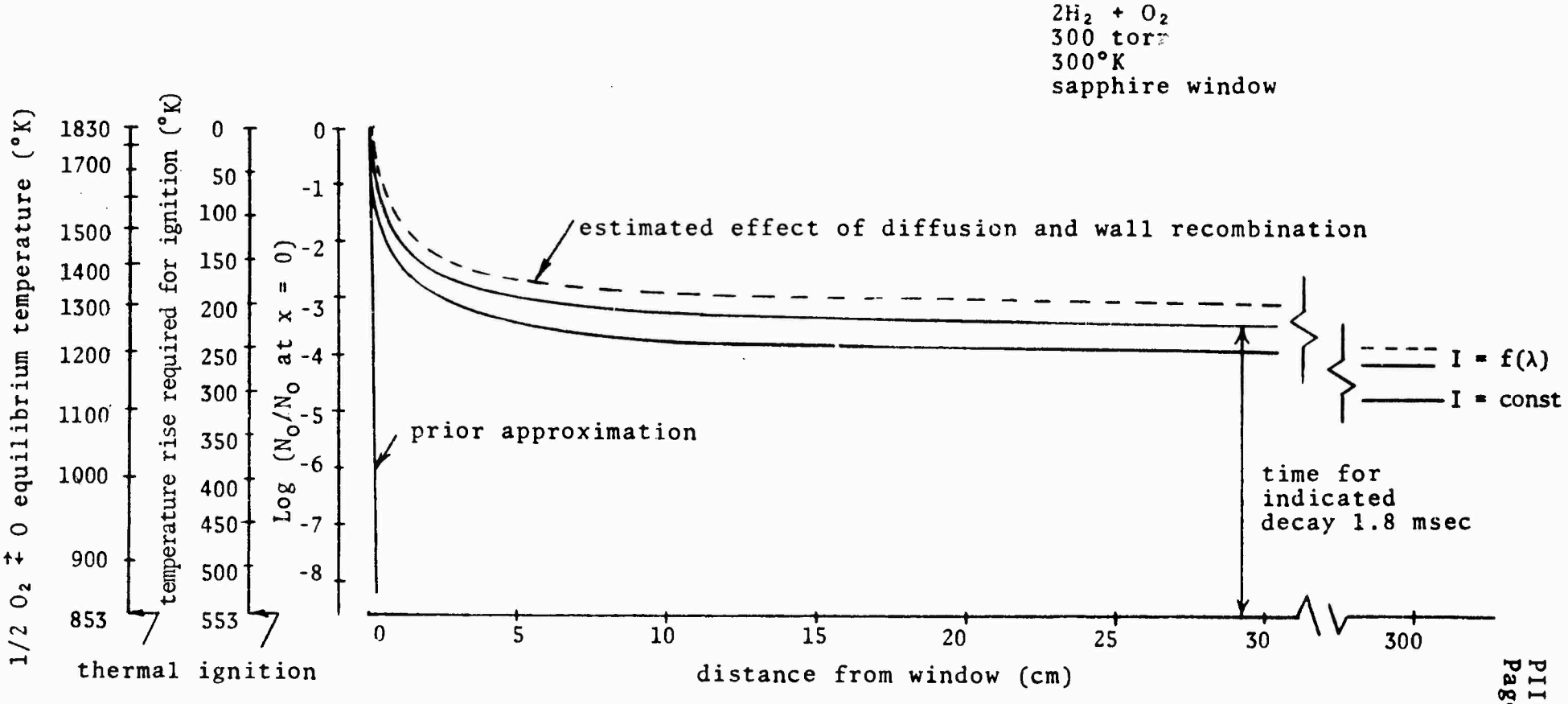

Figure 2B - Penetration of Radiative Combustion Enhancement for a Stoichiometric Hydrogen-Oxygen Mixture at a Pressure of 300 torr

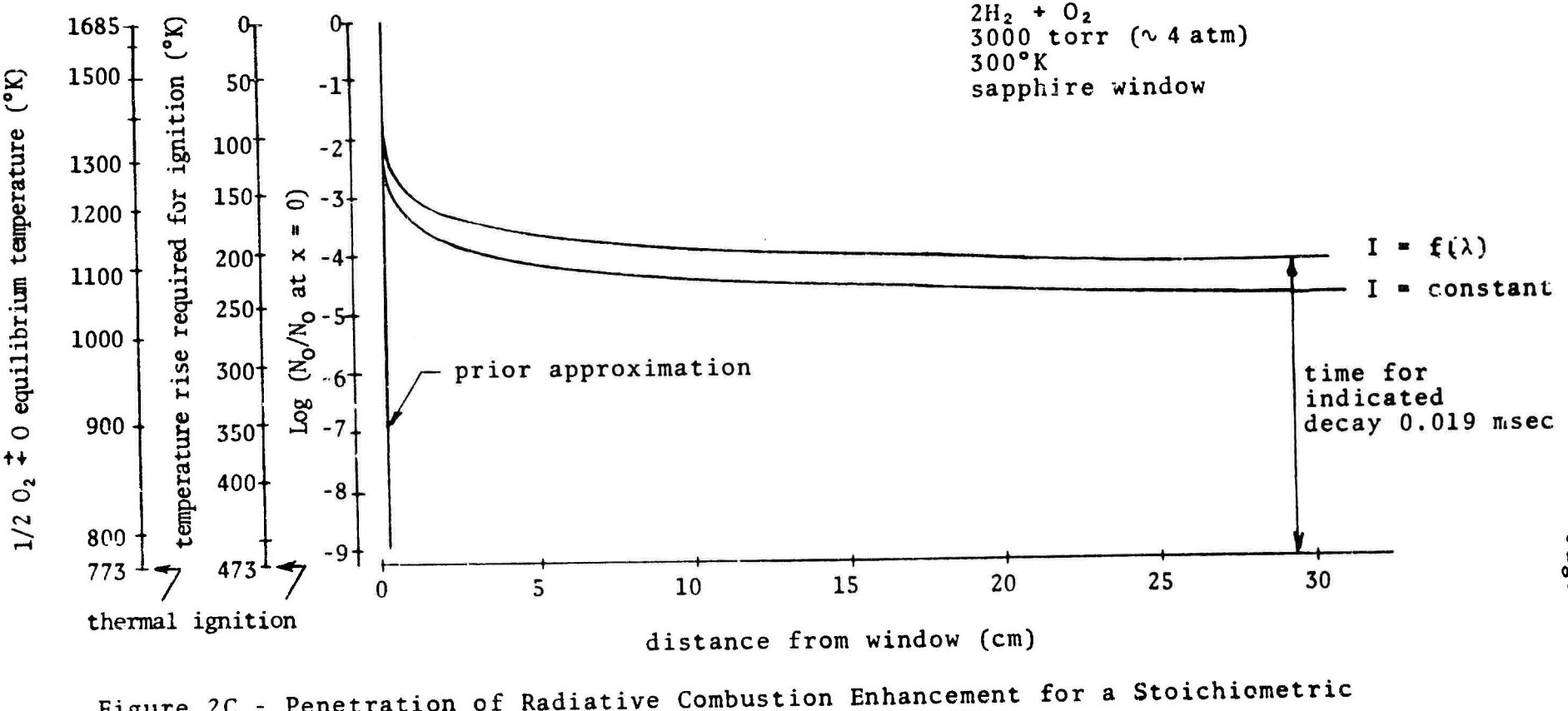

Figure 2C - Penetration of Radiative Combustion Enhancement for a Stoichiometric Hydrogen-Oxygen Mixture at a Pressure of 3000 torr

Table 1

Wavelength Regions of Importance for Combustion Enhancement - Based on Knowledge of Stoichiometric Hydrogen-Oxygen Mixtures

Effect	Wavelength Range (Å)
Total range of interest	1050 to 2450
Practical range (sapphire)	1400 to 2450
Ignition 0-0.01 cm	1450 to 1650
Propagation 0-3 cm	1450 to 1800
Propagation 3-30 cm	1550 to 1850
Propagation 30-300 cm	1750 to 2450

D. SUMMARY

- The photochemical combustion technique creates sufficient oxygen atom concentrations at in-depth region of the reactant mixture to result in a combustion enhancement effect which acts to reduce the temperature increase required for ignition below that normally required.

- Coupling of phase plane and radiant penetration data provides the necessary information to calculate the magnitude of the enhancement effect. Whereas photochemical ignition requires oxygen atom concentrations in excess of about 10^{14} atoms/cm^3, photochemical enhancement only requires oxygen atom concentrations in excess of about 10^3 to 10^6 atoms/cm^3.

- Different wavelength regions have been identified as being effective in combustion enhancement at various distances into the mixture.

- The combustion enhancement effects discussed, suggest the mechanism responsible for the observation of increased flame propagation velocity in previous photochemical ignition experiments.

E. REFERENCES

1. Cerkanowicz, A. E., Levy, M. E., and McAlevy III, R. F., "Photochemical Ignition of Gaseous Fuel-Oxidizer Mixtures at Subatmospheric Pressures," Final AFOSR Scientific Report No. 70-1664, April 1970.

2. Cerkanowicz, A. E., "Photochemical Initiation of Sustained Combustion in Unsensitized Gaseous Fuel-Oxygen Mixtures," Ph.D. Dissertation, Stevens Institute of Technology, June 1970.

3. Yang, C. H., and Gray, B. F., "On the Unification of the Thermal and Chain Theories of Explosion Limits," J. Phys. Chem., Vol. 69, pp. 2747-2750, 1965.

4. Yang, C. H., and Gray, B. F., "The Determination of Explosion Limits from a Unified Thermal and Chain Theory," Eleventh Symposium on Combustion, pp. 1099-1106, 1967.

5. McBride, B. J., et al, Thermodynamic Properties to 6000°K for 210 Substances Involving the First 18 Elements, p.252, NASA SP-3001, 1963.

6. Lewis, B., and von Elbe, G., Combustion Flames and Explosions of Gases, Academic Press, Inc., 1961.

APPENDIX VII

LASER CALCULATIONS

A. FUNDAMENTAL ABSORPTION CONSIDERATIONS

In some applications, the use of high radiant intensity (laser pulse) to produce photodissociative effects could result in a significant change in the concentration of absorbing species. The usual Beer-Lambert formulation will not apply in this case since the variation of the absorbing species concentration with time and distance must be considered. Starting with the assumption of linear absorption of monochromatic radiation [1], the loss of radiant intensity for absorption by one component of a nonscattering medium is given by

$$\partial I = - I\sigma_i n_i \partial x \qquad (1)$$

where I is the irradiance reaching the absorbing species i at a distance x from the window, σ_i is the absorption cross section of the species and n_i is the number density of the species. Since n_i is a function of distance and time (due to the assumed large photodissociative effect), integration of the above equation does not give the usual Beer-Lambert law but rather the following

$$I = I_o T \exp \left(- \sigma_i \int_0^x n_i \partial x\right) \qquad (2)$$

where I_o is the source irradiance reaching the window and T is the window transmission. Generalizing to a mixture of N absorbing species (i = 1, 2, 3,----N), equation (2) becomes

$$I = I_o T \exp \left(- \sum_{i=1}^{N} \sigma_i \int_0^x n_i \partial x\right) \qquad (3)$$

The energy E_λ absorbed by the mixture per unit volume per unit time at a given wavelength and distance x from the window is given by

$$E_\lambda = -\partial I/\partial x = I_o T \left(\sum_{i=1}^{N} \sigma_i n_i\right) \exp \left(- \sum_{i=1}^{N} \sigma_i \int_0^x n_i \partial x\right) \qquad (4)$$

Finally, for polychromatic radiant input, equation (4) must be integrated with respect to wavelength (note that the quantities I_o, T, and σ_i are all wavelength dependent) to give the energy E absorbed by the mixture per unit volume per unit time at a distance x from the window

$$E = \int_0^\infty E_\lambda d_\lambda = \int_0^\infty I_o T \left(\sum_{i=1}^{N} \sigma_i n_i \right) \exp \left(- \sum_{i=1}^{N} \sigma_i \int_0^x n_i \partial x \right) d_\lambda \qquad (5)$$

Simplification of this expression can be achieved by making the following assumptions:

- The radiant energy is provided by a laser pulse of bandwidth $\Delta\lambda$ centered at wavelength λ. In this limited region, the window transmission and species absorption parameters can be considered to be independent of wavelength, being designated by T^* and σ^*_i, respectively. The radiant intensity of the laser pulse is given by $I^* = \int I_o d_\lambda$.
- The only radiant absorbing species is molecular oxygen ($i = O_2$) which photodissociates via the reaction $O_2 + h\nu \rightarrow O + O$.

As a result of these assumptions, equation (5) can be written in the following form,

$$E_{O_2} = I^* T^* \sigma^*_{O_2} n_{O_2} \exp \left(- \sigma^*_{O_2} \int_0^x n_{O_2} \partial x \right) \qquad (6)$$

B. ATOMIC OXYGEN PRODUCTION

Following absorption of the radiant energy, photodissociation of molecular oxygen occurs resulting in formation of oxygen atoms. Subsequent loss of atoms will then occur due to gas phase kinetics (recombination, ozone formation, etc.), diffusion and wall recombination. However, it will be assumed that the duration of the laser pulse is sufficiently short to allow the loss mechanisms to be neglected. Consequently, the rate of change of oxygen atom concentration is given by the following expression,

$$\partial n_O / \partial t = 2E_{O_2} / D' \qquad (7)$$

where D' is the photon energy absorbed in photodissociation

Combining equations (6) and (7) then gives

$$\partial n_O/\partial t = (?I^*T^*\sigma^*_{O_2}\, n_{O_2}/D') \exp\,(-\,\sigma^*_{O_2} \int_0^X n_{O_2}\partial x) \qquad (8)$$

Additional equations can be written for atom conservation and photodissociation energy,

$$n_O/2 + n_{O_2} = N_{O_2} \qquad (9)$$

$$D' = h\nu^* = hc/\lambda^* \qquad (10)$$

where N_{O_2} is the initial particle density of molecular oxygen (the initial density of atomic oxygen is assumed to be zero), h is Planek's constant, c is the speed of light, ν^* is the frequency of the laser pulse and λ^* is the corresponding wavelength of the laser pulse.

C. SOLUTION OF DIFFERENTIAL EQUATION

Combining equations (8) and (9) to eliminate n_O gives the following

$$\partial\alpha/\partial t = -\,K\alpha \exp\,(-\int_0^X \alpha\partial x) \qquad (11)$$

where $\alpha \equiv \sigma^*_{O_2}\, n_{O_2}$ (12)

and $K \equiv I^*T^*\sigma^*_{O_2}/D'$ (13)

Differentiating equation (11) by x then gives

$$\partial^2\alpha/\partial x\partial t = -\,K\left[(\partial\alpha/\partial x) \exp\,(-\int_0^X \alpha\partial x) - \alpha^2\exp(-\int_0^X \alpha\partial x)\right] \qquad (14)$$

which can then be combined with equation (11) as follows

$$\partial^2\alpha/\partial x\partial t = (1/\alpha)(\partial\alpha/\partial x)(\partial\alpha/\partial t) - \alpha(\partial\alpha/\partial t) \qquad (15)$$

Rearrangement then gives the following

$$\partial[(1/\alpha)(\partial\alpha/\partial x) + \alpha]/\partial t = 0 \tag{16}$$

Consequently, the term in the brackets [] must only be a function of x, say f(x). Thus

$$(1/\alpha)(\partial\alpha/\partial x) + \alpha = f(x) = \partial g(x)/\partial x \tag{17}$$

where $g(x) \equiv \int f(x)dx$ = function of x only.

Further simplification can now be achieved by the following substitution

$$\alpha \equiv \phi \exp\,(g(x)) \tag{18}$$

which then gives

$$(1/\phi)(\partial\phi/\partial x) + \phi \exp\,(g(x)) = 0 \tag{19}$$

the solution of which has the form

$$1/\phi = \int \exp\,(g(x))\,\partial x + h(t) \tag{20}$$

where h(t) = function at t only. Combining equation (20) with equation (18)--and equation (12)--then gives

$$\alpha = \sigma^*_{O_2}\, n_{O_2} = \exp\,(g(x))/\left[\int \exp\,(g(x)) + h(t)\right] \tag{21}$$

Written as an infinite power series, the form of the above solution must be as follows,

$$\alpha = \sum_{n=0}^{\infty} A_n x^n \Big/ \left[\sum_{n=0}^{\infty} A_n x^{n+1}/(n+1) + \sum_{i=0}^{\infty} B_i t^i\right] \tag{22}$$

D. EVALUATION OF SERIES COEFFICIENTS

Evaluation of the A_n constants is accomplished by use of the initial condition for the situation of interest. Assuming homogeneous conditions at the start of irradiation, the initial condition is then given as

$$\text{at } t = o,\ x \geq o \qquad \alpha = \sigma^*_{O_2} N_{O_2} \equiv \alpha_o \tag{23}$$

Substitution into equation (22) gives

$$\alpha_o \left[\sum_{n=o}^{\infty} A_n x^{n+1}/(n+1) + B_o \right] = \sum_{n=o}^{\infty} A_n x^n \tag{24}$$

or after rearrangement

$$\alpha_o \sum_{n=1}^{\infty} A_{n-1} x^n/n + \alpha_o B_o = A_o + \sum_{n=o}^{\infty} A_n x^n \tag{25}$$

Equating coefficients of terms with identical powers of x

$$A_o = \alpha_o B_o \qquad \text{and } A_n = \alpha_o A_{n-1}/n \tag{26}$$

from which the following recursion formula for A_n is obtained

$$A_n = \alpha_o^{n+1} B_o/n! \tag{27}$$

And consequently equation (22) becomes

$$\alpha = \sum_{n=o}^{\infty} (\alpha_o^{n+1} x^n/n!) \Big/ \left[\sum_{n=o}^{\infty} (\alpha_o^{n+1} x^{n+1}/(n+1)!) + \sum_{i=o}^{\infty} (B_i t^i/B_o) \right] \tag{28}$$

Evaluation of the B_i constants is accomplished by substitution of equation (28) into equation (11). This ultimately results in the following expression

$$\sum_{i=o}^{\infty} KB_i t^i = \sum_{i=o}^{\infty} (i+1) B_{i+1} t^i \tag{29}$$

Equating coefficients of terms with identical powers of t

$$B_{i+1} = KB_{i-1}/i \tag{30}$$

from which the following recursion formula for B_i is obtained

$$B_i = K^i B_o/i! \tag{31}$$

Substitution into equation (28) and rearrangement then gives

$$\alpha/\alpha_o = 1\Big/\left[1 + \left(\sum_{i=1}^{\infty} (Kt)^i/i!\right)\Big/\left(\sum_{n=0}^{\infty} (\alpha_o x)^n/n!\right)\right] \tag{32}$$

The infinite series terms in equation (32) are clearly exponential and thus the equation can be written as

$$n_{O_2}/N_{O_2} = \left[1 + (e^{Kt}-1)\Big/(e^{\alpha_o x})\right]^{-1} \tag{33}$$

or in the terms of the oxygen atom concentration as

$$n_O/N_{O_2} = \left[1 + (e^{\alpha_o x})\Big/(e^{Kt}-1)\right]^{-1} \tag{34}$$

An inspection of the above two equations shows that as $x \to \infty$ the conditions expected for a semi-infinite domain are satisfied. Namely

$$\text{at} \quad x \to \infty, \; t \geq 0 \qquad n_{O_2} \to N_{O_2} \text{ and } n_O \to 0 \tag{35}$$

Equation (34) indicates that the maximum oxygen atom concentration occurs for the minimum value of distance ($x = 0$, window location) and the maximum value of time ($t = t^*$, end of the radiant pulse). The equation is general in the sense that it provides for significant changes in the concentration of the absorbing species (bleaching) and thereby departs from the usual Beer-Lambert formulation.

E. LASER PHOTOCHEMICAL IGNITION ENERGY

Threshold photochemical ignition of a reactant mixture via pulsed laser irradiation will be achieved when the oxygen atom concentration near the window at the end of the radiant pulse (maximum value) equals the critical oxygen atom concentration for ignition[1]. Threshold ignition conditions are therefore given by

$$n_O = n_{O\text{-crit}},\ t = t^*,\ x = o \tag{36}$$

Substitution of these conditions into equation (34) along with the use of equations (10) and (13) provides the following expression for the critical radiant intensity for threshold photochemical laser ignition.

$$I^*_{crit} = (hc/T^*\sigma^*_{O_2}{}^*\lambda^*t^*)\ \ell n\left\{1 + \left[(2N_{O_2}/n_{O\text{-crit}})-1\right]^{-1}\right\} \tag{37}$$

However, previous results have shown that $(2N_{O_2}/n_{O\text{-crit}}) >> 1$ and consequently the following approximate form can be used†

$$I^*_{crit} \cong (hc/T^*\sigma^*_{O_2}\ \lambda^*t^*)(n_{O\text{-crit}}/2N_{O_2}) \tag{38}$$

The critical laser pulse energy for photochemical ignition of a reactant mixture is then given by

$$E^*_{crit} = I^*_{crit}\ t^*\ A^* \tag{39}$$

or
$$E^*_{crit}/A^* = (hc/T^*\sigma^*_{O_2}\ \lambda^*)(n_{O\text{-crit}}/2N_{O_2}) \tag{40}$$

where A^* is the beam area of the laser pulse.

---

†Equation (38) could have been derived directly from the usual Beer-Lambert formulation using the stated inequality. However, one of the intents of this effort was to provide a general formulation for those situations where the stated inequality is invalid.

Since $\sigma^*_{O_2}$ is a strong function of wavelength, equation (40) indicates that the critical laser energy for photochemical ignition will also be a strong function of wavelength. A typical result is shown in Figure 1, where the laser radiant energy per unit window area required for photochemical ignition is given as a function of wavelength for a 300 torr, stoichiometric hydrogen-oxygen mixture ($n_{O\text{-}crit}/2N_O \cong 1.17 \times 10^{-4}$)[2] using a UV grade sapphire window for radiant transmission. The energy requirement is a minimum, 60 $\mu J/cm^2$, at a wavelength of about 1500 Å and increases very rapidly for wavelength regions above or below the minimum. An infinite amount of energy is required below 1400 Å due to the cut-off in window transmission and above 2450 Å due to the end of the photodissociation bands.

For comparison, the approximate ordinate position of the incoherent sources (plasma arcs) currently being used for photochemical ignition is also indicated. Assuming that (for these sources) the wavelength region effective in the photochemical ignition process is from 1400 Å to 1800 Å, the ordinate value (100 $\mu J/cm^2$) is determined by dividing the total UV energy in this region by the cross-sectional area of the window. However, this calculation assumes (without experimental verification) that the radiant energy in question is evenly distributed over the window area. Due to effects such as plasma pinch, this area will probably be smaller and, consequently, the effective energy per unit area higher than the value indicated. In any event, the UV energy per unit area required for photochemical ignition using an incoherent source is slightly higher but about the same order of magnitude as the minimum required by a VUV laser source.

F. COMMENTS ON LASER IGNITION TECHNIQUES

Photochemical ignition requires that radiant energy be provided in a particular, limited UV wavelength region (1400 Å to 2450 Å in the case considered above)[2]. When considering lasers as possible sources, three techniques should be explored; direct laser action in the region of interest, frequency multiplication of higher wavelength lasers, and two photon absorption effects. Each of these techniques is discussed below.

(i) Direct Laser Action

Direct laser action resulting in photochemical ignition would require operation in the 1400 Å to 1800 Å (vacuum ultraviolet region) range with the optimum region at about

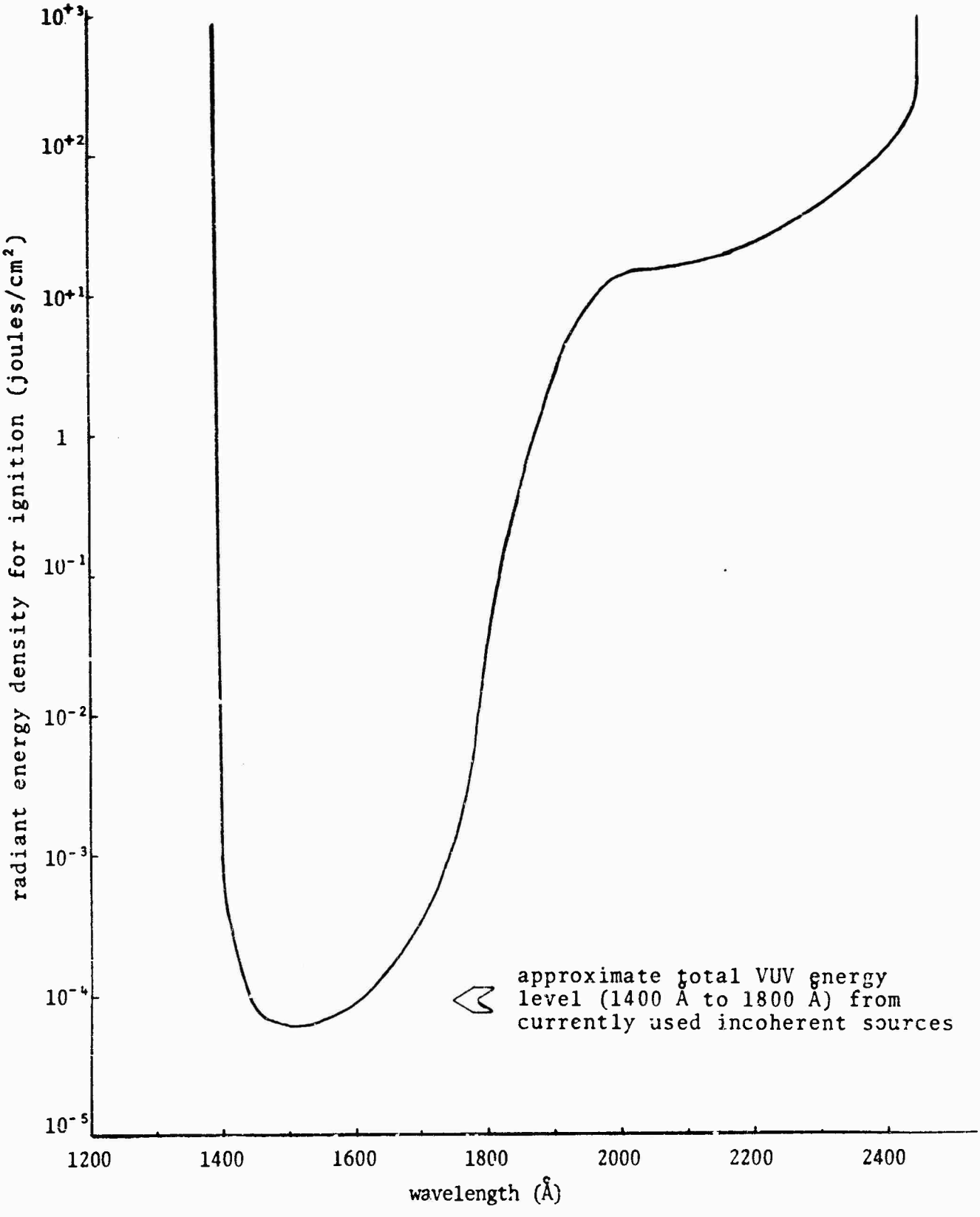

Figure 1 - Threshold Energy Requirements per Unit Window Area for Laser Ignition of a 300 torr, Stoichiometric, Hydrogen-Oxygen Mixture using a UV Grade Sapphire Window

1500 Å. The wavelength region from 1800 Å to 2450 Å is excluded due to the high energy density requirements, as indicated in Figure 1. Only three research groups (Naval Research Laboratory, International Business Machine and Lebedev Institute) have attempted working in this region[3,4]. The major obstacle is that the probability of spontaneous emission increases with the third power of the frequency, so that extremely high pump rates are needed to maintain a population inversion. All three groups use electron beam-impact excitation of a gas within the laser cavity and the primary lasing region is about 1600 Å or 1760 Å.

The NRL laser is characteristic of the VUV lasers currently available in the laboratory and has the following typical operating parameters[4,5]: wavelength - 1600 Å, output energy - 1 mJ, pulse time - 1 nsec, peak power - 1 MW, overall system efficiency - 10^{-4}. Using some of these values, the information provided by Figure 1 and an irradiation cross-sectional area of the same value as used in the photochemical ignition experiments[2] (0.317 cm^2) results in the calculation of an indicated laser input energy requirement of approximately 0.317 J. The most efficient plasma arc source (at the present time) requires an input of 0.25 J for photochemical ignition of the same reactant mixture. Consequently, in terms of input energy required for ignition, the laser and plasma arc sources compare favorably. And the efficiency of both methods will undoubtedly be improved.

Although the VUV laser can possibly compete with a plasma arc source on the basis of energy input required for photochemical ignition, it cannot compete with regard to other practical criteria. The VUV laser (1400 Å to 1800 Å) does not exist outside a few very fundamental research laboratories. In the laboratories where it does exist, it requires a complex support system and does not function reliably[5]. Judging from current VUV laser specifications[3,4], and from the characteristics of UV lasers[6], a VUV laser source would be approximately 1000 times larger, 10 to 100 times heavier and 100 to 1000 times more expensive than a plasma arc source. Consequently, major advancements in availability, complexity, reliability, size, weight and cost of VUV laser systems are necessary before photochemical ignition by direct laser action would be practical. In the meantime, practical plasma arc sources (incoherent) are currently available.

(ii) Frequency Multiplication

The nonlinear effects possible with high intensity light beams (lasers) provides techniques for doubling and tripling laser source frequencies[7].

Radiant energy in the 1400 Å to 1800 Å VUV region could be generated with a UV laser source in the 2800 Å to 3600 Å region by using a frequency doubler. About twelve commercially available UV lasers exist in this region[6], but the doublers are currently only laboratory type devices with efficiencies ranging from 0.1% to 10%[7,8]. Since the best available UV laser in the region of interest has a 1% efficiency (most are only 0.1% efficient), the overall efficiency for VUV radiant energy production by frequency doubling is currently less than 10^{-4}. A frequency doubled UV laser photochemical ignition system will therefore require an input energy level equal to or greater than a direct VUV laser system. Additionally, the complexity, size, weight, and cost of the ignition system would be further compromised.

A frequency tripling device would allow for the use of a laser source in the 4200 Å to 5400 Å region. However, the efficiency of the conversion device is extremely low[7] (on the order of 10^{-6}) and not commercially available. Thus, in this case, the magnitude of input energy required is objectionable in addition to the current complexity, size, weight, and cost limitations.

It appears that consideration of the use of frequency multiplication techniques for laser-photochemical ignition systems will require laser system improvements equivalent to those necessary to develop a direct VUV laser system.

(iii) Two Photon Absorption

Intense laser radiation can result in the absorption of light by a medium that normally absorbs light only at twice the laser frequency. In this process, two photons are absorbed simultaneously, resulting in an excited state species that would normally be produced by absorption of a single photon of twice the frequency[7]. An equation for the cross section σ^* for a two-photon excitation process can be written as follows[9],

$$\sigma^* = (e^2/mc^2)^2(\lambda^{*2}/n^2\Delta\nu)\ F^* \qquad (41)$$

where $e^2/mc^2 = 2.8 \times 10^{-13}$cm, n is the dielectric constant of the medium, λ^* is the radiant wavelength of the laser light, $\Delta\nu$ is the width of the absorption band around $2\nu^*$, and F^* is the incident photon flux. Combining equation (41) and equation (40) then gives an expression for the critical laser pulse energy E^*_{crit} as follows,

$$\frac{E^*}{A^*(t^*)^{1/2}} = \left[\frac{hc}{T^*\lambda^*}\right]\left[\frac{n(\Delta\nu)^{1/2}}{(e^2/mc^2)\lambda^*}\right]\left[\frac{n_{o\text{-}crit}}{2N_{O_2}}\right]^{1/2} \quad (42)$$

The primary oxygen absorption band of interest extends over the wavelength range 1290 Å to 1750 Å and results in dissociation as follows,

$$O_2(^3\Sigma_g^-) + h\nu \rightarrow \left[O_2(^3\Sigma_u^-)\right] \rightarrow O(^1D) + O(^3P) \quad (43)$$

For a two-photon absorption effect in this region, a laser source at a radiant wavelength of 3000 Å (λ^*) would be appropriate. The two-photon effect would then occur at about the mid-point of the wavelength region of interest and the width of the absorption band would be $3.05 \times 10^{14} sec^{-1}(\Delta\nu)$. In the 3000 Å region, the best window material would be quartz with a transmission of 0.923 (T^*) and, as before, a window area of 0.317 cm^2(A^*) will be assumed to allow for direct comparison with the experimental results obtained using incoherent sources. Laser energy and pulse time for two photon, photochemical ignition of a stoichiometric hydrogen-oxygen mixture at 300 torr pressure using a 3000 Å laser is then given by the following relation

$$E^*/(t^*)^{1/2} = 4.76 \times 10^3 \text{ joules/sec}^{1/2} \quad (44)$$

For laser pulse times ranging from 1 to 100 nsec, this equation indicates a pulse energy requirement of 0.15 to 1.5 joules. Of the twelve commercially available UV lasers suitable for this technique[6], only one meets the energy requirement expressed above. The others are lower by more than a factor of ten. However, the energy input required by the one suitable source is about 100 times that required by current incoherent sources. Consequently, consideration of the use of double photon absorption for photochemical ignition will also require a drastic improvement in laser source characteristics, particularly in energy conversion efficiency.

Finally, it should be noted that the use of two photon absorption for reaction initiation has been demonstrated for hydrogen-chlorine reaction[10]. Since the photodissociation band of chlorine occurs at higher wavelengths (2800 Å to 4000 Å) than that of oxygen, a more efficient, red laser light source (6943 Å ruby laser) could be employed. And an apparently successful reaction initiation was achieved when the source was operated in the Q-switched mode (higher intensity), indicating that a two-photon process was involved.

G. LASER RADIANT PENETRATION

The in-depth penetration of a laser pulse can be determined from equation (34), a typical result being illustrated in Figure 2. This figure compares the enhancement (penetration) effects produced in a 300 torr, stoichiometric, hydrogen-oxygen mixture when threshold photochemical ignition is achieved by laser radiation (1600 Å) and plasma arc radiation (1400 Å to 2450 Å). Both sources result in photochemical ignition near the radiant transmitting window (x = 0) but only the plasma arc source exhibits a simultaneous in-depth enhancement effect.

A similar enhancement effect to that achieved using the plasma arc source can be obtained by using an 1800 Å laser source of the same energy. However, as can be seen in Figure 2, this source does not have sufficient energy for photochemical ignition.

As a result, it would require two laser sources (if they existed) to perform the same function that is possible with one distributed light source (plasma arc).

H. DISSOCIATION WAVE VELOCITY

The time history of any radiant pulse effective in producing photodissociation results in the formation of a disturbance which can be referred to as a photodissociation wave. This is particularly evident in the situation where the radiant pulse is of sufficient intensity and duration to result in bleaching the medium behind the wave front. The rate of propagation of the photodissociation wave for a laser pulse can be determined by differentiation of equation (34). This results in the following,

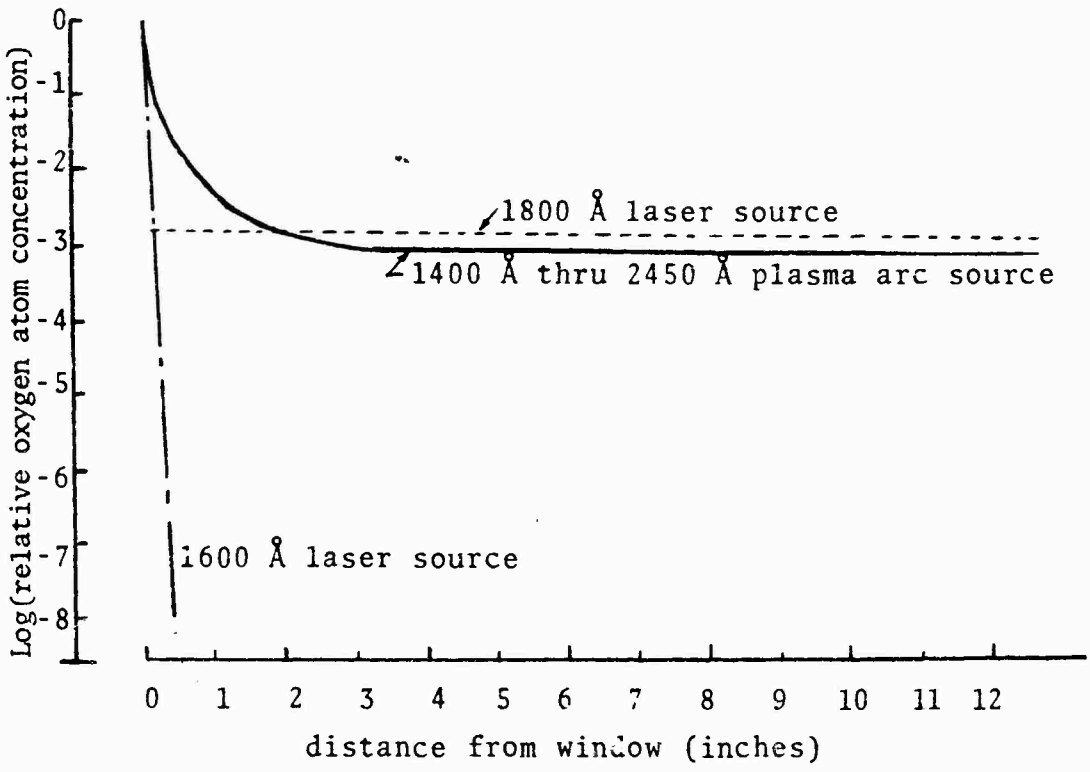

Figure 2 - Penetration of Photodissociation Effects (Ignition or Combustion Enhancement) for Various Radiant Sources in a 300 torr, Room Temperature, Stoichiometric Hydrogen-Oxygen Mixture Using a UV Grade Sapphire Window

$$dx/dt = \left[Ke^{Kt}/\alpha_o e^{\alpha_o x}\right]\left[(2N_{O_2}/n_o) - 1\right] \quad (45)$$

Combining this equation with equation (34) then gives

$$dx/dt = (K/\alpha_o)\left[e^{Kt}/(e^{Kt} - 1)\right] \quad (46)$$

where for $t \to 0$ $dx/dt \to 1/\alpha_o t = 1/\sigma^*_{O_2} N_{O_2} t$ (46a)

and for $t \to \infty$ $dx/dt \to K/\alpha_o = I^*T^*\lambda^*/N_{O_2} hc$ (46b)

The dissociation wave velocity defined by equation (46) does not depend on which point (degree of dissociation) of the wave is observed but only the time from the start of the irradiation pulse. For the initial part of the radiant pulse ($t \to 0$), the velocity is independent of the pulse intensity and depends only on the absorption coefficient, the concentration of the absorbers and the time. However, for times sufficiently long such that $\exp(Kt) >> 1$, the wave velocity approaches a constant, lower value. This value is independent of the absorption coefficient but does depend on the radiant intensity and wavelength--see equation (46b).

I. SUMMARY

It appears that the unique properties of laser sources are of no value for this application and that any practical use of lasers for photochemical ignition is at least one to two decades away, as indicated by the following summation:

- The principle and characteristics of photochemical ignition of combustion reactions can be studied with the currently available plasma arc sources (incoherent sources).
- Laser-photochemical ignition would require a vacuum ultraviolet laser source in the wavelength region 1400 Å to 1800 Å. Such lasers do not now exist outside a few scattered, fundamental research laboratories (IBM, NRL and Lebedev Institute). The existing systems are very complex and do not work reliably. Researchers at NRL have stated that

they get only about one successful lasing action a week and it appears that their program is being abandoned.

- The lowest wavelength lasers commercially available operate in the wavelength region 2650 Å to 3600 Å, which is inappropriate for photochemical ignition. However, if lasers in this region are an indication of what might eventually be available in the VUV, then compared to a plasma arc source they would be approximately 1000 times larger, 10 to 100 times heavier, and 100 to 1000 times more expensive. Frequency multiplication does not solve the problems.

- Disregarding the above two facts, laser sources would still be inappropriate since they cannot produce in-depth enhancement of combustion, as well as ignition. The enhancement effects are a result of absorption of higher wavelength radiation than that needed for ignition. Consequently, a distributed source (plasma arc) is more appropriate.

J. REFERENCES

1. Moor, N. J., Physical Chemistry, p. 820, Prentice-Hall, 1962.

2. Cerkanowicz, A. E., "Photochemical Initiation of Sustained Combustion in Unsensitized Gaseous Fuel-Oxygen Mixtures," Ph.D. Dissertation, Stevens Institute of Technology, June 1970.

3. Staff, "More Laser Power With Electron-Beam Control," Physics Today, Vol. 25, No. 1, pp. 17-19, 1972.

4. Elton, R. C., Waynant, R. W., Andrews, R.A., and Reilly, M. H., "X-Ray and Vacuum-UV Lasers, Current Status and Prognosis," NRL Report 7412, May 1972.

5. Elton, R. C., Private Communication, September 6, 1972.

6. Staff, "Commercial Laser Product Directory," Electro-Optical Systems Design, Vol. 4, No. 10, pp. 17-28, 1972.

7. Giordmaine, J. A., "The Interaction of Light with Light," Scientific American, Vol. 210, No. 4, 1964.

8. Dewey, C. F., "Excitation of Gases Using Wavelength-Tunable Lasers," Modern Optical Methods in Gas Dynamic Research, Plenum Press, pp. 221-270, 1971.

9. Kleinman, D. A., "Laser and Two-Photon Processes," Physics Review, Vol. 125, No. 1, pp. 87-88, 1962.

10. Porter, G., "Initiation of the Hydrogen-Chlorine Reaction by Red Laser Light," Nature, Vol. 215, pg. 502, 1967.

APPENDIX VIII

EXCITED STATE KINETICS

A. INTRODUCTION

The primary step in the process of photochemical initiation and enhancement of combustion in practical fuel-air mixtures has been experimentally determined to be the photodissociation of molecular oxygen[1]. This is accomplished by irradiation of room temperature, reactant mixtures with ultraviolet light below 2450 Å, various wavelength regions of which result in different photodissociation paths[2]. Absorption within the Herzberg band from 1950 Å to 2450 Å results in a forbidden transition, followed by rapid dissociation to two ground state atoms:

$$O_2(^3\Sigma_g^-) + h\nu \rightarrow O_2(^3\Sigma_u^+) \rightarrow 2O(^3P) \qquad (1)$$

Absorption in the Schumann-Runge bands from 1760 Å to 1950 Å results in excitation to one of the vibrational levels of the $O_2(^3\Sigma_u^-)$ state and subsequently provides two ground state atoms via a predissociation mechanism:

$$O_2(^2\Sigma_g^-) + h\nu \rightarrow O_2(^3\Sigma_u^-) \rightarrow O_2(^3\pi_u) \rightarrow 2O(^3P) \qquad (2)$$

In the Schumann continuum, 1290 Å to 1760 Å, the predissociation mechanism is replaced by direct dissociation to an excited and a ground state atom:

$$O_2(^3\Sigma_g^-) + h\nu \rightarrow O_2(^3\Sigma_u^-) \rightarrow O(^1D) + O(^3P) \qquad (3)$$

Photon energies below 1300 Å are suitable for direct photodissociation to two excited atoms:

$$O_2(^3\Sigma_g^-) + h\nu \rightarrow O(^2P) + O(^1S) \qquad (4)$$

The potential energy curves[3] and properties[4] of the various electronic states of molecular and atomic oxygen are summarized in Figure 1.

Previous analyses of photochemical combustion initiation and enhancement made no distinction between excited and ground state (normal) oxygen atoms[1,5,6]. As a result, all atoms were assumed to be in the ground state and "ground state kinetics" were used exclusively. Since in-depth enhancement of combustion has been shown to primarily depend on interaction with ultraviolet radiation above 1760 Å, and consequently involve only ground state oxygen atoms (equations 1 and 2), no problem results from the above assumption. Further, since application of the photochemical combustion effects involves the use of sapphire windows (due primarily to durability), all radiation below 1400 Å will be cut-off and consequently the $O(^2P)$ and $O(^1S)$ excited oxygen species (equation 4) will not be present. However, the $O(^1D)$ excited atomic oxygen species will be present in photochemical combustion initiations due to very strong absorption of ultraviolet light in the 1290 A (1400 A when sapphire windows are used) to 1760 Å wavelength region (equation 3). Since this is the wavelength region of prime importance for photochemical combustion initiation, the possible effect of having half of the generated oxygen atoms in the more reactive $O(^1D)$ excited state should not be ignored.

The purpose of this Appendix is to determine the role of the $O(^1D)$ atom in the combustion processes after its photodissociative production by reaction (4).

B. GENERAL COMMENTS ON EXCITED STATE CHEMISTRY

A major difference between photochemically activated and thermally activated systems is the resulting distribution of excited state species which enter into reaction. In photochemical processes the reacting system can acquire electronic energy as a result of the absorption of radiation, while the majority of thermal processes rarely involve electronically excited species, even at high temperatures[2]. Photochemical processes also provide for the production of vibrationally excited species, either by direct absorption or deactivation of electronically excited species, at vibrational levels significantly above the levels corresponding to thermal equilibrium (Maxwell-Boltzmann) of the reactants. In many cases, the acquisition of energy in the photochemical process is followed by dissociation of the excited species and the resulting production of extremely reactive atoms or radicals. The

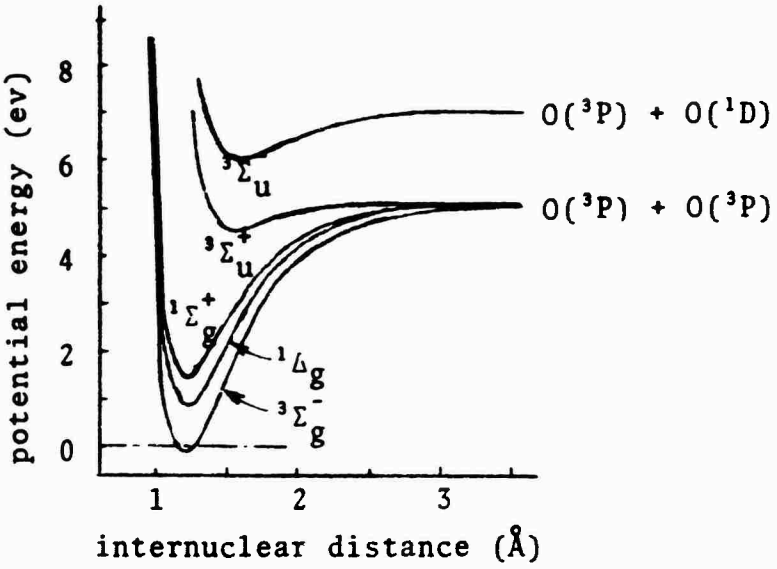

	Species	Relative Energy kcal/mole	(ev)	Dissociation Energy kcal/mole
Molecular:	$O_2(^3\Sigma_g^-)$	0	(0)	118.3
	$O_2(^1\Delta_g)$	22.5	(0.98)	95.7
	$O_2(^1\Sigma_g^+)$	37.5	(1.68)	80.6
	$O_2(^3\Sigma_u^+)$	102.1	(4.43)	15.1
	$O_2(^3\Sigma_u^-)$	141.1	(6.12)	21.3
Atomic:	$O(^3P)$	0	(0)	----
	$O(^1D)$	45.4	(1.967)	----
	$O(^1S)$	96.6	(4.188)	----

Figure 1 - Properties of the First Few Electronic States of Molecular and Atomic Oxygen[34]

highly energetic, non-equilibrium states thus reached are a function of the wavelength of the quantum absorbed and the temperature of the system, and they result in a reaction path that is entirely different from that followed as a result of thermal activation. This is evidenced in the subject work by the ability to initiate many combustion reactions at room temperature by photochemical means but not by thermal means[1,5,6].

In order to establish the reaction path and products of a photochemical reaction it is necessary to determine the fate of the excited state species. Subsequent to electronic or vibrational excitation by radiant absorption, the excited species will undergo one of the following changes[7]:

1. radiative decay (chemiluminescence)
2. dissociation
3. physical deactivation via transfer of energy to a colliding molecule (includes quenching)
4. chemical reaction

Clearly, the lifetime of the excited state undergoing a particular process is also a critical factor in determining the reaction path and the order of the kinetics. For example, the importance of excited states in connection with photochemistry lies in their ability to initiate secondary reactions. Since the secondary reactions have to compete with the spontaneous emission of the excited species (radiative decay), the most desirable states are those with long radiative lifetimes (metastable states).

C. ANALYSIS OF $O(^1D)$ REACTION KINETICS

Radiative decay or deactivation of the $O(^1D)$ species produced by photodissociation of oxygen in the wavelength region 1290 Å to 1760 Å is strongly spin-forbidden since a change in multiplicity would be required in going from the singlet first excited state to the triplet ground state[8]. In fact, the $O(^1D)$ species could be considered stable rather than metastable since the radiative lifetime is on the order of 10^{+2} sec[8]. Consequently, physical and chemical collision processes will dominate the kinetics, thus insuring that the energy of excitation will not be dissipated in an undesirable radiative process.

It is therefore clear that the $O(^1D)$ species must undergo a chemical reaction or a physical deactivation reaction where the energy must be transferred either into translation, vibration in the ground state, or production of excited electronic states. Which of these two processes occur depends on the type of species involved in the collision with the $O(^1D)$ species. And the dominant process in a given reactant system will depend on the reaction rate constants for that kinetic system. Unfortunately, the rate constant data available for $O(^1D)$ is largely qualitative with only a limited amount of quantitative results. Further, almost all the work on $O(^1D)$ kinetics has involved observation of final reaction products (and not direct observation of $O(^1D)$), followed by a calculation of $O(^1D)$ reaction rates based on an assumed series of reactions producing the final products. As a result, the reported literature values for particular $O(^1D)$ reaction rate constants is suspect in regard to the validity of the reaction scheme assumed in the data reduction as well as the experimental apparatus employed. In some cases, reported literature values for the same reaction differ by a considerable amount, thus further confirming the uncertainties involved in the measurements.

Notwithstanding the problems cited above (but keeping the qualifications in mind), a survey was made of the available $O(^1D)$ reaction rate data for the possible reactions of interest to combustion systems. References to a large part of the pertinent literature can be found in review papers written by McGrath and McGarvey (1967)[9] and by Noxon (1970)[10]. The paper by Noxon is also important in that it apparently represents the first successful measurement of reaction rates (it includes physical quenching) by direct observation of the $O(^1D)$ species and consequently may contain more reliable data. Results of the survey have been categorized in terms of the nature of the species colliding with the $O(^1D)$ species and are given below.

- Oxygen ($^3\Sigma_g^-$) Available in practical combustion systems as the primary oxidizing species. For the systems of interest, the $O(^1D)$ - $O_2(^3\Sigma_g^-)$ interaction is one of the most important considerations.

  The physical quenching interaction has been studied analytically and experimentally by a number of investigators[9,10] and is still one of the least determined $O(^1D)$ reactions. On the basis of theoretical reasoning, the quenching reaction is highly favored since both spin conservation and energy level matching (allowing exact

resonance exchange) are satisfied, providing for efficient physical deactivation along the indicated path;

$$O(^1D) + O_2(^3\Sigma_g^-, v'' = 0) \rightarrow O(^3P) + O_2(^1\Sigma_g^+, v'' = 2) \quad (5)$$

However, the reported experimental results regarding this reaction show a conflict of opinion, with a disagreement of about 10^3 for the rate constant. In general, the balance of the more recent and less questionable experiments indicate that the higher rate constant applies. Further, the results of Noxon's work[10], which is based on direct observation of $O(^1D)$, supports the claims favoring the higher rate constant. On the basis of the references reviewed the most probable reaction rate constant for reaction 5 will be taken as $5 \times 10^{-11} cm^3 particle^{-1} sec^{-1}$, with $5 \times 10^{-14} cm^3 particle^{-1} sec^{-1}$ representing the opposing view which claims reaction (5) is inefficient. It should be pointed out, that although the deactivation reaction succeeds in the removal of a chemically reactive species, $O(^1D)$, it results in the production of two other chemically reactive species, $O(^3P)$ and $O_2(^1\Sigma_g^+)$. Consequently, reaction (5) can be thought of as a branching of reactive species rather than a destruction, at least for combusting systems.

The only chemical reaction that might compete with reaction 5 would be the three body recombination process to produce ozone[9]

$$O(^1D) + O_2(^3\Sigma_g^-) + M \rightarrow O_3(^1A) + M^* \quad (6)$$

However, this reaction should be slower than the corresponding reaction with ground state oxygen atoms $O(^3P)$ since it is spin-forbidden and would require that an additional 45.4 kcal/mole (1.96 ev) of excitation energy be taken up by M in addition to the 25.5 kcal/mole normally taken up for the ground state oxygen atom reaction[9,11-13]. The formation of a triplet or electronically excited ozone molecule would be permitted by the selection rules. However, indications are that this state is short lived with a resulting formation of the initial reactant species[13]. Thus reaction (6) is

expected to be considerably slower than the reaction involving the ground state oxygen atom

$$O(^3P) + O_2(^3\Sigma_g^-) + M \rightarrow O_3(^1A) + M \qquad (7)$$

which has a rate constant on the order of 5×10^{-34} cm^6 particle^{-2}sec^{-1}, as previously discussed[1,5].

In summary, the removal of $O(^1D)$ species via interaction with ground state molecular oxygen can be considered to proceed entirely by the physical quenching path of reaction 5. Removal of $O(^1D)$ via the chemical path resulting in the formation of ozone, reaction 6, cannot compete unless the results indicating a slower rate for reaction 5 (by a factor of 10^3) are shown to be true or abnormally extreme pressures are involved in the combustion system. Following physical deactivation of $O(^1D)$ to $O(^3P)$, ozone formation can then take place in the normal manner as indicated by reaction (7).

- Nitrogen ($^1\Sigma_g^+$) Nitrogen is the most prevalent species present in air-breathing combustion systems. Chemical interaction with $O(^1D)$ species is possible and may have been observed in some liquid phase experiments[14]. However, no clear concept of the chemical reaction mechanism has evolved and it appears that the interaction should be dominated (especially in the gas phase) by the physical quenching mechanism[9,10,14].

  General agreement exists in the literature that nitrogen is an efficient quencher of $O(^1D)$ species with a rate constant on the same order of magnitude or somewhat faster than that for oxygen quenching (assuming the higher value for the later interaction). Yet no clear description of the reaction path has evolved except that the absence of available low lying electronic energy levels in nitrogen indicates that the $O(^1D)$ excitation energy would have to be converted into translational or vibrational energy. One possible mechanism which has been proposed is a direct resonance exchange between the $O(^1D)$ species and the seventh vibrational level of the electronic ground state of N_2.

$$O(^1D) + N_2(^1\Sigma_g^+, v'' = 0) \rightarrow O(^3P) + N_2(^1\Sigma_g^+, v'' = 7) \quad (8)$$

The difficulty in accepting this path lies in the fact that it is forbidden by spin conservation rules and the failure to detect the excited nitrogen molecules in experiments. A more plausible path has been proposed which involves the formation of an association complex of $N_2O^{\#}$ which then undergoes a radiationless transition to a predissociating state before sufficient energy is accumulated to allow dissociation to the original reactant species. The predissociative deactivation mechanism then results in the products $N_2(^1\Sigma_g^+)$ and $O(^3P)$ as follows

$$O(^1D) + N_2(^1\Sigma_g^+) \rightarrow N_2O^{\#} \rightarrow N_2(^1\Sigma_g^+) + O(^3P) \quad (9)$$

This process is also spin-forbidden but this may be negated by the occurrence of spin-orbit interaction. At pressures moderately higher than atmospheric, the reaction may involve ternary collisions

$$O(^1D) + N_2(^1\Sigma_g^+) + M \rightarrow N_2O^{\#} + M \rightarrow N_2(^1\Sigma_g^+) + O(^3P) + M \quad (10)$$

In summary, the primary $O(^1D)$ - $N_2(^1\Sigma_g^+)$ interaction is assumed to be a non-chemical deactivation via the formation of a short lived, $N_2O^{\#}$ complex followed by predissociation to ground state species[9]--reaction 9. The efficiency of $O(^1D)$ removal by nitrogen has been experimentally determined to be on the same order of magnitude as removal by oxygen and the rate constant (for reaction 9) will be taken as 5×10^{-11} cm^{3}particle^{-1}sec^{-1} [10].

- Hydrogen ($^1\Sigma_g^+$) Available in combustion systems as the primary fuel, pyrolysis product of higher hydrocarbon fuels or as an intermediary species of the reaction. Interaction between $O(^1D)$ and hydrogen is considered to be solely of a chemical nature with the possibility of physical deactivation being completely excluded[9,15,16].

The chemical reaction of $O(^1D)$ and hydrogen is expected to result in the production of vibrationally excited hydroxyl species up to the ninth vibrational level.

$$O(^1D) + H_2(^1\Sigma_g^+) \rightarrow OH^{\#}(^2\pi) + H(^2S) \qquad (11)$$

Insufficient excess energy is involved in this reaction to result in the production of electronically excited products. The excess energy of the $O(^1D)$ species does, however, result in its being more reactive toward hydrogen than the ground state $O(^3P)$ species. This is evidenced by the fact that the ground state $O(^3P)$-hydrogen interaction has an activation energy of about 8 kcal and the resulting reaction is about 1 kcal/mole endothermic, while the excited state $O(^1D)$-hydrogen interaction approaches a zero activation energy and can be exothermic by as high as 45 kcal/mole!

Assuming that zero activation energy is required for the reaction described by equation 11, then on the basis of a past survey on the ground state reaction rate[1], a rate constant of about 5×10^{-11} $cm^3 particle^{-1} sec^{-1}$ is indicated.

- Hydrocarbons Hydrocarbons are the primary fuel species in practical combustion devices. And as might be expected only an extremely limited amount of information exists in the literature on the interaction of $O(^1D)$ and hydrocarbon species[9,13,17,18]. Consequently, the only reliable statement concerning these reactions that can be made is: reaction paths involved will undoubtedly differ from the ground state $O(^3P)$ reaction path due to both the excess energy of the $O(^1D)$ species and the requirements of spin conservation.

  An illustration of the complexity inherent in $O(^1D)$-hydrocarbon interactions can be seen by considering the possible reaction paths for the simple methane species, which may include the following:

$$O(^1D) + CH_4 + M \rightarrow CH_3OH + M : \text{ insertion} \qquad (12)$$

$$O(^1D) + CH_4 \rightarrow CH_2O + H_2 : \text{ fragmentation or elimination} \qquad (13)$$

$$O(^1D) + CH_4 \rightarrow CH_3 + OH^{\#} \text{ : hydrogen abstraction} \quad (14)$$

$$O(^1D) + CH_4 \rightarrow O(^3P) + CH_4 \text{ : quenching} \quad (15)$$

All four reactions are possible and may in fact proceed via the formation of an excited, short lived alcohol $CH_3OH^{\#}$ intermediary ($ROH^{\#}$ in the general case). Experimental information on which of these reactions dominate is anything but complete and for the higher hydrocarbon other reaction paths may be involved.

As a result of the complexity of the $O(^1D)$-hydrocarbon interactions, the lack of available data, and the limited time available, no detailed summary will be made at this time regarding the $O(^1D)$-hydrocarbon interactions. It can, however, be assumed that the rate of chemical removal of $O(^1D)$ by methane is very efficient and on the same order of magnitude as chemical removal by hydrogen.

- Water(^1B) Unless the incoming air (for air-breathing combustion systems) contains moisture, the only source of water in most combustion systems is from the reaction products. Thus, it is expected that water species would not enter into the initiation process unless the incoming air contains moisture.

  With regard to interaction between $O(^1D)$ and water, the results are similar to those experienced for hydrogen except that even less literature information exists for adequate corroboration[9,13]. No physical deactivation reaction is expected and the chemical interaction is considered to result in the production of hydroxyl radicals, probably in the vibrationally excited state.

$$O(^1D) + H_2O(^1B) \rightarrow 2OH^{\#}(^2\pi) \quad (16)$$

As was the case with hydrogen, insufficient excess energy is involved in this reaction to result in the production of electronically excited species. However, the reaction is expected to proceed considerably faster (although not with zero activation energy) than the corresponding reaction for the ground state $O(^3P)$ atom. Further, the ground

state atom reaction is endothermic by about 16.8 kcal/mole while the excited state atom reaction can be exothermic by as much as 34 kcal/mole.

- Carbon Monoxide ($^1\Sigma$) Carbon monoxide will appear in combustion systems as a reaction intermediary or as a product species in the case of incomplete combustion. Its presence as a reaction intermediary would represent the best chance for interaction with excited $O(^1D)$ atoms.

  Most of the work reported on the $O(^1D)$-carbon monoxide physical deactivation interaction indicate that this process is relatively efficient[9,10,19]. It is not clear if this involves a two body reaction, a three body reaction or an intermediary species formation. A value on the order of 5×10^{-11} $cm^3 particle^{-1} sec^{-1}$ has, however, been generally assigned to the deactivation reaction assuming it proceeds via the two body mechanism.

$$O(^1D) + CO(^1\Sigma) \rightarrow O(^3P) + CO(^1\Sigma)^{\#} \qquad (17)$$

  Chemical reaction between the excited atom and carbon monoxide is spin-allowed, as opposed to the corresponding ground state atom reaction which is spin-forbidden[13]. No clear position has been taken regarding this reaction, with most studies citing the work of Jackson[20] as evidence that this reaction does not readily occur. His results are, however, contrary to the early results of this investigation[1,5] which has proven that reaction (17) must be rapid due to the demonstrated ability to photochemically initiate combustion in a dry oxygen-carbon monoxide mixture. Since carbon monoxide oxidation represents an intermediary stage present in all hydrocarbon-air reactions, the importance of this finding should not be minimized. Apparently, the only available results which agree with this finding are those of Clerc and Barat[21]. Their data indicate a reaction rate constant of about 10^{-11} $cm^3 particle^{-1} sec^{-1}$ and, notwithstanding the absence of verifying data, is recommended by this report for use in kinetics calculations involving reaction (17).

- Carbon Dioxide ($^1\Sigma$) Available as a product of combustion, carbon dioxide should not enter into the photochemical conditions of interest to this work. Its role appears (from the reference literature) to be almost solely that of a physical quencher of $O(^1D)$ species[9,10], although the path taken in the quenching process may be influenced by the possibility of incipient chemical bonding[9].

$$O(^1D) + CO_2(^1\Sigma) \rightarrow O(^3P) + CO_2(^1\Sigma) \qquad (18)$$

A rate constant of 3×10^{-12} $cm^3 particle^{-1} sec^{-1}$ (as determined by Noxon[10]) will be used for kinetics involving this reaction.

- Ozone (^1A) Ozone can be present as an ignition and/or combustion intermediary, particularly when oxygen atoms are available. Formation results from the very rapid three body reaction involving oxygen atoms, molecular oxygen and almost any third body. As shown previously[1], this represents an ozone formation mechanism that apparently cannot be neglected in photochemical ignition processes (see reaction 7). Chemical interaction between oxygen atoms and ozone had previously been neglected as being too slow in comparison to other reactions due to the low concentrations of ozone available in the ignition process. This, however, may not be true when the oxygen atom involved is in the excited (^1D) state due to a considerably higher reaction rate constant than for the ground state[9] (4×10^{-12} $cm^3 particle^{-1} sec^{-1}$ compared to 2×10^{-15} $cm^3 particle^{-1} sec^{-1}$)[22,13]. Additionally, there is a reasonable amount of evidence[9,22,23] that a chain mechanism with yields as high as 44 to 130 occurs in the $O(^1D)$-O_3 reaction sequence. A proposed chain mechanism is as follows;

$$O(^1D) + O_3(^1A) \rightarrow O_2(^3\Sigma_g^-) + O_2(^3\Sigma_u^+) \qquad (19)$$

$$O_2(^3\Sigma_u^+) + O_3(^1A) \rightarrow 2O_2(^3\Sigma_g^-) + O(^1D) \qquad (20)$$

If this is truely the case, then any ozone formed during the photochemical ignition process will be rapidly removed with subsequent formation of molecular oxygen. And, consequently, the role of ozone in the photochemical ignition kinetic is undoubtedly still of minor importance.

- Miscellaneous Some information on $O(^1D)$ interaction kinetics is also available for combustion intermediaries (such as OH, H_2O_2, C_2N_2), combustion products (such as NO, N_2O, NO_2), and other incidental species (such as Kr, Xe, He, Ar, NH_3, Cl_2, Br_2, F_2, HCl, SF_6). The review papers by McGrath and McGarvey[9] or Noxon[10] should be consulted for information concerning these species.

D. ANALYSIS OF ELECTRONICALLY EXCITED O_2 KINETICS

A direct consequence of some of the $O(^1D)$ kinetics [physical quenching by $O_2(^3\Sigma_g^-)$] is the formation of electronically excited $O_2(^1\Sigma_g^+)$ species which carries about 37.5 kcal/mole excitation energy. The energy transferred to electronic excitation of the diatomic species is not lost as it results in increasing the reaction rate of these species compared to their ground state reaction rates. As with the $O(^1D)$ species, the ensuing reactions must involve either physical quenching or chemical reaction (depending on the interacting species) since radiative transitions to the ground state are strongly forbidden for the excited species of interest.

The existing knowledge of excited molecular oxygen kinetics is in a more rudimentary state than that related to excited atomic oxygen kinetics. A detailed presentation will therefore be avoided. All relevant quenching reactions will be considered first with rates based on the survey presented by Noxon[10]. This will be followied by consideration of some possible chemical reaction kinetics of interest with rates based on the appropriate modification of ground state kinetic data.

- Physical Quenching Quenching rates of $O_2(^1\Sigma_g^+)$ by the following interactions are relatively well determined[10],

$$O_2(^1\Sigma_g^+) + O_2(^3\Sigma_g^-) \rightarrow 2O_2(^3\Sigma_g^-)^{\#} \qquad (21)$$

$$O_2(^1\Sigma_g^+) + N_2(^1\Sigma_g^+) \rightarrow O_2(^3\Sigma_g^-) + N_2(^1\Sigma_g^+)^\# \quad (22)$$

$$O_2(^1\Sigma_g^+) + CO_2(^1\Sigma) \rightarrow O_2(^3\Sigma_g^-) + CO_2(^1\Sigma)^\# \quad (23)$$

$$O_2(^1\Sigma_g^+) + CO(^1\Sigma) \rightarrow O_2(^3\Sigma_g^-) + CO(^1\Sigma)^\# \quad (24)$$

In the order presented, the quenching rates will be taken as 1.5×10^{-16}, 2.0×10^{-15}, 3.0×10^{-13}, 3.0×10^{-15} cm^3 $particle^{-1}sec^{-1}$, with the excess energy assumed to reside in vibration levels of the products.

- Chemical Reaction Chemical reaction rates of interest will be calculated by using the kinetic data available for ground state kinetics but with activation energies modified to account for the excess energy available in the excited species. For the $O_2(^1\Sigma_g^+)$ species the excess energy amounts 37.5 kcal/mole. However, even for a simple species such as hydrogen, very little information about the rate coefficients for the ground state reaction is available.

  For hydrogen, the most probable reaction is the formation of two hydroxyl radicals,

$$O_2(^1\Sigma_g^+) + H_2 \rightarrow 2OH \quad (24a)$$

although the following reaction may also occur,

$$O_2(^1\Sigma_g^+) + H_2 \rightarrow H + HO_2 \quad (24b)$$

Considerable difference of opinion exists concerning the activation energy for the ground state reaction corresponding to equation (24a), with estimates ranging from 45 kcal/mole to 70 kcal/mole[25-28]. This in turn results in an extremely large uncertainty in the kinetic rate for the reaction, extending from 3×10^{-13} $cm^3 particle^{-1}sec^{-1}$ on the

high side[26] to 4 x 10^{-34} $cm^3 particle^{-1} sec^{-1}$ on the low side[25], a variation of 21 orders of magnitude!! The corresponding reaction rates for ground state species would be 1 x 10^{-40} $cm^3 particle^{-1} sec^{-1}$ to 2 x 10^{-61} $cm^3 particle^{-1} sec^{-1}$, considerably slower than for the excited state reaction. Obviously the state of knowledge of the kinetics in question is seriously lacking.

The information available on methane-molecular oxygen interactions is also in the same questionable state[24,26,28] Rate constants for the reaction indicated below vary

$$O_2(^1\Sigma_g^+) + CH_4 \rightarrow CH_3 + HO_2 \qquad (25)$$

from 3.64 x 10^{-16} $cm^3 particle^{-1} sec^{-1}$ on the high side[26] to 6.64 x 10^{-31} $cm^3 particle^{-1} sec^{-1}$ on the low side[24]. However, even if the highest rate constant were used for reaction (25) it would still be an order of magnitude slower than the physical quenching reaction with the most prominent species in a fuel-air combustion system (see equation 22). The corresponding ground state reaction would be about 27 orders of magnitude slower.

For carbon monoxide, the reaction of interest would be given by the following,

$$O_2(^1\Sigma_g^+) + CO \rightarrow O_2 + O \qquad (26)$$

Based on the work and summary of Brokaw, et al[29] a reaction rate of 7 x 10^{-14} $cm^3 particle^{-1} sec^{-1}$ will be assumed for this reaction. The corresponding ground state reaction is indicated to be 27 orders of magnitude slower.

E. PHOTOCHEMISTRY OF H_2-N_2-O_2 SYSTEM

In order to obtain some idea of the role in the combustion reactions of electronically excited species [$O(^1D)$ and $O_2(^1\Sigma_g^+)$] produced as a result of the photochemical technique, the hydrogen-air system will be considered. The trends indicated can be related to those expected for a hydrocarbon-air system, consideration of which would require a more complicated kinetic scheme.

A proposed reaction mechanism for photochemical initiation and subsequent initiation kernel reactions is presented in Figure 2. Reaction a is the primary photochemical initiation reaction which results in ground and excited electronic states of atomic oxygen. Relevant excited atomic oxygen reactions are given by reactions b, c and d, while the important excited molecular oxygen (created via reaction b) reactions are given by e, f and g. It should be noted that considerable uncertainty exists in the choice of a reaction rate constant for reaction g. Ozone formation, which had previously been determined to be an important reaction, is accounted for by reaction h. Finally, the standard ground state kinetics for the hydrogen-air system is given by reactions i thru m. However, the last three reactions (k, l, m) will be neglected due to their low reaction rate constants.

Consideration will be given only to the time interval from the start of the radiant pulse to the point where either the initial reactant species concentrations change appreciably, or the intermediary species concentrations build to a level where intermediary-intermediary reactions become significant. Thus, it will be assumed that initial reactant species concentrations do not change and that intermediary-intermediary reaction can be neglected. These assumptions can be shown to be valid during the time of the radiant pulse and for a "short" time after the end of the radiant pulse.

Based on the proposed reaction mechanism and the above assumptions, the following equations can be written for the concentration (designated by []) changes of the excited state intermediaries O^* and O_2^*, and the normal intermediaries O, H, OH and O_3.

$$d[O^*]/dt = k_a[O_2]e^{-[O_2]\sigma x} - k_b[O_2][O^*] - k_c[N_2][O^*] - k_d[H_2][O^*] \qquad (27)$$

Figure 2 - Reaction Mechanism for Photochemical Initiation and the Subsequent Initial Combustion Phase of a H_2-N_2-O_2 System

Type	Reaction	Rate Constant ($cm^3 particle^{-1} sec^{-1}$)
initiation	(a) $O_2 + h\nu \rightarrow O + O^*$	photodissociation rate
O^* removal	(b) $O^* + O_2 \rightarrow O + O_2^*$	5×10^{-11} (5×10^{-14})
	(c) $O^* + N_2 \rightarrow O + N_2$	5×10^{-11}
	(d) $O^* + H_2 \rightarrow H + OH$	5×10^{-11}
O_2^* removal	(e) $O_2^* + O_2 \rightarrow 2O_2$	1.5×10^{-16}
	(f) $O_2^* + N_2 \rightarrow O_2 + N_2$	2×10^{-15}
	(g) $O_2^* + H_2 \rightarrow 2OH$	3×10^{-13} (4×10^{-34}) high uncertainty
O_3 formation	(h) $O + O_2 + M \rightarrow O_3 + M$	5×10^{-34} $cm^6 particle^{-2} sec^{-1}$
standard ground state kinetics for H_2-O_2 system (ref. 25, 26)	(i) $OH + H_2 \rightarrow H_2O + H$	1×10^{-14}
	(j) $O + H_2 \rightarrow OH + H$	2×10^{-16}
	(k) $H + O_2 \rightarrow OH + O$	2×10^{-24} slow
	(l) $OH + O_2 \rightarrow HO_2 + O$	1×10^{-47} slow
	(m) $O_2 + H_2 \rightarrow 2OH$	1×10^{-40} (2×10^{-61}) slow

Notes:
1. The excited state species $O(^1D)$ and $O_2(^1\Sigma_g^+)$ are designated by O^* and O_2^* respectively.
2. The proposed mechanism is assumed to apply only for times in which insufficient intermediary (radical) concentrations exist for the intermediary-intermediary interactions to be important compared to intermediary-reactant species interactions. During this time, it is also assumed that reactant species concentrations will not change significantly.

$$d[O_2^*]/dt = k_b[O_2][O^*] - k_e[O_2][O_2^*] - k_f[N_2][O_2^*] - k_g[H_2][O_2^*] \quad (28)$$

$$d[O]/dt = k_a[O_2]e^{-[O_2]\sigma x} + k_b[O_2][O^*] + k_c[N_2][O^*] - k_h[O_2][M][O] - k_j[H_2][O] \quad (29)$$

$$d[H]/dt = k_d[H_2][O^*] + k_i[H_2][OH] + k_j[H_2][O] \quad (30)$$

$$d[OH]/dt = k_d[H_2][O^*] + 2k_g[H_2][O_2^*] + k_j[H_2][O] - k_i[H_2][OH] \quad (31)$$

$$d[O_3]/dt = k_h[O_2][M][O] \quad (32)$$

$$\text{and } k_a \equiv I_o T\sigma/D' \quad (33)$$

where the following definitions apply at the wavelength(s) of interest

- σ = absorption cross section of molecular oxygen
- D' = energy absorbed in the photodissociation process
- T = window transmission
- I_o = instantaneous square wave irradiance at the window
- $[M]$ = total particle concentration
- x = distance into the reactant mixture measured from the window

The effects of diffusion and wall recombination are neglected for the purpose of these calculations.

- Excited O* Species

The solution of equation (27), with the initial condition of $[O^*] = 0$ at $t = 0$, is straightforward and results in an equation for excited O* concentrations of the following form

$$[O^*] = f_o k_a [O_2] e^{-[O_2]\sigma x} \tag{34}$$

where $$f_o \equiv (1 - e^{-A_3 t})/A_3 \tag{35}$$

$$A_3 \equiv k_b[O_2] + k_c[N_2] + k_d[H_2] \tag{36}$$

The maximum O* concentration is thus indicated to occur at the ignition site (x = 0) and at the end of the radiant pulse (t = τ). However, it can be shown that an equilibriun value corresponding to this maximum value is reached before the end of the radiant pulse. For equilibrium to be reached, the time dependency (contained in the f_o term) must be negligible. This can be expressed as follows

$$e^{-A_3 t_{e_0}} << 1 \tag{37}$$

Assuming that this inequality is satisfied by equating the indicated term to 0.01, the time to equilibrium (t_{e_0}) then is given by

$$t_{e_0} = 4.6/A_3 \tag{38}$$

For most systems of interest this time will be considerably less than the radiant pulse time. And in that event the peak excited state oxygen atom concentration is given by

$$[O^*]_{max} = k_a[O_2]/A_3 \tag{39}$$

- Ground State O Species

Combining equations (29) and (34) results in a differential equation for ground state oxygen atom species

$$d[O]/dt = (1 + f_o A_2) k_a [O_2] e^{-[O_2 \sigma x]} - B[O] \tag{40}$$

where $$A_2 \equiv k_b[O_2] + k_c[N_2] \tag{41}$$

$$B \equiv k_h[O_2][M] + k_j[H_2] \tag{42}$$

Solution of this differential equation for the initial condition of [O] = 0 at t = 0, gives the following expression for oxygen atom concentration

$$[O] = \{f_1 + (f_1-f_0)A_2/(A_3-B)\}\, k_a[O_2]e^{-[O_2]\sigma x} \qquad (43)$$

where $$f_1 \equiv (1-e^{-Bt})/B \qquad (44)$$

As with the excited oxygen atom species, the maximum ground state oxygen atom concentration is indicated to occur at the ignition site (x = 0) and the end of the radiant pulse. A photo-stationary state would not be reached until times (t_{e_2}) on the order of

$$t_{e_2} = 4.6/B \qquad (45)$$

which corresponds roughly to the end of the radiant pulse for the kinetics of interest.

- Excited O_2^* Species

Combining equations (28) and (34) results in a differential equation for excited oxygen molecule species

$$d[O_2^*]/dt = f_o A_1 k_a[O_2]e^{-[O_2]\sigma x} - C[O_2^*] \qquad (46)$$

where $$A_1 \equiv k_b[O_2] \qquad (47)$$

$$C \equiv k_e[O_2] + k_f[N_2] + k_g[H_2] \qquad (48)$$

Solution of this differential equation for the initial condition of $[O_2^*] = 0$ at t = 0, gives the following expression for the excited oxygen molecule concentration.

$$[O_2^*] = \{(f_2-f_o)A_1/(A_3-C)\}k_a[O_2]e^{-[O_2]\sigma x} \qquad (49)$$

where $$f_2 \equiv (1-e^{-ct})/C \qquad (50)$$

A photo-stationary state would not be reached until times (t_{e_2}) on the order of

$$t_{e_2}) = 4.6/C \tag{51}$$

which would not be reached before the end of the radiant pulse for the kinetics of interest. Consequently, the maximum excited oxygen molecule concentration will be reached at the ignition site at the end of the radiant pulse.

- Ground State O_3 Species

Substitution of equation (43) into equation (32) provides a simple differential equation which can easily be solved for the initial condition $[O_3] = 0$ at $t = 0$, resulting in the following expression for the ozone concentration

$$[O_3] = \{F_1 + (F_1-F_0)A_2/(A_3-B)\}(k_h[O_2][M])k_a[O_2]e^{-[O_2]\sigma x} \tag{52}$$

where $F_0 \equiv (t-f_0)/A_3$ (53)

$F_1 \equiv (t-f_1)/B$ (54)

Once again, it can be shown that the maximum concentration during irradiation is achieved at the end of the radiant pulse. The time to an equilibrium state has not been derived.

- Other Intermediary Species

A relatively simple differential equation can be obtained for the time history of the sum of hydrogen atom and hydroxyl species concentration by adding equations (30) and (31) followed by substitution of equations (34), (43) and (49). Solution for the combined [H + OH] concentrations with the initial condition that [H + OH] = 0 at t = 0 results in the following expression

$$d[H + OH]/dt = (Q_1 + Q_2 + Q_3)2k_a[O_2]e^{-[O_2]\sigma x} \tag{55}$$

where $Q_1 \equiv F_0k_d[H_2]$ (56)

$$Q_2 \equiv \{F_0+(F_1-F_0)A_2/(A_3-B)\}k_j[H_2] \quad (57)$$

$$Q_3 \equiv \{(F_2-F_0)A_1/(A_3-C)\}k_g[H_2] \quad (58)$$

and $$F_2 \equiv (t-f_2)/C \quad (59)$$

The maximum value for [H + OH] concentration occurs at the end of the radiant pulse.

- Specific Cases

A number of numerical solutions to the above equations were obtained, corresponding to various conditions of pressure, stoichiometry, diluent concentration and assumed reaction rate chemistry. In obtaining these solutions, the following parameters were kept constant at their indicated values,

$T\sigma = 10.51 \times 10^{-16}$ cm^2 Å/molecule (in the ignition wavelength region)

$\tau = 10^{-4}$sec (square wave pulse assumed)

$A = 0.323$ cm^2 (corresponds to window diameter of 0.25")

$E = 1$ µj/100 Å @ 1500 Å (unit pulse energy)

$D' = 5.1$ ev $= 8.18 \times 10^{19}$ joules/molecule

$T = 300°K$ (room temperature)

consequently

$I_o = E/A\tau = 3.1 \times 10^{-4}$ joules/cm^{2}sec Å (UV pulse intensity)

$k_a \equiv I_o T\sigma/D' = 0.3976$ sec^{-1}

Additionally, since the maximum concentration of any species always occurred at the end of the radiant pulse ($t = \tau$) and near the window ($x = 0$), all tabulated values were calculated for this condition.

The results presented in Table 1 are for a stoichiometric hydrogen-oxygen system ($2H_2 + O_2$) and indicate the effect of pressure and assumed excited state kinetics on intermediary species concentrations generated during ultraviolet irradiation. Four reaction kinetic cases were considered;

Case A - all the excited state kinetics indicated in Figure 2 occur and the highest value of the indicated rate constants apply ($k_b=5x10^{-11}$, $k_g=3x10^{-13}$).

Case B - no positive contribution of electronically excited molecular oxygen, Reaction g, to the formation of intermediaries occurs ($k_b=5x10^{-11}$, $k_g=4x10^{-34} \cong 0$).

Case C - the formation of electronically excited molecular oxygen, Reaction b, is inefficient and, consequently, this species is of minimal consequence in the kinetics ($k_b=5x10^{-14}$, $k_g=3x10^{-13}$).

Case D - neglects the presence of excited state species and assumes only ground state kinetics (k_b thru $k_g = 0$).

Table 2 compares the concentration of intermediaries generated by ultraviolet absorption, with and without excited state kinetics, for various stoichiometries of hydrogen-oxygen-nitrogen mixtures from stoichiometric to fuel-lean. Finally, Figure 3 graphically presents the results of Table 2 for lean fuel-air mixtures.

F. DISCUSSION

Although disagreement exists regarding the rate constant for most excited state reactions, an indication of the importance of such reactions can be established. This is demonstrated by the consideration of a hydrogen-oxygen-nitrogen kinetic system with the inclusion of the possible kinetics for the appropriate excited states of atomic and molecular oxygen. In this system, the combustion initiation process, or kernel, will involve the following intermediary species - O, O^*, O_2^*, O_3, OH and H.

For the photochemical initiation conditions of interest, the equations in the previous section indicate that a photostationary state (steady state) of excited state species is achieved during the time of irradiation. Table 1 indicates that for stoichiometric mixtures the concentrations achieved for O^* and O_2^* are on the order of 10^9 particles/cm^3 and 10^{11} particles/cm^3, respectively, and are essentially independent of the mixture pressure. The concentrations of other intermediary species are on the order of 10^{13} to 10^{14} particles cm^3. For fuel-lean mixtures, somewhat higher O_2^* concentrations are achieved, see Table 2.

Table 1 - Effect of Excited State Kinetics on Intermediary Species Concentrations for a Stoichiometric Hydrogen-Oxygen System at Various Pressures (1)

Case	Pressure (torr)	(particles/cm^3)						
		[O]	[O*] (3)	[O_2^*] (3)	[O_3]	[OH+H]	[Σ] (2)	[Σ] - [O_3]
A	~0	1.67×10^{13}	2.65×10^{9}	2.21×10^{11}	1.50×10^{11}	2.53×10^{13}	4.23×10^{13}	4.22×10^{13}
B	30	1.67×10^{13}	2.65×10^{9}	4.24×10^{12}	1.50×10^{11}	1.72×10^{13}	3.40×10^{13}	3.39×10^{13}
C	30	1.25×10^{13}	3.97×10^{9}	3.31×10^{8}	1.13×10^{11}	2.56×10^{13}	3.83×10^{13}	3.82×10^{13}
D	30	2.50×10^{13}	0	0	2.27×10^{11}	3.78×10^{11}	2.56×10^{13}	2.54×10^{13}
A	300	8.26×10^{13}	2.65×10^{9}	2.21×10^{11}	8.03×10^{13}	2.67×10^{14}	4.30×10^{14}	3.50×10^{14}
B	300	8.26×10^{13}	2.65×10^{9}	2.56×10^{13}	8.03×10^{13}	1.83×10^{14}	3.46×10^{14}	2.66×10^{14}
C	300	6.20×10^{13}	3.97×10^{9}	3.31×10^{8}	6.02×10^{13}	2.64×10^{14}	3.87×10^{14}	3.26×10^{14}
D	300	12.39×10^{13}	0	0	12.05×10^{13}	2.00×10^{13}	2.65×10^{14}	1.44×10^{14}
A	760	4.22×10^{13}	2.65×10^{9}	2.21×10^{11}	3.75×10^{14}	6.65×10^{14}	10.80×10^{14}	7.05×10^{14}
B	760	4.22×10^{13}	2.65×10^{9}	1.01×10^{14}	3.75×10^{14}	4.54×10^{14}	8.71×10^{14}	4.96×10^{14}
C	760	3.16×10^{13}	3.97×10^{9}	3.32×10^{8}	2.82×10^{14}	6.62×10^{14}	9.76×10^{14}	6.94×10^{14}
D	760	6.33×10^{13}	0	0	5.63×10^{14}	3.70×10^{13}	6.63×10^{14}	1.00×10^{14}

Case A - excited state chemistry contributes ($k_b=5\times10^{-11}$, $k_g=3\times10^{-13}$)

Case B - neglects the positive value of O_2^* ($k_b=5\times10^{-11}$, $k_g=4\times10^{-34}\approx 0$)

Case C - neglects the formation of O_2^* ($k_b=5\times10^{-14}$, $k_g=3\times10^{-13}$)

Case D - neglects all excited state kinetics (k_b thru k_g = 0)

Notes: 1 - for details on the parametric condition set in the compilation of Table 1, see associated text.

2 - for case B, the [Σ] does not include the [O_2^*] concentration as the ultimate fate of this species is destruction without contribution to the total effective intermediary concentration.

3 - for the conditions considered, these values represent steady state concentrations (i.e., a photostationary state in O* and O_2^* is achieved).

Table 2 - Effect of Excited State Kinetics on Intermediary Species Concentrations for Various Hydrogen-Oxygen-Nitrogen Stoichiometries

Stoichiometry	Case	(particles/cm^3)						
		[O]	[O*]	[O_2^*]	[O_3]	[OH+H]	[Σ]	[Σ]-[O_3]
$2H_2+O_2$	A	8.26×10^{13}	2.65×10^{9}	2.21×10^{11}	0.80×10^{14}	2.67×10^{14}	4.30×10^{14}	3.50×10^{14}
	D	12.39×10^{13}	0	0	1.20×10^{14}	2.00×10^{13}	2.65×10^{14}	1.44×10^{14}
$2H_2+4.76O_2$	A	13.41×10^{13}	5.63×10^{9}	2.28×10^{12}	3.22×10^{14}	5.467×10^{14}	10.05×10^{14}	6.83×10^{14}
	D	15.70×10^{13}	0	0	3.77×10^{14}	1.29×10^{13}	5.47×10^{14}	1.70×10^{14}
$2H+10\ O_2$	A	8.04×10^{13}	6.63×10^{9}	5.51×10^{12}	2.35×10^{14}	6.28×10^{14}	9.49×10^{14}	7.14×10^{14}
	D	16.08×10^{13}	0	0	4.71×10^{14}	7.90×10^{12}	6.40×10^{14}	1.69×10^{14}
$2H_2+(O_2+3.76N_2)$	A	6.78×10^{13}	1.16×10^{9}	0.95×10^{11}	2.54×10^{13}	5.25×10^{13}	1.46×10^{14}	1.20×10^{14}
	D	7.94×10^{13}	0	0	2.98×10^{13}	4.96×10^{12}	1.14×10^{14}	0.84×10^{14}
$2H_2+2(O_2+3.76N_2)$	A	8.21×10^{13}	1.38×10^{9}	2.24×10^{11}	3.73×10^{13}	4.81×10^{13}	1.67×10^{14}	1.30×10^{14}
	D	8.99×10^{13}	0	0	4.04×10^{13}	3.44×10^{12}	1.34×10^{14}	0.93×10^{14}
$2H_2+5(O_2+3.76N_2)$	A	9.33×10^{13}	$1.54\ 10^{9}$	6.03×10^{11}	4.80×10^{13}	3.88×10^{13}	1.81×10^{14}	1.33×10^{14}
	D	9.71×10^{13}	0	0	4.99×10^{13}	1.67×10^{12}	1.49×10^{14}	0.99×10^{14}
$2H_2+10(O_2+3.76N_2)$	A	9.79×10^{13}	1.60×10^{9}	11.625×10^{11}	5.25×10^{13}	3.24×10^{13}	1.84×10^{14}	1.31×10^{14}
	D	9.99×10^{13}	0	0	5.35×10^{13}	0.89×10^{12}	1.54×10^{14}	1.01×10^{14}

Case A - excited state chemistry contributes
Case D - neglects all excited state chemistry
Note - for details on the parametric conditions set in the compilation of Table 2, see associated text.

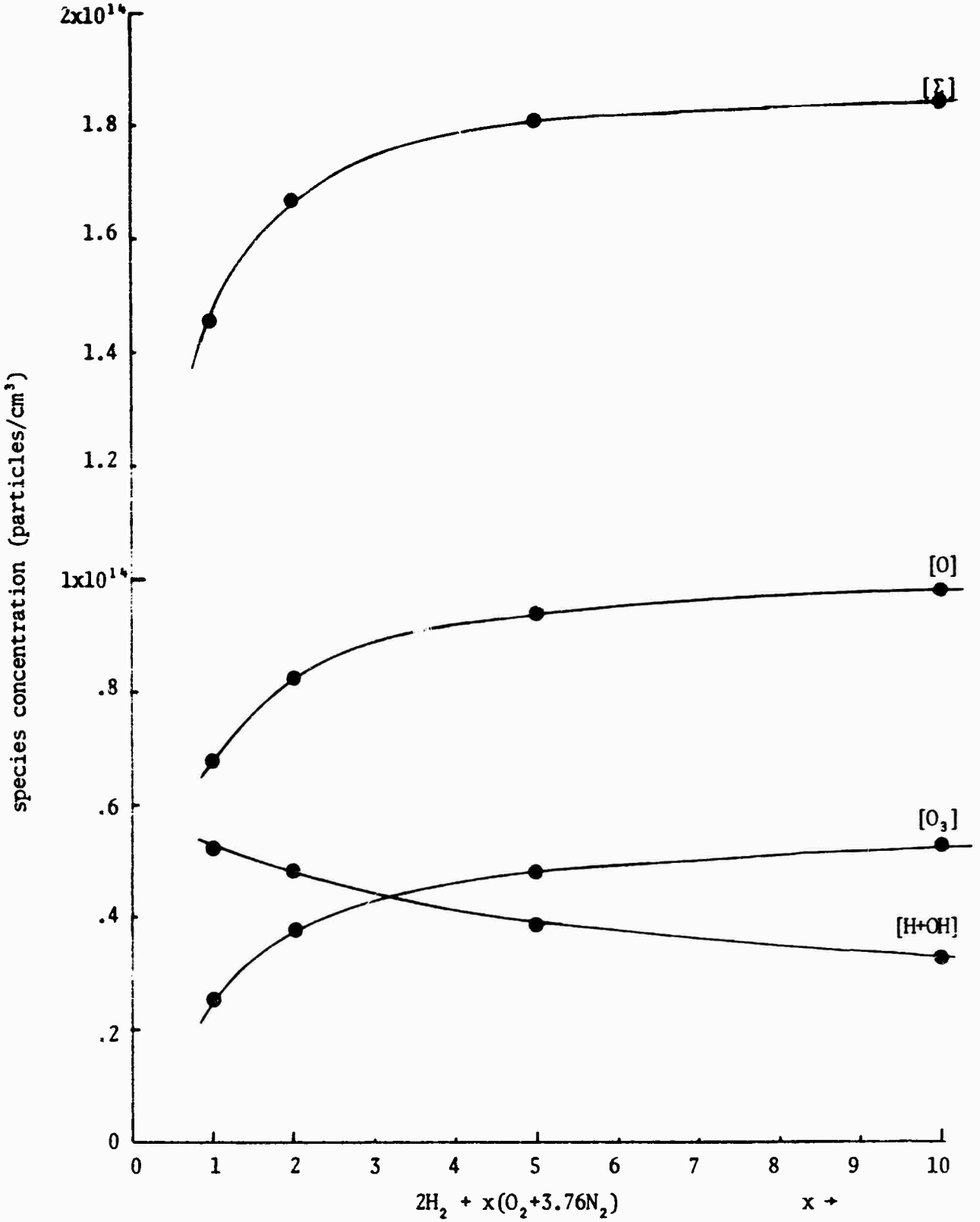

Figure 3 - Intermediary Species Concentrations vs Increasing Air Dilution of a Hydrogen-Air Reactant Mixture
($[\Sigma]=[O]+[O^*]+[O_2^*]+[O_3]+[OH]+[H]$)

While the steady state concentrations achieved for O^* and O_2^* are two to five orders of magnitude below other intermediary concentrations, the presence or availability of these species has a pronounced effect on the ignition kinetics. This can be illustrated by comparing cases A thru D in Table 1. If the reactivity of O_2^* with fuel species (Reaction g, Figure 2) is considered to be inefficient or comparable to the ground state then the results of case B apply. In this circumstance, the total concentration of active intermediaries (indicated by $[\Sigma]$) produced in the ignition kernel is reduced about 20% below that possible if the excited state kinetics were considered effective (case A). Thus the contribution of O_2^* species to the ignition process is effective and must be considered unless the slower rate constants for Reaction g, indicated in some of the literature, are eventually substantiated.

The importance of O_2^* species can be further demonstrated by the conditions considered in case C. In this case, the O_2^* species are considered to be very reactive with fuel species but the O_2^* formation process (Reaction b, Figure 2) is assumed to be somewhat inefficient. The resulting effect is a reduction of the total intermediary concentration by about 10%.

Finally, if the presence of O^* species is neglected (and consequently O_2^* species as well), the results of case D would apply. A comparison between this case of ground state chemistry and the excited state chemistry (case A) indicates that a loss of about 40% in total intermediary species in the ignition kernel occurs when excited state species are not involved in the combustion process.

A consideration which should eventually be explored further is the role of ozone species in the kinetic scheme. For the purpose of determining the importance of electronically excited species, details on the ozone kinetics were disregarded. And the concentration of ozone species was included in the total intermediary species count. A more detailed consideration of ozone kinetics would have complicated the calculations presented by accounting for photodissociation, thermal decomposition, reformation of atomic and molecular oxygen, and interaction with fuel species. The general aspects of the results would, however, have been the same since loss of ozone by these reactions results in the formation of a replacement intermediary species, such as atomic oxygen.

An exception to this possibility would be a chain reaction sequence as indicated by equations 19 and 20, wherein the net result is the loss of ozone and the formation of ground state molecular oxygen species. In this case, ozone formation represents a termination path in the intermediary species kinetic scheme and the ozone concentration

should therefore not be included in the total intermediary concentration. The last column in Tables 1 and 2 indicate the results in this situation. Referring to Table 1, it can be seen that the presence of excited species becomes even more important, as the total intermediary concentration would drop between 40 to 85% if only ground state kinetics were considered. It is therefore clear that the presence of excited state species contributes significantly to the total intermediary species concentration, regardless of the role of ozone species in the kinetic scheme.

In addition to the quantitative effect on intermediary species concentration, the presence of excited state kinetics qualitatively alters the intermediary species type present in the ignition kernel. Without excited state species, the major contribution to the intermediaries would be O and O_3 in proportions which depend on the mixture pressure, with minimal (order of magnitude lower in concentration) contribution from OH and H species. However, if excited state kinetics are involved, the OH and H species represent a major contribution to the total intermediary concentration at all pressures, in addition to the O and O_3 species.

The effect of excited state chemistry on the total intermediary species concentration in fuel lean hydrogen-oxygen and hydrogen-air mixtures is indicated by the results presented in Table 2. As before, it is apparent that excited state species contribute significantly to the formation of intermediaries and should therefore not be neglected in fuel-lean kinetic calculations. Further, the results indicate that the total intermediary species concentration generally increases as the mixture becomes more fuel lean (see Figure 3, for example). Consequently, the ignition kernel will not suffer a depletion of intermediaries as the mixture becomes more fuel lean and hence the ignition energy required will not necessarily increase.

G. SUMMARY

The following statements provide an abridgment of the key results of this Appendix:

- The presence of electronically excited state species [$O(^1D)$ and $O_2(^1\Sigma_g^+)$] created as a result of the photochemical ignition technique cannot be neglected in the pertinent kinetic calculations. This has been shown to be the case even when the wide variation in literature values for the kinetic rate constants of these species is taken into account.

- A major factor leading to the importance of the $O(^1D)$ and $O_2(^1\Sigma_g^+)$ species results from the radiative decay to the ground state being spin forbidden. Consequently, the excitation energy can only be lost via collisional transfer with another species in the reactant system.

- A better knowledge of the $O_2(^1\Sigma_g^+)$-fuel kinetic rate constant is needed.

- A better knowledge of the $O_2(^1\Sigma_g^+)$ formation (or the $O(^1D)$ collision de-excitation with molecular oxygen) rate constant is needed.

- A photostationary state in $O(^1D)$ and $O_2(^1\Sigma_g^+)$ species is achieved with respective concentrations on the order of 10^9 particles/cm^3 and 10^{11} particles/cm^3 for typical photochemical combustion initiation conditions.

- The character of the ignition kernel is changed when excited state kinetics is involved by virtue of the fact that significant concentrations of OH and H species are formed in addition to the O and O_3 species which are dominant species when ground state kinetics prevail.

- The kinetics of the photochemical combustion initiation process is such that the use of leaner fuel-air mixtures does not result in the depletion of intermediary species in the ignition kernel. Thus, this indicates that the ignition energy required by the photochemical technique will not be seriously affected by the use of fuel lean mixtures.

H. REFERENCES

1. Cerkanowicz, A. E., "Photochemical Initiation of Sustained Combustion in Unsensitized Gaseous Fuel-Oxygen Mixtures," Ph.D. Dissertation, Stevens Institute of Technology, June 1970.

2. Calvert, J. G., and Pitts, J. N., Photochemistry, John Wiley and Sons, 1966.

3. Herzberg, G., Molecular Spectra and Molecular Structure -I. Spectra of Diatomic Molecules, D. Van Nostrand Co., 1950.

4. Johnston, H. S., "Gas Phase Reaction Kinetics of Neutral Oxygen Species," NSRDS-NDS 20, 1968.

5. Cerkanowicz, A. E., Levy, M. E., and McAlevy III, R. F., "Photochemical Ignition of Gaseous Fuel-Oxidizer Mixtures at Subatmospheric Pressures," Final AFOSR Scientific Report No. 70-1664, April 1970.

6. Cerkanowicz, A. E., "Photochemical Enhancement of Combustion and Mixing in Supersonic Flows," Interim AFOSR Scientific Report No. 73-0563, March 1972.

7. Laidler, K. J., "The Chemical Kinetics of Excited States," Oxford at the Clarendon Press, 1955.

8. Allen, C. W., Astrophysical Quantities, The Athlone Press, 1963.

9. McGrath, W. D., and McGarvey, J. J., "The Production, Deactivation and Chemical Reactions of $O(^1D)$ Atoms," Planet Space Science, Vol. 15, pp. 427 to 455, 1967.

10. Noxon, J. F., "Optical Emission from $O(^1D)$ and $O_2(b^1\Sigma_g)$ in Ultraviolet Photolysis of O_2 and CO_2," J. Chem. Phys., Vol. 52, No. 4, pp. 1852 to 1873, 1970.

11. Sullivan, J. O., and Warneck, P., "Reactions of ^1D Oxygen Atoms. III. Ozone Formation in the 1470-Å Photolysis of O_2," J. Chem. Phys., Vol. 46, No. 3, pp. 953 to 959, 1967.

12. Meaburn, G. M., Perner, D., LeCalve, J., Bourene, M., "A Pulsed-Radiolysis Study of Atomic Oxygen Reactions in the Gas Phase," J. Phys. Chem., Vol. 72, No. 11, pp. 3920 to 3925, 1968.

13. Leighton, P. A., Photochemistry of Air Pollution, Vol. 9 of: Physical Chemistry--A Series of Monographs, p. 122, 1961.

14. DeMore, W. B., and Raper, O.F., "Reactions of $O(^1D)$ with Nitrogen," J. Chem. Phys., Vol. 37, p. 2048, 1962.

15. McGrath, W. D., and Norrish, R. W., "Studies of the Reactions of Excited Oxygen Atoms and Molecules Produced in the Flash Photolysis of Ozone," Proc. Royal Soc. A254, pp. 317 to 326, 1960.

16. Basco, N., and Norrish, R. W., "The Production of Vibrationally Excited Hydroxyl Radicals Under Isothermal Conditions by Flash Photolysis," Proc. Royal Soc. A260, pp. 293 to 303, 1961.

17. DeMore, W. B., and Raper, O. F., "Reaction of $O(^1D)$ with Methane," Vol. 46, No. 7, pp. 2500-2505, 1967.

18. Yamazaki, H., and Cventanovic, R. J., "Collisional Deactivation of the Excited Singlet Oxygen Atoms and Their Insertion into the CH Bonds of Propane," J. Chem. Phsy. Vol. 41, pp. 3703-3710, 1964.

19. DeMore, W. B., "$O(^1D)$ Quencning Efficiency of O_2 Relative to Other Gases," J. Chem. Phys., Vol. 52, No. 8, pp. 4309-4310, 1970.

20. Jackson, W. F., "A Study of the Photochemical Carbon Monoxide Oxidation," J. Am. Chem. Soc., Vol. 56, pp. 2631-2635, 1934.

21. Baulch, D. L., Drysdale, D. D. and Lloyd, A. C., "High Temperature Reaction Rate Data - No. 1," Leeds, England, 1968.

22. Snelling, D. R., Baiamonte, V. D., and Bair, E. J., "Decomposition of Ozone by $O(^1D)$," J. Chem. Phys., Vol. 44, No. 11, pp. 4137-4144, June 1966.

23. Volman, D. H., "Photochemical Gas Phase Reactions in the Hydrogen-Oxygen System," Advances in Photochemistry, Vol. 1, pp. 43 to 82, 1963.

24. Mayer, S. W. and Schieler, L., "Computed Rate Constants and Activation Energies for the Abstraction Reaction of Ground-State and Excited Oxygen with Fuels," Western States Combustion Institute, Paper No. 68-2, 1968.

25. Bahn, G. S., Reaction Rate Compilation for the H-O-N System, Gordon and Breach - Science Publishing, 1968.

26. Bowman, C. T., "Application of Kinetics Calculations to the Interpretation of Shock Tube Data," Western States Combustion Institute, Paper No. 68-50, 1968.

27. Asaba, T., Gardiner, W. C., and Stubbeman, R. F., "Shock-Tube Study of the Hydrogen-Oxygen Reaction," Comments Section p. 302, Tenth Symposium on Combustion, 1965.

28. Higgin, R. M., and Williams, A., "A Shock-Tube Investigation of the Ignition of Lean Methane and n-Butane Mixtures with Oxygen," Twelfth Symposium on Combustion, pp. 579 to 590, 1969.

29. Brabbs, T. A., Belles, F. E., and Brokaw, R. S., "Shock-Tube Measurements of Specific Reaction Rates in the Branched-Chain H_2-CO-O_2 System," Thirteenth Symposium on Combustion, pp. 129 to 136, 1971.

APPENDIX IX

COMBUSTION INSTABILITY PHENOMENA

A. DISCUSSION

Advanced phase plane analysis schemes (C. F. Yang and B. F. Gray) have shown that for combustible mixtures where a negative temperature coefficient exists, instabilities (cool flames) can result[1-3]. The temperature-species concentration plane then has three regions associated with the status of the mixture, a stable region of non-combustion, an oscillatory combustion region and a region of "hot" rapid reaction. Such a system is depicted in Figure 1.

Starting from the stable point (A), if the temperature of the mixture is increased only to the point where the first separatrix (line EBF, through saddle point B) is crossed, rapid combustion will not occur. The mixture will be "trapped" in a region of slow burning and exhibit an oscillatory combustion behavior about a limit cycle curve. Consequently, this establishes a possible mechanism whereby oscillations can be experienced in practical combustors. To avoid this problem, the heat input to the unburned mixture must be sufficient to increase the temperature above the second separatrix (line GDH, through saddle point D).

A possible alternative solution for the establishment of rapid combustion and the avoidance of oscillatory behavior is use of the photochemical technique. Qualitatively, it can be seen that it is easier to avoid the slow burning region by initiating combustion via species concentration changes since a "shorter" path has to be traversed between the two separating curves (EBF and GDH). This is verified to some extent by the previous experimental observations where ultraviolet irradiation of methane-air mixtures occasionally resulted in a two-stage combustion-flame front (cool flame)[4]. Apparently, some of the test radiant conditions happened to place the mixture within the narrow, slow burning region. Since measurements were performed with incremental energy inputs, the upper limit for the energy separation between the stable and rapid burning region (via the photochemical path) is given by the energy increment used. This amounts to only about 1.0 microjoule of energy in the oxygen absorption region of interest.

The use of ultraviolet radiant sources would provide an extra degree of freedom in exploring instabilities of this nature by permitting the establishment of rapid changes in intermediary species concentrations.

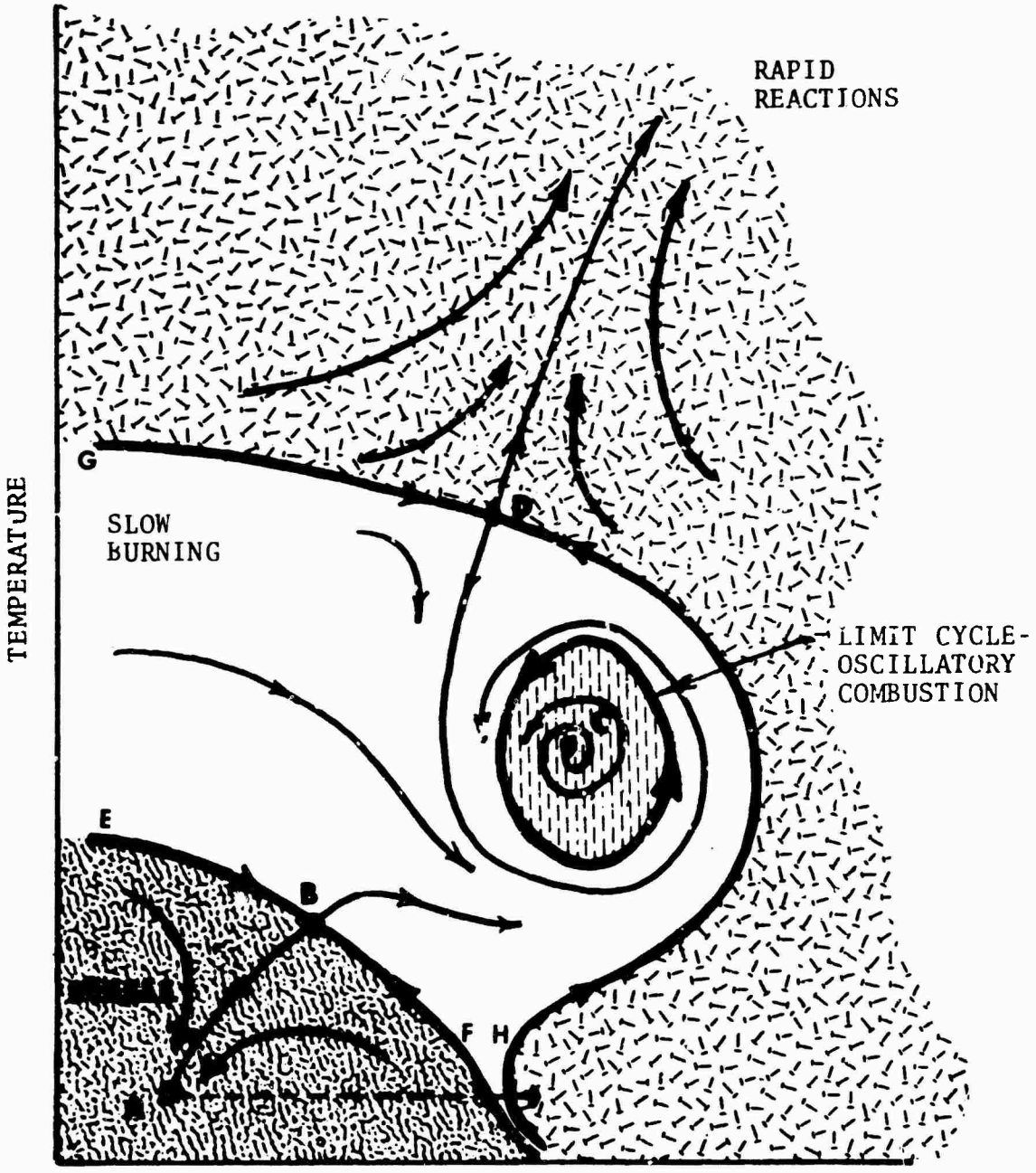

FIGURE 1 - PHASE PLANE ANALYSIS FOR A REACTING SYSTEM WITH A NEGATIVE TEMPERATURE COEFFICIENT

B. REFERENCES

1. Gray, B. F. and Yang, C. F., "On the Unification of the Thermal and Chain Theories of Explosion Limits," J. Phys. Chem., pp. 2747-2750, Vol. 69, No. 8, 1965.

2. Yang, C. H. and Gray, B. F., "On the Slow Oxidation of Hydrocarbon and Cool Flames," J. Phys. Chem., pp. 3395-3406, Vol. 73, No. 10, October 1969.

3. Yang, C. H., "Two-Stage Ignition and Self-Excited Thermokinetic Oscillation in Hydrocarbon Oxidation," J. Phys. Chem., pp. 3407-3413, Vol. 73, No. 10, October 1969.

4. Cerkanowicz, A. E., "Photochemical Initiation of Sustained Combustion in Unsensitized Gaseous Fuel-Oxygen Mixtures," Ph.D. Dissertation, Stevens Institute of Technology, June 1970.

APPENDIX X

COMPENDIUM: DISSEMINATION OF PHOTOCHEMICAL COMBUSTION KNOWLEDGE

A. REPORTS AND PAPERS

A bibliography of all published literature pertaining to the photochemical combustion investigation since its inception is presented below:

1. Cerkanowicz, A. E., Levy, M. E., and McAlevy III, R. F., "Photochemical Ignition of Gaseous Fuel-Oxidizer Mixtures at Subatmospheric Pressures," AFOSR Scientific Report 68-1553, June 1968.

2. Cerkanowicz, A. E., Levy, M. E., and McAlevy III, R. F., "Photochemical Ignition of Low Pressure Fuel-Oxidizer Mixtures," Western States Section - Co bustion Institute Paper 68-42, Fall 1968.

3. Cerkanowicz, A. E., Levy, M. E., and McAlevy III, R. F., "Ignition of Subatmospheric Gaseous Fuel-Oxidant Mixtures by Ultraviolet Irradiation," AIAA Paper No. 69-88, 7th Aerospace Sciences Meeting, January 1969.

4. Cerkanowicz, A. E., Levy, M. E., and McAlevy III, R. F., "Photochemical Ignition of Gaseous Fuel-Oxidizer Mixtures at Subatmospheric Pressures," AFOSR Scientific Report No. 69-2153, May 1969.

5. Cerkanowicz, A. E., Levy, M. E., and McAlevy III, R. F., "The Photochemical Ignition Mechanism of Unsensitized Fuel-Air Mixtures," AIAA Paper No. 70-149, 8th Aerospace Sciences Meeting, January 1970.

6. Cerkanowicz, A. E., Levy, M. E., and McAlevy III, R. F., "Photochemical Ignition of Gaseous Fuel-Oxidizer Mixtures at Subatmospheric Pressures," Final AFOSR Scientific Report No. 70-1664, April 1970.

7. Cerkanowicz, A. E., "Photochemical Initiation of Sustained Combustion in Unsensitized Gaseous Fuel-Oxygen Mixtures," Ph.D. Dissertation, Stevens Institute of Technology, June 1970.

8. Cerkanowicz, A. E., "Photochemical Enhancement of Combustion and Mixing in Supersonic Flows," Interim AFOSR Scientifc Report No. 73-0563, March 1972.

9. Cerkanowicz, A. E. and McAlevy III, R. F., "Photochemical Ignition and Flame Holding: A New Approach to the Control of Combustion," Chemical Propulsion Information Agency Publication 231, Vol. II, pp. 347-355, December 1972.

10. Cerkanowicz, A. E., and McAlevy III, R. F., "Photochemical Ignition and Combustion Enhancement in High Speed Flows of Fuel-Air Mixtures," AIAA Paper No. 73-216, 11th Aerospace Sciences Meeting, January 1973.

B. PRESENTATIONS

Documentation of all presentations pertaining to the photochemical combustion work is provided below:

1. AFOSR 3rd Contractors Meeting on Combustion Dynamics Research, Cocoa Beach, Florida, June 1967 - by M. E. Levy.

2. Seminar, Stevens Institute of Technology, Hoboken, New Jersey, Spring 1968 - by A. E. Cerkanowicz.

3. AFOSR 4th Contractors Meeting on Combustion Dynamics Research, Madrid, Spain, July 1968 - by M. E. Levy.

4. Western States Combustion Institute Meeting, Stanford Research Institute, California, Fall 1968 - by A. E. Cerkanowicz.

5. AIAA 7th Aerospace Sciences Meeting, New York, New York, January 1969 - by A. E. Cerkanowicz.

6. AFOSR 5th Contractors Meeting on Combustion Dynamics, Denver, Colorado, June 1969 - by A. E. Cerkanowicz.

7. AIAA 8th Aerospace Sciences Meeting, New York, New York, January 1970 - by A. E. Cerkanowicz.

8. AFOSR 6th Contractors Meeting on Combustion Dynamics, Sherman Oaks, California, June 1970 - by A. E. Cerkanowicz.

9. Presentation to Air Force Personnel, Photochem Industries, New Jersey, November 1970 - by R. F. McAlevy III.

10. AFOSR 7th Contractors Meeting on Combustion Dynamics Research, La Jolla, California, June 1971 - by A. E. Cerkanowicz.

11. Presentation at Wright-Patterson Air Force Base, Dayton, Ohio, September 1971 - by A. E. Cerkanowicz.

12. Presentation at General Electric-Aircraft Engines Division, Evendale, Ohio, March 1972 - by A. E. Cerkanowicz.

13. First International Symposium on Air Breathing Engines, Paris, France, June 1972 - by R. F. McAlevy III.

14. AFOSR 8th Contractors Meeting on Combustion Dynamics Research, Chicago, Illinois, August 1972 - by A. E. Cerkanowicz.

15. Ninth JANNAF Combustion Meeting, Monterey, California, September 1972 - by R. F. McAlevy III.

16. AIAA 11th Aerospace Sciences Meeting, Washington, D. C., January 1973 - by A. E. Cerkanowicz.

17. Presentation at Cambridge Research Laboratory, Cambridge, Massachusetts, January 1973 - by A. E. Cerkanowicz.

18. AFOSR 9th Contractors Meeting on Combustion Dynamics Research, Los Angeles, California, August 1973 - by A. E. Cerkanowicz.